LAPPEENRANTA
UNIVERSITY OF TECHNOLOGY

Ville Särkimäki

RADIO FREQUENCY MEASUREMENT METHOD FOR DETECTING BEARING CURRENTS IN INDUCTION MOTORS

Thesis for the degree of Doctor of Science (Technology) to be presented with due permission for public examination and criticism in the Auditorium 1383 at Lappeenranta University of Technology, Lappeenranta, Finland on the 28th of May, 2009, at noon.

Acta Universitatis
Lappeenrantaensis
341

Supervisor	Professor Jero Ahola LUT Energy Lappeenranta University of Technology Finland
Reviewers	Dr.-Ing. Annette Muetze School of Engineering University of Warwick United Kingdom
	D.Sc. Pertti Pakonen Electrical Engineering Tampere University of Technology Tampere, Finland
Opponent	Dr.-Ing. Annette Muetze School of Engineering University of Warwick United Kingdom

ISBN 978-952-214-746-2
ISBN 978-952-214-747-9 (PDF)
ISSN 1456-4491
Lappeenrannan teknillinen yliopisto
Digipaino 2009

ABSTRACT

Ville Särkimäki

Radio Frequency Measurement Method for Detecting Bearing Currents in Induction Motors

Lappeenranta 2009

118 p.

Acta Universitatis Lappeenrantaensis 341

Diss. Lappeenranta University of Technology

ISBN 978-952-214-746-2, ISBN 978-952-214-747-9 (PDF), ISSN 1456-4491

Induction motors are widely used in industry, and they are generally considered very reliable. They often have a critical role in industrial processes, and their failure can lead to significant losses as a result of shutdown times. Typical failures of induction motors can be classified into stator, rotor, and bearing failures. One of the reasons for a bearing damage and eventually a bearing failure is bearing currents. Bearing currents in induction motors can be divided into two main categories; classical bearing currents and inverter-induced bearing currents. A bearing damage caused by bearing currents results, for instance, from electrical discharges that take place through the lubricant film between the raceways of the inner and the outer ring and the rolling elements of a bearing. This phenomenon can be considered similar to the one of electrical discharge machining, where material is removed by a series of rapidly recurring electrical arcing discharges between an electrode and a workpiece.

This thesis concentrates on bearing currents with a special reference to bearing current detection in induction motors. A bearing current detection method based on radio frequency impulse reception and detection is studied. The thesis describes how a motor can work as a “spark gap” transmitter and discusses a discharge in a bearing as a source of radio frequency impulse. It is shown that a discharge, occurring due to bearing currents, can be detected at a distance of several meters from the motor. The issues of interference, detection, and location techniques are discussed. The applicability of the method is shown with a series of measurements with a specially constructed test motor and an unmodified frequency-converter-driven motor.

The radio frequency method studied provides a nonintrusive method to detect harmful bearing currents in the drive system. If bearing current mitigation techniques are applied, their effectiveness can be immediately verified with the proposed method. The method also gives a tool to estimate the harmfulness of the bearing currents by making it possible to detect and locate individual discharges inside the bearings of electric motors.

Keywords: bearing current, bearing damage, induction motor, electric motor, variable-frequency drive, inverter, frequency converter, radio frequency, condition monitoring

UDC 621.313.333 : 621.822 : 621.3.014.7 : 537.862

ACKNOWLEDGEMENTS

This research work has been carried out during the years 2005–2008 at Lappeenranta University of Technology. The research has been partly funded by ABB Oy.

I would like to thank all the personnel working at the Department of Electrical Engineering at LUT during these years. Especially, I would like to express my deepest thanks to my colleagues Professor Jero Ahola, Professor Tuomo Lindh, and M.Sc. Risto Tiainen for the experience they have shared, for the comments they have given, and for the time I have had pleasure of spending with them.

I would like to thank the pre-examiners of this doctoral thesis, Dr.-Ing. Annette Muetze and D.Sc. Pertti Pakonen for their valuable comments and corrections to improve the manuscript. I am very grateful to PhD Hanna Niemelä for proofreading the thesis and improving the English language of the text. Special thanks go to Tapio Haring from ABB Oy for giving the initial push for this research topic.

The financial support by the Lappeenranta University of Technology Foundation, the Ulla Tuominen Foundation, the Lahja and Lauri Hotinen Fund, the Jenny and Antti Wihuri Foundation, and the Walter Ahlström Foundation is greatly appreciated.

To my parents, I wish to express my gratitude for always supporting me on my chosen path as well as giving me excellent opportunities to achieve my goals in education and in life. Most of all, I am grateful to Suvi Simpanen for patience and support during the preparation of this thesis.

Västerås, May 1st, 2009

Ville Särkimäki

CONTENTS

ABBREVIATIONS AND SYMBOLS

Roman letters

A_H	Hertzian contact area
B	width of a bearing
C	specific heat capacity
$C_{1,2}$	capacitor
C_b	bearing capacitance
C_{DE}	bearing capacitance at the drive-end
C_{NDE}	bearing capacitance at the non-drive-end
C_{sr}	stator-to-rotor capacitance
C_{wr}	winding-to-rotor capacitance
C_{ws}	winding-to-stator capacitance
c	speed of light
D	outer diameter of a bearing
d	inner diameter of a bearing
d_c	thickness of the lubrication film in a bearing
d_r	radial bearing play
E_b	energy stored in parasitic capacitances
f	frequency
f_s	switching frequency
i	current
i_b	bearing current
J	local bearing current density
J_b	apparent bearing current density
k	location at time-axis
L	inductor
L_{frame}	inductance due to frame construction
L_{rotor}	inductance due to rotor construction
l	length
m	mass
N	number of points of DFT
N_b	number of rollers in a bearing
n	sample
P	power
R	resistor
R_b	bearing resistance
R_{frame}	resistance due to frame construction
R_{rotor}	resistance due to rotor construction
r	radius
r_b	radius of rollers in a bearing
S	heat of fusion
S_{21}	forward voltage gain
T	temperature
t	time
t_{op}	time of operation
U_b	voltage from shaft to ground (bearing voltage)
U_c	common-mode voltage
U_{th}	bearing threshold voltage
U_{ug}	phase-to-ground voltage

U_{vg}	phase-to-ground voltage
U_{wg}	phase-to-ground voltage
V	volume
W	electrical bearing stress
w	window function
x	signal

Greek letters

δ	skin depth
ε_0	permittivity of free space
ε_r	relative permittivity
κ	metal conductivity
λ	wavelength
μ_0	permeability of free space ($4\pi*10^{-7}$ H/m)
μ_r	relative permeability
ρ	resistivity
ω	angular velocity

Acronyms

AC	Alternating Current
A/D	Analog-to-Digital (conversion)
AUT	Antenna Under Test
BVR	Bearing Voltage Ratio
CM	Common Mode
CSI	Current Source Inverter
DC	Direct Current
DE	Drive End
DFT	Discrete Fourier Transform
DSP	Digital Signal Processor
EDM	Electrical Discharge Machining
EMI	Electromagnetic Interference
FEM	Finite Element Method
FFT	Fast Fourier Transform
FICORA	Finnish Communications Regulatory Authority
FPGA	Field Programmable Gate Array
HF	High frequency
HV	High Voltage
IGBT	Insulated-Gate Bipolar Transistor
LV	Low Voltage
NDE	Non Drive End
MV	Medium Voltage
PC	Personal Computer
PD	Partial Discharge
PE	Polyethylene
PM	Permanent Magnet
PWM	Pulse Width Modulation
RF	Radio Frequency

RFID	Radio Frequency Identification
RMS	Root Mean Square
SNR	Signal to Noise Ratio
SRD	Short Range Device
STFT	Short Time Fourier Transform
UHF	Ultra High Frequency
VFD	Variable-Frequency Drive
VHF	Very High Frequency
VNA	Vector Network Analyzer
VSI	Voltage Source Inverter

1 INTRODUCTION

Induction motors are widely used in industry, and they are generally considered to be very reliable. There can be hundreds or thousands of induction motors in a single factory. Induction motors are often in a critical role in industrial processes, and their failure can lead to significant losses as a result of shutdown times. Typical failures of an induction motor can be classified into stator, rotor, and bearing failures. For example, (Thorsen, 1999) reports a survey made in offshore oil industries, petrochemical industries, gas terminals, and refineries, where 51.6% of all failures of electric motors were bearing failures. According to an older study (Albrecht, 1986), bearing failures account for 41% of all failures. Based on these studies, bearing failures can thus be considered the most common failures of electric motors.

One of the many reasons for a bearing damage and eventually a bearing failure is bearing currents. This thesis concentrates on bearing currents with a special reference to bearing current detection in induction motors. Bearing currents occur also in synchronous motors, such as permanent magnet and synchronous reluctance motors; nevertheless, these are not discussed any further here, as the study focuses on induction motors only. However, the following introduction to bearing currents is applicable to electric machines in general. The method studied in this thesis has been verified with induction motors, and its applicability to other types of machines is discussed in brief in Chapter 5.

A bearing current detection method based on radio frequency measurement is studied and verified with tests. The detected radio frequency impulses are due to sparking in the bearings of an electric motor, and this sparking is directly related to bearing currents. The method studied in this thesis makes it possible to detect harmful bearing currents immediately when commissioning a new drive system. Typically, bearing currents have been suspected if the bearings fail before their expected lifetime, and any bearing current measurements have usually been conducted after the failure. If bearing currents are properly detected at an early point, countermeasures can be implemented and the lifetime of the bearing can be substantially increased. To this end, the main focus in the thesis is on inverter-induced bearing currents and more specifically on EDM (electrical discharge machining) bearing currents. The reason for this is that the measurements are made with a test setup where EDM bearing currents are dominating. However, the results are applicable to all kinds of bearing currents, including classical bearing currents if they generate electrical discharges (sparking) in the bearings of a motor. This statement is discussed in more detail in Section 1.4.

1.1 Bearing currents in induction motors

Bearing currents in induction motors can be divided into two main categories[1]; classical bearing currents and inverter-induced bearing currents. The latter can be further divided into four sub-categories; capacitive bearing currents, EDM bearing currents, HF (high-frequency) circulating bearing currents, and bearing currents caused by rotor ground currents (Muetze, 2006B). This categorization is shown in Fig. 1-1.

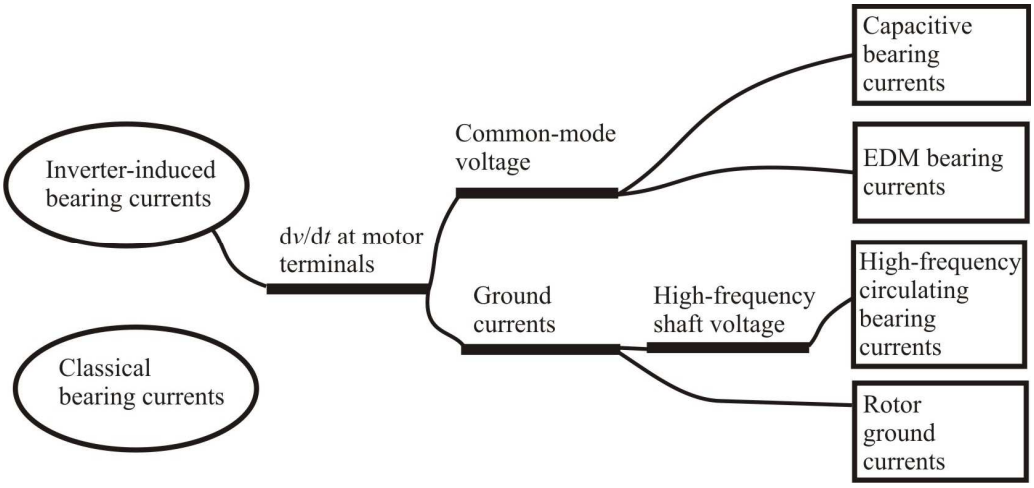

Fig. 1-1 Categorization of bearing currents according to their source and generation mechanism (Muetze, 2006B).

1.2 Classical bearing currents

Classical bearing currents occurring in sine-wave-operated alternating current (AC) motors have been known almost for a century. The phenomenon of motor shaft voltages producing circulating shaft currents has been recognized since the 1920s. These “classical” bearing

[1] This classification is true for electric machines in general and is applicable to, for example, permanent magnet and synchronous reluctance motors, even though they are outside the scope of this thesis.

currents are mostly caused by magnetic asymmetries that produce a variable magnetic flux in the stator, which induces a voltage on the shaft of an electric motor (Alger, 1924). Previously, this was problematic only in larger motors, because only then the voltage induced on the shaft was high enough to rise above the breakdown voltage of the oil film in a bearing of the motor. Since then, design and manufacture of electric motors have improved and classical bearing currents are not considered problematic anymore. A different mechanism causing bearing currents is electrostatic charging of a shaft, as presented in (Ammann, 1988). An example of this mechanism is steam brushing of the turbine blades in a generator, which could lead to high shaft voltages. Classical bearing currents are outside the scope of this thesis, the main focus being on inverter-induced bearing currents in induction motors.

1.3 Bearing currents in inverter-driven motors

Variable-frequency drives (VFDs) have numerous benefits; they offer energy savings, and at the same time they allow high dynamic operation. Unfortunately, they are also a source of a "new" kind of bearing currents. These inverter-generated bearing currents may destroy bearings within a short time of operation. (Bell, 2001) reports a case with two similar motors: One of the motors was equipped with a PWM (Pulse Width Modulation) inverter, and its bearings failed after only six months of operation; this was seven times faster than in the case of the other machine without a PWM inverter. (Boyanton, 2002) mentions a case where bearings of variable-speed AC motors had to be replaced in less than three years because of bearing currents. According to (Oh, 2007), motors controlled by frequency converters may have bearing problems after only a month of operation, and bearing currents are classified as a serious problem among motor manufacturers. The above-mentioned times to failure are rather short for typical induction motors when compared for example against the operational times of 20 000–40 000 hours, which are recommended by a large international motor manufacturer for a small (frame size 160) four-pole motor (ABB, 2005).

The bearing currents do not always flow through the bearings of a motor; they can also destroy the bearings of a load or a sensor connected to the shaft of a motor. (Dahl, 2008) mentions a case where the bearings of encoders connected to two motors failed after seven months from the start-up. After nine months from the start-up, also one of the bearings of the motor failed. A fluting pattern indicating bearing currents was observed from all of these bearings. Table 1-1 presents a summary of the main reasons for electric motor failures. The table is partially modified from the original given in (Tavner, 2008), which is based on various surveys and Tavner's expertise. Based on results given in the table it can be said that roughly a half of the failures are related to bearings. However, it is not useful to compare different surveys from different years, because the sizes and voltage levels of the motors vary and the studies do not specify what percentages of the motors were driven with a frequency converter. Nevertheless, it should be noted that in the two most recent surveys from 1995 to 1999 (Tavner, 2008), the proportion of bearing failures is substantially high, ranging from 75% to 95% of all failures. In these studies, no specific reasons for bearing failures are given, and thus it is not possible to say how serious a problem bearing currents really are in the present drives.

Table 1-1. Reasons for motor failures (Tavner, 2008).

Year and reference	Year 1985. (O'Donnell, 1985)	Year 1986. (Albrecht, 1986)	Year 1995. (Thorsen, 1995)	Years 1995–1997. (Tavner, 2008)	Year 1999. (Tavner, 1999)
Types of electric motors	>150 kW MV & HV motors	>75 kW MV & HV motors	>11 kW MV & HV motors	<150 kW LV motors and generators	<750 kW LV motors and generators
Bearings	41%	41%	42%	75%	95%
Stator	37%	36%	13%	9%	2%
Rotor	10%	9%	8%	6%	1%
Other	12%	14%	38%	10%	2%

In (Hoppler, 2007), some reasons for bearing faults are specified in more detail. These are shown in Fig. 1-2, where typical reasons for bearing failures are given in percentages. As can be seen, most of the main reasons for bearing failures are of a type that can be avoided by careful maintenance and condition monitoring operations; such reasons are for example aged or missing lubricant or a dirty bearing. Bearing currents are mentioned as the fifth most important reason for a failure. In (Hoppler, 2007), it is not mentioned whether these motors have been operated with a frequency converter or not. It can be approximated that currently over 20% of all the motors in industry are driven with frequency converters. It is probable that if the percentage of frequency-converter-driven motors were higher, also the amount of bearing failures caused by bearing currents would be higher.

It should be emphasized that so far there has not been an easy-to-apply and reliable method available to detect bearing currents. At the initial phase, the bearing damage caused by bearing currents is impossible to detect without disassembling the bearing and using a microscope to study the bearing races. At this point, the damage is due to very small micro craters and it is not detectable with a vibration measurement. The actual bearing failure is due to bearing-current-generated micro cratering and the dynamic effect when bearing rollers are passing over these craters. Further, it is possible that the lubricant has lost some of its properties because of arcing and metal particles, which are loosened from the bearing. This can accelerate the bearing damage. If the bearing is disassembled and studied after a failure has occurred, it is possible that the origin for the failure is difficult to detect correctly. For these reasons, it is possible that a bearing failure caused by bearing currents is often wrongly categorized and underestimated. Damages caused by bearing currents are discussed in more detail in Section 1.4.

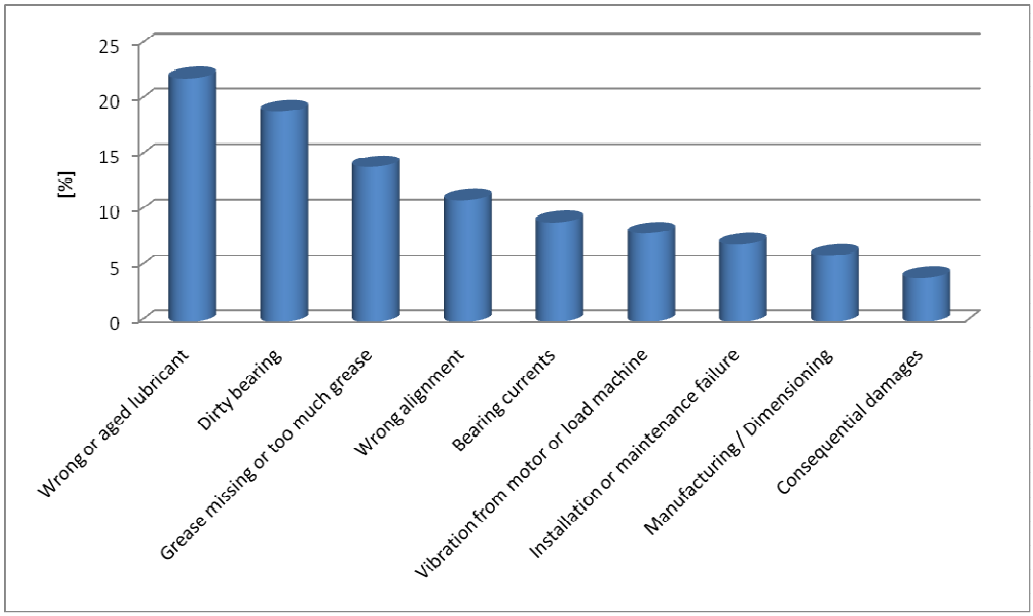

Fig. 1-2. Reasons for a bearing failure according to (Hoppler, 2007).

The main reasons for inverter-induced bearing currents are the common-mode voltage caused by the inverter and especially the influence of the fast voltage rise and fall times (high du/dt) at the motor terminals (Chen, 1996). This nonzero and high-frequency common-mode voltage can be considered to be the root cause for different kinds of bearing currents. These inverter-induced bearing currents can be further categorized into small capacitive currents, EDM currents, circulating bearing currents, and rotor ground currents.

The common-mode voltage U_c in the two-level inverter can be calculated from the phase-to-ground voltages U_{ug}, U_{vg} and U_{wg}, as shown in Eq. (1-1).

$$U_c = \frac{U_{ug} + U_{vg} + U_{wg}}{3} \tag{1-1}$$

The common-mode voltage is usually referred to the ground potential or negative DC bus. Since the line-to-ground voltages are driven either to the positive or the negative DC bus of a frequency converter, it is not possible to sum up these voltages to zero at all instants of time. This means that there is always a nonzero common-mode voltage present at the motor terminals if a typical two-level frequency converter is used to drive a motor. In certain multilevel converter topologies, it is possible to choose modulation and switching combinations to obtain a zero common-mode voltage (Zhang, 2000). However, this is not always practical or possible, because it would have a negative effect on the dynamic performance of a motor.

Common-mode current is a result of the common-mode voltage and the parasitic capacitances of an electric motor that provide low-impedance paths for high-frequency currents. These parasitic capacitances can be neglected at normal operating frequencies, but at the high du/dt of the common-mode voltage they can become important. The parasitic capacitances that have a significant effect on the emergence of bearing currents are the winding-to-stator capacitance

C_{ws}, the winding-to-rotor capacitance C_{wr}, the stator-to-rotor capacitance C_{sr}, and the bearing capacitance C_b. These are illustrated in Fig. 1-3.

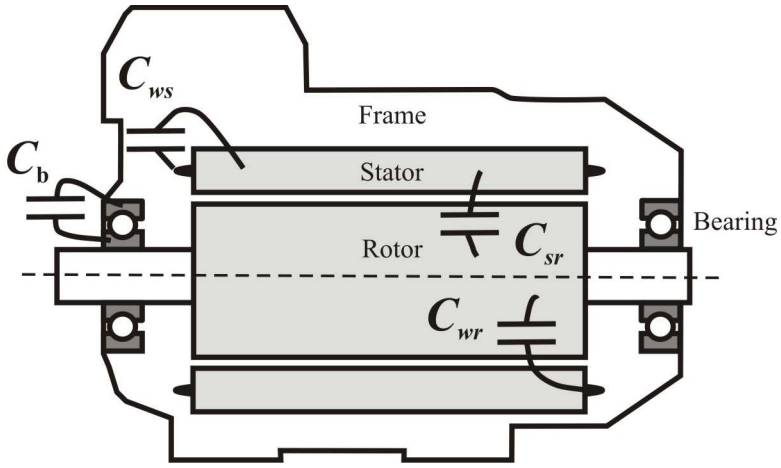

Fig. 1-3. Illustration of some of the parasitic capacitances of an electric motor, which are important at frequencies much higher than the normal operating frequency. These are the winding-to-stator capacitance C_{ws}, the winding-to-rotor capacitance C_{wr}, the stator-to-rotor capacitance C_{sr}, and the bearing capacitance C_b. These parasitic capacitances are the reason for high-frequency common-mode currents and the emergence of bearing currents.

As mentioned previously, these parasitic capacitances are not important at low frequencies, such as the normal operating frequency of 10–100 Hz in most applications. The carrier frequency of an inverter can be up to a few kilohertz, which can also be considered to be a relatively low frequency. The most important reason for common-mode currents is the fast switching of the IGBT (Insulated-Gate Bipolar Transistor). The frequencies present caused by a high du/dt can reach up to several megahertz (Link, 1999). These fast voltage rise and fall times generate high-frequency currents that flow through parasitic capacitances. This can lead to the emergence of different types of bearing currents that are discussed in more detail in the following subsections.

1.3.1 Small capacitive currents

The high du/dt of the common-mode voltage causes HF common-mode currents to flow from the windings through the stator lamination, the air gap, the rotor, the shaft, and the bearings to the frame. This occurs every time when an IGBT switches on or off (Wang, 2000). When bearing rollers are running on top of a lubrication film at higher motor speeds, there is a thin insulation layer between the bearing rollers and rings. This insulating oil/grease layer forms the bearing capacitance (C_b) in the bearing, between the shaft and the frame. In this case, a capacitive current (i_b) is formed according to Eq. (1-2), where U_b is the voltage across bearings.

$$i_b = C_b \cdot \frac{dU_b}{dt} \tag{1-2}$$

These capacitive currents are typically in the range of 5–10 mA. Because capacitive currents are rather small, they are usually considered to be harmless (Muetze, 2006B). The path of the small capacitive current from the rotor through the bearings is illustrated with the dashed line in Fig. 1-4. The current path from the stator winding to the rotor is not included in the illustration.

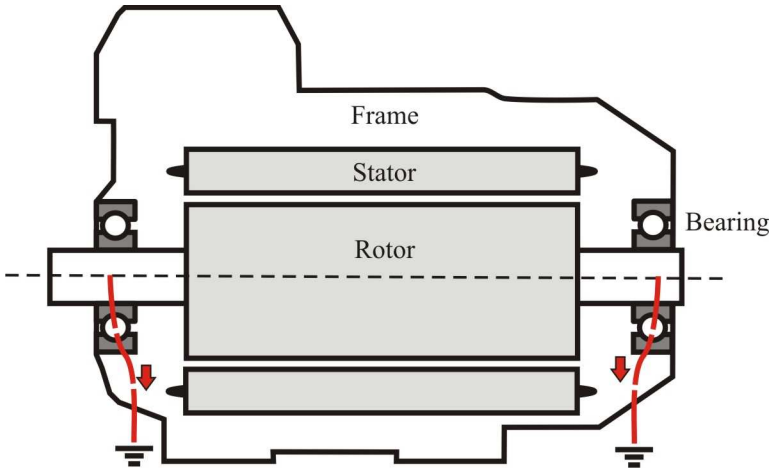

Fig. 1-4. Small capacitive currents and EDM currents flow from the shaft through the bearings to the frame and finally to the grounding point. The current path is illustrated with the dashed line. Only the EDM bearing currents are considered to be harmful to the bearings of an electric motor.

1.3.2 EDM bearing currents

Parasitic capacitances in the motor and the high frequency of the common-mode voltage can also cause another type of bearing currents. The requirement is that the motor is running at a sufficient speed for the bearing rollers to roll on top of a lubrication film so that the bearing capacitance is formed as previously explained. Because of a capacitive coupling of the winding to the rotor, the bearing capacitance and other parasitic capacitances are charged and the voltage at the shaft of the motor rises to a certain value. If the charged voltage at the shaft exceeds the breakdown voltage of the lubrication film, the energy in the capacitances discharges through the bearings and causes the flow of the EDM current (Chen, 1996).

The path of the EDM current is from the shaft to the inner ring of the bearing, through the rollers to the outer ring, and to the frame of the motor. The path is illustrated in Fig. 1-4. The bearing capacitance and the breakdown voltage of the lubrication film are not constant, because the lubricant film thickness depends on many factors, such as fluid velocity, fluid viscosity, load acting on the bearings, temperature, dielectric strength of the lubricant, additives in the lubricant, and surface roughness of the bearing (Busse, 1997B). For these reasons, discharges can occur randomly and are not directly linked to the switching moments of the IGBT. According to (Binder, 2008), maximum EDM bearing currents occur slightly below or at the rated speed of the motor. At higher speeds, the thickness of the lubrication film and hence the insulation thickness is greater and the EDM currents are reduced. The lubricant thickness ranges from 0.2 to 2.0 μm in the bearings, and it is estimated in (Busse, 1997B) that the dielectric strength of the lubricant is 15 V/μm. This leads to an assumption that shaft voltages between 3 and 30 V can be large enough to cause discharges in the bearings.

The magnitude of the shaft voltage[2] depends on the common-mode voltage, because it is determined via a capacitance voltage divider from the common-mode voltage (U_c). In (Busse, 1997B), this capacitance voltage divider has been termed as BVR (Bearing Voltage Ratio). With the BVR and the common-mode voltage, the voltage across the bearing can be estimated as given in Eq. (1-3)

$$U_b = U_c \cdot \mathrm{BVR} = U_c \cdot \frac{C_{wr}}{C_{wr} + C_{sr} + 2C_b} \tag{1-3}$$

where C_{wr} is the capacitance between the winding and the rotor and C_{sr} is the capacitance between the stator and the rotor. According to (Muetze, 2007B), the BVR is typically in the range of 3–10%. As an example, with a 400 V AC supply, shaft voltages up to ~40 V can be expected. This is more than the breakdown voltage of the lubrication film, and thus EDM bearing currents are likely to occur.

1.3.3 High-frequency circulating bearing currents

High-frequency circulating bearing currents are somewhat more complicated than the current types introduced above, and they can be briefly explained as follows: A high du/dt of the voltage at the motor terminals together with the parasitic capacitances between the motor winding and the stator laminations C_{ws} cause an additional HF common-mode current with frequencies up to several megahertz. The current enters the motor through the windings and leaves via the lamination and the frame. This current excites a HF circular magnetic flux around the motor shaft, which in turn induces a shaft voltage along the shaft of a motor. If this induced shaft voltage is high enough, it can discharge through the bearings and generate a circulating current through the bearings, the shaft, and the frame of a motor.

This phenomenon was first presented by Chen et al. in (Chen, 1996B;1998). Later, (Muetze, 2004) and (Mäki-Ontto, 2005) have explained this kind of a bearing current in more detail. The magnetic flux is distributed axially on the stator frame as illustrated in Fig. 1-5. In the figure, the sizes of the circles indicate the magnitude of the flux. This kind of linear flux distribution is a result of a high-frequency current reducing linearly in the axial direction of the motor frame. Because of the high frequency of the current, skin effect becomes important. At the frequencies present, the skin depth is less than the thickness of each stator lamination. The current flows through each of these laminations to the grounding point. The HF current and the magnetic flux

[2] In some articles ‘shaft voltage’ is referred to as ‘bearing voltage’.

have their maximum values in the laminations near the grounding point, and the flux decreases linearly lamination by lamination. Therefore, the induced voltage on the shaft has a potential difference between the shaft ends, which can exceed the breakdown voltage level of the lubricant and lead to a circulating bearing current. The path of the HF circulating bearing current is from the shaft through the bearing to the frame and back to the shaft through the other bearing as illustrated with the dashed line in Fig. 1-5.

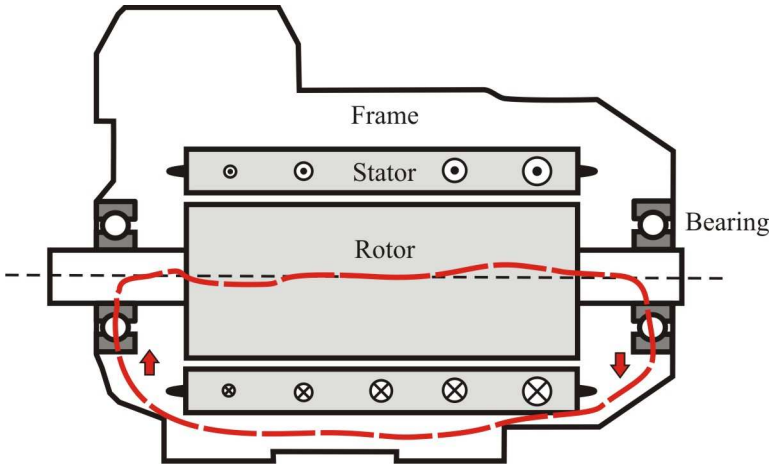

Fig. 1-5. High-frequency circulating bearing currents flow in a loop formed by the shaft, bearings, and the frame of an electric motor as illustrated with the dashed line.

1.3.4 Rotor ground currents

If the frame of an electric motor is poorly grounded, rotor ground currents (sometimes referred to as shaft grounding currents) can occur in the system. This may take place when the rotor ground impedance is significantly lower than the grounding impedance of the motor frame. Typically this means that the rotor is well grounded through the driven load. This type of a bearing current was first discussed in (Ollila, 1997).

The generation mechanism of rotor ground currents is as follows: The high du/dt at the motor terminals creates a HF common-mode current to the motor frame (see Section 1.3.3). If the rotor is better grounded than the stator, this current flows through the bearings of the motor, the shaft, and the load machine back to the frequency converter. The path of the rotor ground current is illustrated with the dashed line in Fig. 1-6.

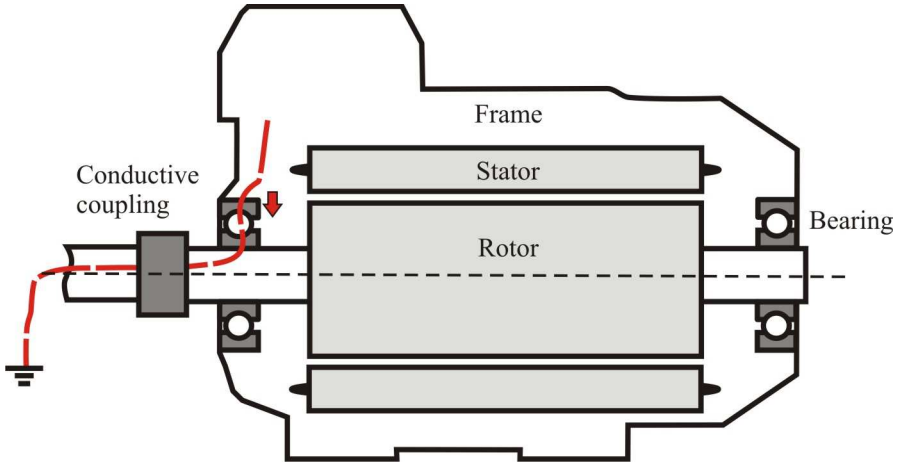

Fig. 1-6. Rotor ground currents flow to the low-impedance ground through the shaft and the load machine as illustrated with the dashed line. The reason for this is the poor grounding of the frame of a motor and high d*u*/d*t* at the motor terminals.

1.4 Bearing damages caused by bearing currents

According to (Binder, 2008), small motors of up to typically 20 kW are likely to suffer from EDM bearing currents, whereas larger motors are more affected by circulating bearing currents. It should be noted that there can be also EDM bearing currents in larger machines if shaft voltage can build up to a certain level required for lubrication film breakdown. Rotor ground currents occur only with motors with the shaft grounded through a load and are not necessarily influenced by the size of the motor. It is still somewhat uncertain whether the damage mechanism behind these different currents is always the same.

According to (Prashad, 2001), damages caused by electric currents in bearings can be divided into two categories. The first type of damage is related to currents through a bearing without sparking. The second type of damage is caused by discharge currents. The first type of damage is possible if a low-resistivity lubricant is used, or a motor is running at such a low speed that there is no sufficient insulating lubrication film in the bearings. In this case, bearing currents may cause surface heating and decompose the lubricant. These can accelerate bearing damages that are mainly due to the dynamic effect of the rollers and not due to electrical pitting. In the second type of damage, the requirements are that a high-resistivity lubricant is used and the motor is running at a sufficient high speed so that there is a thin insulating lubrication film between the rollers and the races of the bearing. In this case, bearing currents cause discharges (sparking) in the bearings. As discussed in Section 1.3.1, only capacitive currents can flow through bearings and lubrication without considered to be harmful to the bearings. What comes to the HF circulating bearing currents or rotor ground currents, there is no clear picture of the damage mechanism. The focus in this thesis is on EDM bearing currents, which are known to cause sparking in the bearing. The method studied in this thesis can be used to detect this discharging type of bearing currents. The method is also applicable to detect other kind of bearing currents only if they cause electrical discharges (sparking) in the bearings.

There are no EDM bearing currents if the shaft voltage stays below a critical threshold voltage of the lubricant (Busse, 1997C). If the shaft voltage exceeds this threshold level, a discharge occurs. This phenomenon can be thought to be similar to electrical discharge machining, where material is removed by a series of rapidly recurring electrical arcing discharges between an electrode and a workpiece. This is fully explained and tested for example in (Jagenbrein, 2005). It is also mentioned in the reference that the destructive effect of bearing current is due to rapid energy release and is not associated with the presence of current or voltage. Discharges can take place at any moment, and their occurrence is difficult to predict. The threshold level at which the discharge occurs is determined by the breakdown voltage of the lubrication film. However, the breakdown voltage of the lubrication film in the bearing is not constant, as the thickness of the lubrication film is changing when the motor is running. The reasons are for example vibration, load variation, temperature changes, and the surface finish of the bearing. For instance, the surface roughness of the bearing races may cause random puncturing of the lubrication film. The quality of the bearing finish may have an effect on the discharge rate, and discharge activity may grow when bearing is partially damaged (Macdonald, 1999). It was mentioned above that the root cause for EDM bearing currents is the common-mode voltage at the motor terminals. Nevertheless, it is not possible to accurately predict the time of the discharge from the common-mode voltage. For example, in (Muetze, 2007) it is stated that EDM bearing currents generally occur at the moment when the rise of the common-mode voltage has finished. This might be partially true, because then there has been more time for parasitic capacitances to charge, and the shaft voltage is close to the maximum value. There are also other issues affecting the threshold level thereby making discharges occur randomly, as will be shown later with measurements.

When the voltage between the shaft and the frame exceeds the breakdown voltage of the lubricant film, the voltage at the shaft discharges releasing energy charged in the bearing capacitances as well as other parasitic capacitances discussed in Section 1.3 (this is further discussed in Section 2.3.1). The discharge generates heat that is concentrated on a very small area on the bearing ring causing local melting of the bearing surface. In other words, the local bearing current density J along with the metal conductivity κ is the reason for a high local power loss density P/V as given in Eq. (1-4). This causes very high local temperatures in very small areas and melting of the bearing race (Muetze, 2006). This means that a small crater is formed every time when a discharge occurs as a result of a bearing current flowing through the bearing. Eventually, multiple craters are formed and particles of molten material are transferred to different places (Preisinger, 2001). This is the starting point for the actual bearing damage. According to (Prashad, 2001), the probability of a crater formation is higher on the inner race of a bearing, because the lubrication film thickness is smaller between the inner race and the rolling elements than between the outer race and the rolling elements.

$$\frac{P}{V} = \frac{J^2}{\kappa} \tag{1-4}$$

The reason why bearing currents are not detected at the early stage is that sparking typically generates micro-cratering where the size of a crater is only 0.5 µm in diameter (Muetze, 2006). These craters are not visible to the bare eye and can only be detected with a microscope. Vibration caused by small craters is too small to be picked up by vibration-analysis equipment (Macdonald, 1999). Because of this, a damage is not often observed before it develops to fluting. Fluting is a pattern of multiple grey lines on bearing raceways and is caused by the

dynamic effect of the rolling elements when they constantly roll over small craters (Muetze, 2006). In other words, the root cause for fluting is electrical discharges taking place inside the bearings.

Bearing sparking can also cause the lubricant in the bearing to change its composition and degrade rapidly. The local high temperature can cause burning or charring of the base oil (Preisinger, 2001). Further, metal particles are transferred to the lubricant because of electric discharging. These issues can accelerate the development of a bearing damage and finally lead to a bearing failure.

There are no exact limits for the shaft voltage or the bearing current which, if exceeded, can cause bearing damage. At least the following suggestions can be found from the literature: In (Prashad, 2001) it is stated that shaft voltages above 200 mV can increase discharges in the bearings of a motor; (Erdman, 1996) in turn gives the following values: <0.3 V is safe, 0.5–1 V may be harmful, and a shaft voltage over 2 V may destroy the bearing. Similarly, (Muetze, 2006) gives recommendations for safe bearing current values. The currents are given as apparent bearing current densities J_b, that is, the peak bearing current i_b divided by the Hertzian contact area A_H as given in Eq. (1-5). Bearing current densities below 0.1 A/mm^2 do not have an effect on the bearing life, whereas bearing current densities over 0.7 A/mm^2 may shorten the bearing life. In (Busse, 1997B), similar values are given; it is stated that current densities below 0.4 A/mm^2 are not dangerous, values between 0.6–0.8 A/mm^2 may be dangerous, and finally, bearing current densities over 0.8 A/mm^2 are probably harmful. An example of how to calculate the Hertzian contact area for a bearing is given in (Busse, 1997E).

$$J_b = \frac{\hat{i}_b}{A_H} \tag{1-5}$$

The bearings of a motor depend on the motor size, the field of application, and operation conditions. Therefore, according to (Muetze, 2006), the absolute values of bearing currents are not the appropriate measure for evaluating the endangerment of bearings because of bearing currents. It is also possible that occasionally there is metal-to-metal contact in the bearing at lower rotation speeds. In this kind of a situation, a current may discharge through the bearing without causing sparking and damage to the bearing. However, (Muetze, 2006) also proposes a different approach to predict the harmfulness of bearing currents. An equation is presented that can be used to calculate the dissipated electric energy in the bearing. Taking into account the apparent bearing current density, the time of operation t_{op} and the switching frequency $f_{s,}$ the electrical bearing stress W can be expressed as given in Eq. (1-6). It is shown in (Muetze, 2006) with experiments that the aging of the grease is directly proportional to W and the degree of melting of the bearing race is function of W.

$$W \approx J_{\mathrm{b}} \cdot t_{\mathrm{op}} \cdot f_{\mathrm{s}} \tag{1-6}$$

1.5 Measurement of bearing currents

Measuring bearing currents is problematic in many ways. Most importantly, bearing currents cannot be measured directly. It is impossible to place a transducer in the path of the bearing current inside a bearing. It is also impossible to measure the current between the outer ring of the bearing and the motor frame. This is true also for measurements between the inner ring of the bearing and the shaft of a motor. Probably the easiest method is to insulate the bearing from the frame and then bypass this insulation with a short wire. The current through this wire can then be measured with a high frequency current probe. This way it is possible to measure the bearing current flowing through the bearing. This works for all kinds of bearing currents. However, it should be noted that it is still not known how the bearing current is distributed inside the bearing, for example, where the discharge or discharges occur. Because of this limitation, bearing currents have to be measured indirectly from the wire, and the actual current has to be approximated or modeled. However, there is still some inaccuracy due to the electrical parameters of the measuring setup. These are the capacitance due to bearing insulation and the resistance and inductance due to wire loop. According to (Muetze, 2007), the knowledge of the following parameters gives a good estimate of the actual bearing current inside a bearing: bearing currents at both ends of the motor (measured with insulated bearings), shaft voltage, common-mode current, stator ground current, rotor ground current, and stator winding common-mode voltage. The reference also covers extensively the measurement of these parameters and explains how the measurement circuitry affects the results.

Bearing currents with insulated bearings are typically measured only in a laboratory, because modification of an existing motor for bearing current measurement is a demanding task. It is time consuming to insulate normal bearings of an existing motor, because this typically requires inserting an additional insulation layer between the bearings and the frame of a motor. A simpler, but an expensive method is to replace the existing bearings with insulated bearings. However, insulating both bearings mitigates bearing current, or in the worst case, moves it to the bearings of the load machine. What makes the situation even more complicated is that based on current measurements alone it is not necessarily possible to say how harmful bearing currents are. This was discussed in the previous section.

In an industrial environment, one way to measure bearing currents without insulated bearings is to measure bearing currents with Rogowski coils. These are coils which can be opened and placed around a shaft, power cables, and grounding cables to measure the current through these. Today they are also available for HF high-current applications. (Link, 1999) shows how common mode currents can be measured in an industrial environment. This way it is possible to get indication of HF circulating bearing currents and rotor ground currents. For example, a Rogowski coil can be placed around the motor phase cables at the frequency converter end to measure the total common-mode current. To find out whether some part of this common-mode current is flowing through the bearings, additional measurements are needed. These include for example measurement of the return current through the grounding cable, auxiliary ground currents, and the shaft current. Based on these measurements, an analysis can be made about the possibility of bearing currents. There can be many auxiliary grounds present in the system making the measurement more difficult. The stator ground current (common-mode current that leaves the motor through the stator frame) can be measured in certain cases. Generally, this

means that the motor is placed on an insulated bed and grounded with a cable, from which the current can be measured. However, stator ground currents do not necessarily indicate that there are bearing currents present in the motor. To measure rotor grounding currents, a Rogowski coil can be placed around the shaft between a motor and a load machine. This is illustrated in (Rechberger, 2006). On the other hand, this current can also be an EDM current, which is flowing through the bearings of a load machine. Circulating currents can be measured with reasonable accuracy, but this requires that the Rogowski coil is placed around the shaft between the bearings of the motor. So this means that the Rogowski coil is installed inside the motor, which can be very problematic. Furthermore, the reliability of using Rogowski coils can be questioned because of strong electromagnetic fields present that might alter the results.

The shaft voltage is relatively easy to measure compared with the bearing currents. This measurement can be done with a brush connected to the shaft of the electric motor. The shaft voltage is mentioned to be a good indicator of bearing currents in (Busse, 1997C) and (Dahl, 2008). In the case of a VFD, there is always a shaft voltage present that will follow the common-mode voltage waveform, as discussed in Section 1.3.2. It is possible to simultaneously measure the common-mode voltage and the shaft voltage and compare these two to see whether discharges take place. If the shaft voltage waveform differs at some point from the common-mode voltage waveform, the reason for this can be assumed to be that the shaft voltage has been discharged to the ground through the bearings of the motor. This requires an experienced person to analyze voltages and to predict whether there are discharges and bearing currents in the bearings of the motor. For instance, it is possible that the shaft voltage discharges through the load machine without being harmful to the bearings of the motor. In other words, it is practically impossible to say anything about the magnitude and/or destructiveness of the bearing currents based on shaft voltage measurements only. A common-mode voltage measurement is typically needed to properly detect time instances at which the shaft voltage discharges. It should also be emphasized that knowledge of the magnitude and rise/fall times of the common-mode voltage is not sufficient to detect bearing currents.

The measurements discussed in this section are illustrated in Fig. 1-7. A problem with most of these measurements is the high-frequency EMI (electromagnetic interference) from the inverter, which should be taken account. This interference is discussed in more detail in Section 3.3.1.

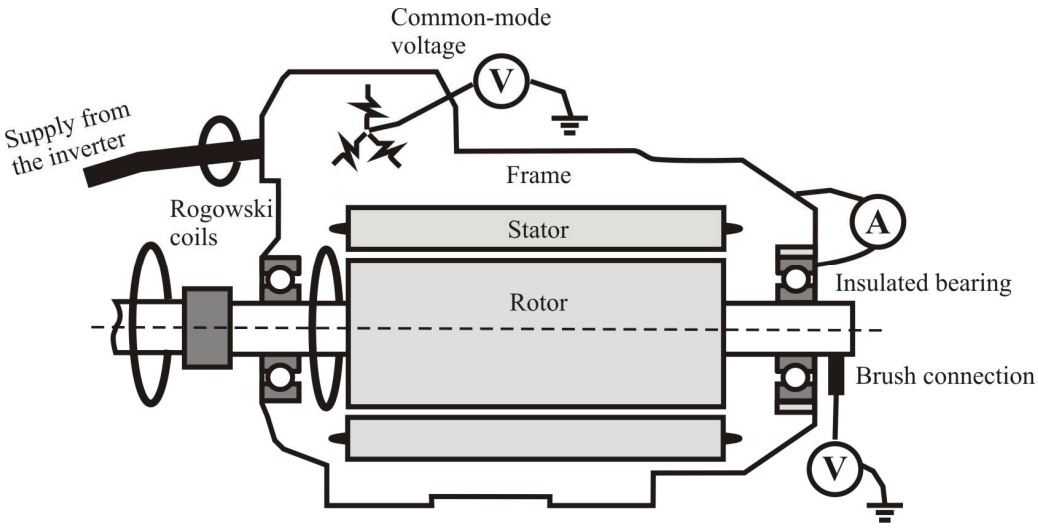

Fig. 1-7. Various measurements that can be used to detect and/or measure bearing currents from an electric motor. Indication of some types of bearing currents can be obtained with Rogowski coils even from an unmodified motor. A more reliable measurement requires insulated bearings that are shorted with a wire. The bearing current can be measured from the wire with a current transducer. Shaft voltage and common-mode voltage measurements can also give some indication of a bearing current problem.

1.6 Bearing condition monitoring methods

An induction motor is a robust and fault-tolerant machine and very popular in industrial drives. During normal operation of an induction motor, both electromagnetic and mechanical forces are designed to interact in such a way that they are balanced and motor vibration is minimized. If there is a fault in the motor, the balance between these forces is lost. The reason for the fault can be an ambient factor, such as errors in design or manufacture, defective installation or use, and normal wear and aging. In most cases, there is not just one reason for a motor fault. The faults can be divided either into electrical and mechanical faults or rotor, stator, and bearing faults. Common electrical faults are winding faults at the stator. At the rotor, such are short circuits of rotor laminations and broken rotor bars. Typical mechanical faults are eccentricity in the rotor and the stator and core slacking in the stator (Singh, 2002).

A common mechanical fault in induction motors is a bearing fault, according to studies presented in (Singh, 2002), (Albrecht, 1986), and (Thorsen, 1999). Multiple monitoring techniques have been developed for bearing condition monitoring. These are, for example, vibration monitoring, temperature monitoring, chemical analysis, acoustic emission monitoring, sound pressure monitoring, laser monitoring, and current monitoring (Zhou, 2007). However, only a few of these methods are widely used in industry. According to (Lindh, 2003), the most important methods are based on the measurement of vibration, acoustic emission, and temperature. However, none of these methods is very useful for detecting bearing currents at an early stage.

The basis of **vibration measurement** is simple. A small defect in the bearing allows radial movement of the rotor and the rolling element of the bearing and causes a mechanical impulse that can be measured with vibration measurement (Lindh, 2003). Accelerometers and vibration

velocity transducers are commonly used for the measurement. Measurements are taken on the bearings, bearing support housing, or other structural parts of the machine. The simplest approach is to measure the overall root-mean-square (RMS) level and crest factor. The crest factor is the ratio of peak value to RMS value of acceleration. However, frequency domain or spectral analysis of the vibration signal is perhaps the most widely used approach for bearing defect detection (Tandon, 1999). In this method, resonant frequencies of certain bearing elements are observed in the frequency domain. This method cannot detect bearing currents directly, only the damage they eventually cause together with mechanical stress that is due to the movement of bearing rollers.

Acoustic emission occurs when a small surface displacement within the material is produced. A transient elastic wave is generated as a result of the rapid release of strain energy caused by the structural alteration in the solid material under mechanical or thermal stresses. Acoustic emission operates in a range from hundred kilohertz up to megahertz, in other words, from audible noise to ultrasonic frequencies. The method can be used to detect, for example, generation and propagation of cracks. Parameters that are typically measured include the peak amplitude of the signal and number of pulses that are over certain threshold level (Tandon, 1999). There are no research data available that would indicate that this method is applicable for direct or early detection of bearing currents.

Degradation of the grease or the bearing can cause a **temperature rise** in the bearing, which can be detected with a temperature sensor installed at the bearing. However, other factors such as power losses in the motor and motor operating speed also affect the temperature of a bearing. This means that further investigation is required to reveal the origin of the temperature rise, and it is possible that the origin is elsewhere than in the bearing. Because the temperature rise is not necessarily linked to bearing currents, this method does not give clear indication of bearing currents and is thereby not applicable to early detection of them.

Chemical analysis of the lubricant is based on the fact that the composition of the lubricant and different chemical products in it is altered because of the heat. Also mechanical wear degrades the bearings, and metal particles are transferred to the lubricant. Except for the approach presented in this thesis, this is the only method that can detect or give indication of sparking and hence bearing currents in the bearing without disassembling it. However, this method is applicable only when lubricating grease is available. Generally this means that this method is available only for motors with a circulating lubricating system. There are also cases where a bearing failure has been caused by electric erosion but no significant changes in the lubricant could have been detected (Ost, 2005). Hence, we may conclude that chemical analysis is not fully appropriate and reliable method to detect bearing currents. Also, real-time indication of bearing currents is not possible to attain with this method.

As indicated above none of these methods is capable to directly detect bearing currents. Most of these methods are applicable only when the damage caused by bearing currents together with mechanical stress has developed to a certain point. Bearing currents can be present in a drive system from the point when a motor is turned on, but it takes some time before the damage caused by bearing currents is developed to such a point where it can be detected with the methods presented in this section. For example, surface damage has to develop to a certain extent before the measured vibration exceeds a certain threshold and an action is taken. Even at this point it may be impossible to say what the root cause for the damage of the bearing is. This requires disassembling the bearing and visual inspection by experienced maintenance personnel to pinpoint the actual cause. It may also require chemical analysis of the lubricant and careful inspection of the bearing surface races with a microscope to be certain whether the damage is

due to the bearing currents. If a healthy bearing needs to be inspected to check the possibility for bearing currents, it means that the bearing is destroyed. The methods presented in this section do not provide a tool that could be used to detect a bearing current from the very beginning of a motor operation. It is also preferable that the detection could be made without disturbing the normal operation of the motor. The method studied in this thesis gives a solution for this problem.

1.7 Mitigation of bearing currents

Multiple techniques have been proposed to mitigate harmful bearing currents. Unfortunately, most of them have certain drawbacks. They may be difficult or impossible to implement on existing systems and typically always raise the cost of the system. Applicability and effectiveness of these techniques also depend upon the type and source of the bearing current present in the system (Schiferl, 2004). Mitigation techniques can be divided into two classes depending on whether they are applied on the inverter side or at the motor. Common-mode filters, shielded cables, carrier frequency reduction, and special modulation techniques are examples of inverter-side mitigation techniques. Some of the techniques used at the motor end are electrostatic shielding between the rotor and the stator, shaft voltage mitigation with slip-rings or brushes, insulated bearings, ceramic rollers, and conductive grease.

Shaft voltage mitigation with **slip-rings or brushes** is a well-known technique. In this method, an apparatus that connects the shaft to the frame of the motor is attached to the shaft of the electric motor. For example, carbon or copper brushes can be used. The brush bypasses the bearing currents through a low-impedance path, and thus no currents are flowing through the bearings and voltage build-up at the shaft is prevented. Ideally, brushes work perfectly against EDM and circulating bearing currents. They are also inexpensive and easy to install afterwards. However, field experience has shown that it is hard to maintain low-resistance contact to the ground because of brush wear and the build-up of an oxide layer. This leads to a need for regular maintenance. A solution for these problems is proposed in (Oh, 2007), where a conductive microfiber ring is presented. This is a brush made of millions of conductive microfibers. According to (Muetze, 2008) this technique involves hardly any direct frictional wear and can be considered as maintenance-free and robust against contamination. Similarly, using **conducting grease** in the bearings grounds the motor shaft and provides a low-impedance path for common-mode currents. In other words, conducting grease works similarly as slip-rings or brushes. Unfortunately, according to (Oh, 2007) this technique has been abandoned, because conductive particles in the lubricant may increase wear and can cause premature failures.

Electrical insulating of the bearings blocks the bearing current path, thus preventing damage to the bearing. This can be done with an insulating layer between the bearings and the motor frame or using ceramic rollers. Insulating layers are typically used in laboratory tests, but are difficult to implement afterwards to the motor. Better solutions are insulated bearings that have a thin oxidation layer deposited on the outer surface of the bearing ring or hybrid bearings, where ceramic rollers are used instead of metallic ones (Preisinger, 2001). The insulation thickness has to be adequate to properly insulate high-frequency bearing currents. It is proposed in (Muetze, 2006C) that the insulating coat has to be at least 250 μm to sufficiently reduce the high-frequency circulating currents. However, insulating the bearings may shift the problem elsewhere, for example to the bearings of a load machine. This may occur, for example, when there are EDM currents present and the bearings of the motor are insulated. If only one end is insulated, the noninsulated bearing may fail twice as fast. If both bearings are insulated and there is a galvanic connection through the shaft to the load machine, the bearings of the load

machine may fail instead. In the case of circulating currents, it suffices if only one end of the motor is properly insulated. A disadvantage of insulated bearings is their high price compared with normal ones. The price of an insulated bearing can be 2–10 times the price of a normal one. Some experiences with such insulated bearings are reported, for example, in (Muetze, 2006B). **Insulated coupling** between the motor and the load can be used to prevent damage to the load machine. By inserting an insulated coupling between the motor and the load, the path of bearing currents to the bearings of the load machine can be effectively blocked. Rotor ground currents can also be mitigated, because the grounding path to the load is cut off. Nevertheless, this method does not have any effect on the EDM and circulating type bearing currents in the motor. In the worst case, this can even lead to reduction of the lifetime of the motor bearings if bearing currents have previously flown through the bearings of the load machine.

Proper grounding and **cable selection** have no effect on the EDM bearing currents, because they are not related to the stator ground currents. For HF circulating currents and rotor ground currents, grounding and cable type can make a difference. According to a measurement reported in (Bentley, 1997) there are significant differences in common-mode currents between drives with different cables. However, the authors have not made any bearing current measurements, and hence it is not possible to tell what the differences in bearing currents are. It is shown by measurement results presented in (Muetze, 2006B) that shielded cables can actually increase circulating currents, because the lower grounding impedance of a shielded cable increases stator ground currents, which results in a higher magnetic flux and hence a higher shaft voltage. Nevertheless, the authors of (Muetze, 2006B) agree that rotor ground currents can be mitigated with a proper grounding and shielded cables. This is shown to be true in (Guttowski, 2006), where these methods were used in a practical application at a paper mill, and in (Rechberger, 2006) where measurements were carried out in a laboratory. Disadvantages of these techniques are the higher cost of special cabling. An additional advantage is that properly shielded cables also reduce the radiated EMI.

Various inverter **output filters** are targeted at mitigating the common-mode voltage and especially to reduce the effects of the high du/dt of the phase voltages, hence reducing also the bearing currents that are affected by this parameter. However, most of these filter structures affect mainly the du/dt and do not significantly reduce the common-mode voltage itself. Thus, these filters have the main effect on the HF circulating currents and the rotor ground currents, because the du/dt is reduced and the EDM bearing currents are not significantly affected if the common-mode voltage stays the same (Muetze, 2006B). There are also filters that can reduce or even eliminate the common-mode voltage and thus can be effective also against EDM bearing currents. These filters require a connection to the DC link of the inverters. Numerous passive and active filter topologies have been presented and tested, for example in (Akagi, 2004, 2006), and (Hyypio, 2005). A problem with filters is that they are expensive and therefore raise the cost of the system.

An effective method is to reduce the common-mode voltage at the inverter end and design a modulator in such a way that the generated common-mode voltage is small or nonexistent (Wang, 2000). This requires a multi-level inverter. Different **modulation techniques** are experimented for example in (Baiju, 2004), (Naumanen, 2008), and (Jouanne, 2002). Problems with these are that they need multilevel converters and cannot be used in existing installations without changing the frequency converter. A different approach to the common-mode voltage reduction by redesigning the common-mode circuitry (motor topology modification) is discussed in (Wang, 2000). However, these methods are only introduced in the article and no measurements are given. Furthermore, most of them are problematic in one way or another, and most of these methods cannot completely eliminate the common-mode voltage. **Carrier**

frequency reduction does not mitigate bearing currents, but it may give a longer lifetime to the bearing. The reasons are that carrier frequency reduction does not have an effect on the fast switching times (high d*u*/d*t*) of the IGBT, but it reduces the number of times when switching occurs during a given time period. This should reduce the times when bearing currents pass through the bearings, hence giving a longer lifetime to the bearing. Disadvantages are changes in the motor performance, increased losses, and increased noise level.

An **electrostatic shielding** between the rotor and the stator is proposed in (Busse, 1997). The idea is to diminish the capacitive coupling between the stator and the rotor with a Faraday shield. This will effectively mitigate EDM currents, because no voltage can be built up on the shaft. The shield works well if properly installed; however, this kind of a mitigation technology raises the total cost of the system and is practically impossible to install afterwards. Proposed construction methods and results attained are discussed in more detail in (Busse, 1997). A somewhat similar method targeted against circulating bearing currents is presented in (Mäki-Ontto, 2003), where **conductive shielding** in the stator slots is suggested. The idea is to prevent high-frequency current to flow from the windings to the stator lamination. Instead, it is guided elsewhere, along the conductive shielding, back to ground. This prevents a circumferential magnetic flux in the stator, and hence there is no induced voltage at the shaft that could generate HF circulating bearing currents. The effectiveness of the method is proved with simulations in (Mäki-Ontto, 2003) and found to be very effective against circulating bearing currents.

Finally, it is important to consider possible differences between **voltage source inverters** (VSI) and **current source inverters** (CSI) with respect to the harmfulness of bearing currents. The majority of the low-voltage and medium-voltage frequency converters used in the industry are based on voltage source inverters. The reason for this is certain advantages of the VSI over the CSI in these applications, and it is not reasonable to assume that this will change in the near future, even if the CSI were less harmful than the VSI to the bearings of an electric motor. Because of the popularity of the VSI, most of the papers published on bearing currents are focused on the VSI. This thesis is no exception in this respect, because the frequency converter used in the measurements in this work is a VSI. If the output voltage and the common-mode voltage of the CSI are considered, it is clear that even though the current waveform is more closely sinusoidal, there are still a high d*u*/d*t* and common-mode voltage present at the output of a typical two-level CSI. This leads to an assumption that the CSI does not differ significantly from the VSI if the harmfulness of bearing current is considered. This is shown in (Delli Colli, 2005), where common-mode voltage and shaft voltage are measured with the VSI and the CSI. The common-mode voltage waveforms differ, but the shaft voltage amplitudes are similar. This suggests that EDM bearing currents are similar in both cases. On the other hand, the harmonic content (both frequency and amplitude) of the output voltage of the CSI is somewhat lower than in the VSI, which suggests that there might be less HF circulating bearing currents and rotor ground currents present.

As mentioned previously, all of these methods have their drawbacks. Further, many of the easy-to-install and relatively cheap solutions are effective only against certain type of bearing currents. A combination that can be thought to be effective against all kinds of bearing currents consists of one or preferably two insulated bearings, a shaft brush, and adequate high-frequency grounding at the motor. It should be taken care that the problem is not transferred to the bearings of a load machine, for example, with an insulated coupling between the motor and the load machine. This is an inexpensive solution, which should work against all types of bearing currents and which can be installed in existing systems. Another solution is to eliminate the source of the bearing currents. In (Akagi, 2006) it is shown with experiments that a passive common-mode filter with access to the DC link neutral point and motor star point can be

effectively used to eliminate all kinds of bearing currents. However, a solution of this kind can be very costly and the connections to the DC link neutral point and the motor star point are not necessarily available.

In addition to what has been discussed here, several other techniques have been proposed in the literature to mitigate bearing currents. Many of them require special drive hardware or a motor winding solution and cannot be applied to the existing drives, and are therefore not discussed here. A review of these techniques is given in (Mäki-Ontto, 2006). Table 1-2 provides a summary of the applicability of each mitigation technique to different types of bearing currents. The table is collected from publications where different mitigation techniques have been tested and/or proposed (Schiferl, 2004), (Busse, 1997), (Guttowski, 2006), (Dahl, 2008), (Muetze, 2003, 2006B, 2006C), (Jouanne, 1998), (Mäki-Ontto, 2003), (Link, 1999), (Delli Colli, 2005), (Akagi, 2006), and (Boyanton, 2002).

Table 1-2. Applicability of various mitigation techniques to different types of bearing currents.

Bearing current type / Mitigation technique	**EDM current**	**Circulating current**	**Rotor ground current**
Shaft grounding brush	Good (connection must be of low impedance)	Good (connection must be of low impedance)	Risk to make the problem even worse
Insulated bearings or ceramic rollers	Good. Requires that both bearings are well insulated	Good. One insulated bearing is enough	Good. Requires that both bearings are well insulated
Proper grounding and/or shielded cables between VFD and motor	Does not work	No significant influence. In worst case possibility to make the problem even worse	Good
Output filters	Requires filter that mitigates common mode voltage and not only du/dt	Good	Good
Insulated coupling at the shaft between the load motor and the load machine	Does not work. Might shift the problem from the bearings of the load to the bearings of the motor	Does not work	Good
Faraday shield between the stator and the rotor	Good	Does not work	Does not work
Carrier frequency reduction	May reduce the currents and give more lifetime to the bearings	May reduce the currents and give more lifetime to the bearings	May reduce the currents and give more lifetime to the bearings
Modulation technique to reduce the common-mode voltage	Good if the common-mode voltage can be mitigated	Good if the common-mode voltage can be mitigated	Good if the common-mode voltage can be mitigated
Conductive shielding in the stator slots	Does not work	Good	Proper grounding is required.
CSI instead of VSI	No difference	May be less harmful	May be less harmful

1.8 Motivation of the study

It is not well known how significant a problem bearing currents and especially inverter-induced bearing currents really are, because the results from different studies vary. One of the reasons is that in many of the studies on electric motor failures, no difference is made between frequency-converter-driven motors and motors that are not equipped with a frequency converter. The second reason is that bearing currents cannot be easily measured, and bearing-current-generated faults are often ascribed to a wrong origin. Based on Section 1.3, we can roughly estimate that 50% to 90 % of the electric motor failures are caused by bearing faults; in these, the proportion of bearing-current-generated faults can be anything from 10% upwards. If there were a relatively simple-to-use and reliable method to detect bearing currents, the figures could be more accurate.

As discussed in Section 1.5, all of the commonly used methods to measure or detect bearing currents are problematic in some respect and/or have their limitations. Most importantly, none of the methods reliably indicates whether there is sparking inside the bearings or not. Current measurement is the best indicator, but as mentioned above, there can be bearing currents without sparking. It was stated in Section 1.4 that the root reason for a bearing damage caused by EDM bearing currents is small micro craters that are generated when a bearing current discharges through the lubrication film and melts the surface of the bearing ring. When it comes to the other type of bearing currents, it is not well known whether they sometimes cause sparking in the bearings or not.

These are the reasons that lead to a need for another measurement method to detect bearing currents, and more precisely, only those bearing currents that cause electrical discharges in the bearing. Preferably, this method should be easy to apply in different situations, and it should not require any changes to the electric motor. Moreover, industry is going towards condition-based maintenance through condition monitoring. To this end, it is possible to detect a damaged bearing with vibration analysis and change it before it fails as discussed in Section 1.6. However, it would be even better if it were possible to take action even earlier provided it is known that there are bearing currents present in the system. As discussed in Section 1.7, there are suitable mitigation techniques available for the purpose. However, it is important to assess whether these actions have been effective or not. The measurement method studied in this thesis provides a tool that can be used to approach these issues.

1.9 Objectives of the study

The objective of this doctoral thesis is to show that it is possible to detect the sparking inside the bearing from outside the motor by measuring RF (radio frequency) emission that is generated by this sparking. This way, it is possible to detect those bearing currents that discharge through the lubricant film melting the bearing races. The method is based on detecting the high-frequency emission resulting from an electric discharge (sparking) in a bearing.

It is important to have a good understanding of the complete chain of effects associated with a measurement technique and the parameters related to it. This is also true if the RF method is to be applied to bearing current detection. First of all, knowledge of the sparking inside a bearing is required. For example, the magnitude and spectrum of a discharge have to be known or at least estimated. Secondly, it is necessary to know how the electric motor behaves as an antenna to determine whether the emission can radiate outside the motor. Additional knowledge of the effects of the environment and interference present is required to know how the signal changes on its way from the motor to the receiving antenna. For example, a frequency converter is a

source of relatively high-frequency and strong RF interference that can easily overlap the signal from the discharge in the bearing. It is also important to know what kind of information can be obtained from the discharge pulse with the RF method. Finally, the requirements and limits for this method need to be known.

As far as the author knows, there are no publications available where a similar RF bearing current detection method as the one presented in this thesis has been studied to this extent. There are some related studies, for example (Prashad, 1999), where the magnetic flux density is measured from the outer and inner ring of a bearing with a hall probe to determine the current passing through the bearing. A similar study is presented in (Cech, 2007), where the magnetic field around a bearing was measured with different probes. It is not mentioned how the shaft voltage was generated, or how far from the bearing the measurement was conducted. It is nevertheless mentioned in the paper that the measured frequencies were between 1 and 2 MHz, which leads to a conclusion that the magnetic field in the close proximity of the bearing was measured.

A major bearing manufacturer has recently published an apparatus (SKF, 2008) to detect bearing currents applying similar techniques as studied in this thesis. The author of this thesis has no experience with this device, but according to the information given it is based on measuring the magnetic field induced by the discharge current in the close proximity (max. 30 cm) of the bearing. There are numerous patents related to discharge detection at a general level and one that is more closely related to this subject (SKF, 2007). Detecting high-frequency emission from sparking has been previously used in partial discharge detection. Such RF partial discharge detection has been applied, for example, to transformers and generators and is discussed in more detail in Section 3.1.

None of the above-mentioned studies discusses detection of inverter-induced bearing currents by measuring the discharge emission also in the far field as it is done in this thesis. It is somewhat unclear whether all the measurements are actually taken in the far field, because there is no definite border between the far field and the near field. However, it can be said that the measurements are taken much further away than in the close proximity of the bearing. The method was found to be working as far as three meters away, which was the maximum distance tested because of space limitations. Most of the measurements presented in this thesis are taken at a distance of one meter from an electric motor. The reason for this is further discussed in Section 4.1. The RF method presented in this thesis and parts of the results have been previously published by the author in (Särkimäki, 2008).

1.10 Scientific contributions of the thesis

The main scientific contributions of this thesis include the following:

1. A method is presented for detecting bearing currents in an induction motor. The method is based on measuring radio frequency emission caused by sparking in a bearing of the motor.

2. It is theoretically shown how an electric motor can work as a “spark gap” transmitter. These include, for example, an analysis of the transmitted RF signal and its spectrum. The feasibility of the theoretical approach is verified by measurements. The operation of an electric motor as an antenna is shown by measurements.

3. A series of measurements is presented to show that the RF method can be used to detect bearing currents from the motor with an antenna and an oscilloscope. A modified motor is used, that allows bearing currents to be measured from the bearings of the motor with current transducer. The applicability of the method is verified also with an unmodified motor.

4. A special test bench was developed that allows shaft voltage variation, bearing current measurement, and motor operation with or without a frequency converter.

5. It is analyzed experimentally how different parameters, such as the shaft voltage affect the discharge emission. Potential application areas of the RF method are also analyzed; for example, whether it is possible to predict the bearing current magnitude or the magnitude of the shaft voltage by measuring the emission from the discharge.

6. A frequency converter is identified as a source of an impulsive interference transmitter that has a high impact on the applicability of the RF method presented. For this reason, different techniques are studied and proposed to mitigate the inverter-generated interference and make detection of discharges possible.

7. Techniques for the localization of RF emission sources are studied and their applicability is discussed. One method is chosen and verified with measurements. The purpose of this is to be able to accurately pinpoint the source of discharges and thereby the motor in which bearing currents are suspected.

1.11 Outline of the thesis

This doctoral dissertation studies a method for detecting bearing currents, or more specifically, a method for detecting electrical discharges in the bearings of an electric motor. Bearing currents are related to discharges in such a way that an individual discharge is a cause for a bearing current flow through the bearing. The detection method is based on the fact that a discharge generates a high-frequency current pulse. Part of this current pulse can radiate as an electromagnetic wave, which is then captured and measured with an antenna and an oscilloscope. It is shown theoretically and verified with measurements that this kind of a method can be used to detect electric discharges (sparking) in the bearings of an electric motor.

The contents of this thesis are divided into the following five chapters.

Chapter 1 gives general information about bearing currents. It is claimed that bearing currents can be considered to be the single largest reason for shortening the lifetime of an induction motor when a frequency converter is used. Different kinds of bearing currents are presented and possible mitigation techniques discussed. Problems with measuring the bearing currents are also discussed. Finally, the chapter provides the background and motivation for the thesis and presents its scientific contributions.

Chapter 2 introduces the theory of the RF method. An electric motor is considered to work similarly to a spark gap transmitter. Based on this assumption, several parameters related to this effect are studied. These are for example the approximation of the energy released and radiated during a discharge, the spectrum of the discharge, and the motor parameters, if the motor is considered to operate as an antenna.

Chapter 3 discusses the occurrence of interference and techniques that can be used to accurately detect the emission signal from the discharge. Propagation of radio waves is discussed in brief, because it has a major impact on the RF method developed. The interference that is due to inverter switching is discussed and measured. It is shown that additional signal processing is required to be able to detect discharge pulses when a frequency converter is used. These techniques are presented and experimentally verified. Design suggestions for a real-time bearing current (sparking) detector are also given.

Chapter 4 presents a series of different measurements. The objective of these measurements is to show that the RF method can be used as theoretically developed in Chapter 2. The applicability of the RF method is verified with a series of measurements and a special test bench. These measurements are: measurements with an adjustable voltage source, measurements with a frequency converter, and antenna analysis of the test motor with a network analyzer.

Chapter 5 concludes the study presented in this thesis. Here, the advantages and limitations of the RF method are discussed and suggestions for future work are given.

2 ELECTRIC DISCHARGES IN THE BEARINGS OF AN ELECTRIC MOTOR

In this chapter, bearing sparking and especially RF emission emitted from an electric discharge inside the bearings of an electric motor are discussed. Electric discharges occur between the inner ring of a bearing and the rolling element and between the outer ring of a bearing and the rolling element. The question is whether it is possible to detect a discharge event by measuring high-frequency emission from the discharge. This way, EDM bearing currents can be detected, because they are linked to discharges.

To study this phenomenon, an electric motor is considered to work like a spark gap transmitter. Based on the assumption that an electric motor is similar to a radio transmitter, several parameters are then analyzed. For simplicity, only the EDM bearing currents are considered in this study. The results should be applicable to both rotor ground currents and circulating bearing currents, if they cause sparking in a bearing. From now on, when discussing the discharges inside a bearing, it is assumed that these discharges always generate sparking in the bearing and hence RF emission as it will be shown later in this chapter.

The key topics in this chapter are: The energy charged in parasitic capacitances, which is released during a discharge, is approximated. It is important to know whether this energy is enough to cause damage in a bearing and generate measurable RF emission. It is shown that the discharge generates high-frequency RF emission that has enough energy to radiate outside an electric motor and also generate micro-cratering as was discussed previously in Section 1.4. The frame, the bearing, and the rotor of an electric motor together comprise a transmitting antenna that determines how the emission spreads into the environment. It is verified with different sizes of LV (low-voltage) motors that such motors work as antennas.

2.1 Introduction to a spark gap transmitter

A spark gap transmitter was the first radio transmitter introduced, and it started the era of radio. As early as in 1888, Heinrich Hertz used a spark gap transmitter to transmit “information” utilizing electromagnetic waves (IEEE, 2008). He used a microscope to verify that small sparks appeared between the electrodes of the receiver when the transmitter was powered. There are various constructions of the spark gap transmitter; one of the simplest of which is illustrated in Fig. 2-1. It consists of a power source, an energy storage, a spark gap, and an oscillatory circuitry with an antenna. The construction works as follows: The voltage source charges the capacitor C_1 until it discharges through the spark gap. The energy released oscillates in the oscillatory circuitry formed by the capacitor C_2 and the inductor L_1 and generates a decaying pulse that radiates from the antenna as an electromagnetic wave.

Spark gap transmitters are no longer used, because they generate very wideband transmission that wastes the limited bandwidth. In the beginning of the 20th century, it was also difficult to modulate analog signal such as speech to the spark gap transmission. For these reasons, transmission utilizing continuous carrier wave became popular. Recently, UWB (ultra wide band) data transmission has gained popularity, and this has similarities to spark gap transmission. As in spark gap transmission, also in UWB short impulses are transmitted instead of using a continuous carrier wave. However, UWB is nowadays used at far higher frequencies than at which spark gap transmission was used. Also, the transmission power is typically in the order of milliwatts in the UWB, while in the spark gap transmission it reached kilowatts.

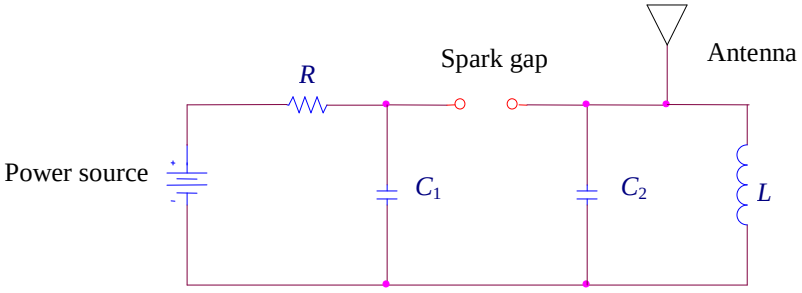

Fig. 2-1. Schematic of a simple spark gap transmitter. It consists of a power source, an energy storage, a spark gap, and an oscillatory circuitry with an antenna.

2.2 Electric motor as a spark gap transmitter

The discharge in a bearing caused by bearing currents can be thought to be similar to the spark occurring in a spark gap transmitter. Fig. 2-2 shows a model of an electric motor, illustrating the motor as a spark gap transmitter.

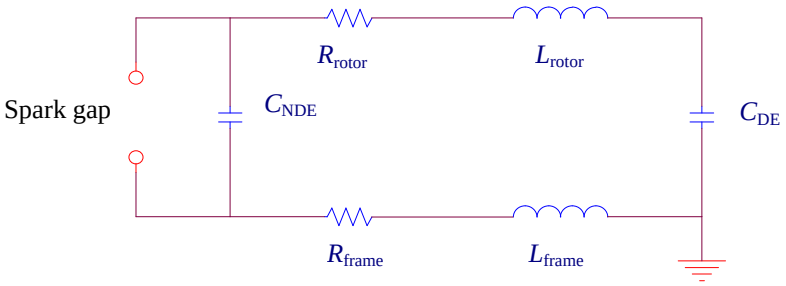

Fig. 2-2. Schematic of an electric motor modeled as a spark gap transmitter (compare with Fig. 2-1). The capacitances C_{NDE} and C_{DE} are the bearing capacitances including other relevant parasitic capacitances and form the main energy storage. The voltage source is not included, because it is the shaft voltage that is determined by the common-mode voltage and BVR. Moreover, the antenna structure is not as clear as in the case of a typical radio transmitter, and therefore it is not included in the model.

The voltage source is not included in the model, because the voltage is generated as a result of the common-mode voltage at the motor terminals and motor parasitic capacitances. In the model, the capacitances C_{NDE} and C_{DE} are the capacitances that are charged because of the common-mode voltage. These represent the capacitances exhibited by the bearings of a typical electric motor, and they can be considered to form the main energy storage. In these capacitances are also included the parasitic capacitances C_{sr} and C_{wr}[3], which were introduced previously in Section 1.3. The C_{ws} is important with circular currents, but is not included, because only EDM currents are considered here. These capacitances are now considered together as an energy storage that discharges during the breakdown. These are discussed below in more detail. It is important to bear in mind that the capacitances C_{sr} and C_{wr} have an important role when analyzing shaft voltage charging. A detailed discussion of the origin of the EDM bearing current, the shaft voltage, and bearing capacitance charging has been given in Section 1.3.2.

The voltage at the shaft of an electric motor is mirrored from the common-mode voltage at the motor terminal, and for this reason it is constant only for short periods of time (Busse, 1997B). It was stated that the shaft voltage can be approximated with Eq. (1-3). If the voltage rises above the breakdown voltage level of the lubricant film, it discharges through a spark gap to the ground. The spark gap is formed between the bearing rings and the rollers of a bearing at the moment of discharge. It should be emphasized that the threshold level when the spark gap closes is not constant because of the rolling of the bearing. The lubrication thickness changes constantly, and the bearing races have a surface roughness that can cause a discharge at a notably lower voltage than the expected lubrication breakdown voltage in a steady case.

At the exact instant when the spark gap closes, the charge in the bearing capacitances and parasitic capacitances discharges to the frame and to the ground through the spark gap. The discharge can take place in either one of the motor bearings. In Fig. 2-2 it is assumed that the discharge takes place in the bearing at the NDE (Non Drive End) of the motor. It is assumed that there are some resistances (R_{rotor} and R_{frame}) and inductances (L_{rotor} and L_{frame}) resulting from the rotor and frame material and geometry. These together with the capacitances C_{NDE} and C_{DE} form the oscillating circuitry similar to the spark gap transmitter illustrated in Fig. 2-1.

Differing from the spark gap transmitter schematic presented in Fig. 2-1, no antenna is included in the motor model in Fig. 2-2. The reason is that there is no clear antenna construction in a normal electric motor. The bearing is located inside a metal frame, and at first thought, it seems impossible that there is any radiation leaking outside from this metal structure when the sparking occurs in the bearing. However, this is not a correct conclusion, because it can be

[3] According to (Muetze, 2007B), the bearing capacitance C_b is about the same size as C_{wr}, which in turn is approximately 1/10–1/20 of the C_{sr}.

assumed that the whole frame of the motor works as an antenna. The reason for this is that whenever there are accelerating charges, there is a changing electromagnetic field, which in turn generates radiating electromagnetic waves. It should also be borne in mind that at the moment of the discharge, the charge at the shaft discharges through the bearing to the frame and eventually to the ground. So there are accelerating charges in the shaft, the bearing, and the frame, and all of these are radiating. This is discussed in more detail in Section 2.5.

2.3 Energy released during a discharge inside a bearing

It is important to know whether there is enough energy released during the discharge to damage the bearing and also to generate RF radiation that can be detected. The first issue has been studied for example in (Prashad, 2001) and (Jagenbrein, 2005). For the bearing current detection method presented here, the RF radiation aspect is more interesting, because the applicability of the RF detection method depends significantly on it. In the following analysis, this problem is studied in three parts: the bearing capacitance and other relevant parasitic capacitances as the energy storage in Section 2.3.1, the shaft voltage due to the common-mode voltage in Section 2.3.2, and the radiated power that is dependent on the energy storage and discharge time period in Sections 2.3.3 and 2.3.4. These in turn will be considered in the following subsections.

2.3.1 Bearing and parasitic capacitances of an electric motor

As previously described, the focus is on EDM bearing currents. In this type of bearing current, the shaft voltage is charged by the common-mode voltage because of the capacitive voltage divider. To approximate the energy released during the discharge, the capacitances where energy is charged need to be known. First, the bearing capacitance is considered. A few different equations can be found in the literature to calculate the bearing capacitance of an electric motor: In (Hayt, 1989), the first model for bearing capacitance is given; see Eq. (2-1). In the equation, N_b is the number of rollers, ε_r is the relative permittivity of lubrication, r_b is the radius of one roller, and d_r is the radial play of the bearing. This is a very simple model, which assumes that the capacitance is formed between two spheres having radii of r_b and r_b+d_r. The inner sphere is the roller, and the outer sphere is determined by the bearing rings around the roller. The total bearing capacitance is N_b times the capacitance of one roller.

$$C_b = \frac{N_b 4\pi\varepsilon_0\varepsilon_r}{\left(\frac{1}{r_b} - \frac{1}{r_b + d_r}\right)} \qquad (2\text{-}1)$$

Another model for the bearing capacitance is introduced in (Muetze, 2007B). In this model, it is approximated that the bearing capacitance is mainly determined by the load-carrying zone of the bearing. Therefore the Hertzian contact area A_H is taken as the area of the capacitor plates. The thickness of the lubrication film d_c depends for example on the rotating speed and the loading of the bearing. According to (Busse, 1997B), the thickness of the lubrication film can be considered to be between 0.2 and 2.0 µm. It is also assumed that the capacitances between the outer ring and the rolling element and between the inner ring and the rolling element are the same. Because of the series connection of these capacitances, the capacitance for one bearing can be calculated as expressed in Eq. (2-2).

$$C_{\mathrm{b}} = 0.5\frac{\varepsilon_0 \varepsilon_{\mathrm{r}} A_{\mathrm{H}}}{d_{\mathrm{c}}} \tag{2-2}$$

To calculate the bearing capacitances, the dimensions of the bearing are required. In this analysis, the bearing type was chosen to be the same as the one used in the test motor (detailed information of the test motor is given in Section 4.1 and Appendix I). The type of the bearing is 6209. Figure 2-3 illustrates the bearing, and its dimensions are given in Table 2-1. The bearing capacitance is calculated with the lubrication thicknesses of 0.2–2 μm, the relative permittivity of the lubricant being 2.2. The radial play for the Eq. (2-1) is calculated according to (Muetze, 2007B), which states that the thickness of the lubrication film is approximately an order of magnitude smaller than the radial bearing play of a bearing. The results are plotted in Fig. 2-4. The bearing capacitance is calculated with Eq. (2-1), indicated with the solid line, and with Eq. (2-2), illustrated with the dashed line. The bearing capacitances in the motor are connected in parallel as can be seen in Fig. 2-2. For this reason, the total bearing capacitance is two times the calculated capacitance of one bearing, which has to be taken into account. In reality, there is some inductance between these capacitances as is shown in Fig. 2-2. This has not been taken into account in the following calculations, but in reality it limits the current pulse at the discharge event.

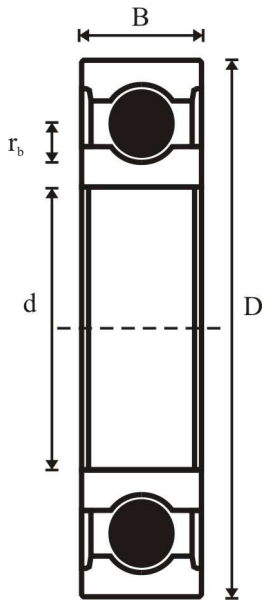

Fig. 2-3. Illustration of the bearing.

Table 2-1. Dimensions and parameters for the bearing used in the test motor.

Bearing type	6209
D	85 mm
d	45 mm
B	19 mm
r_b	6.5 mm
N_b	9 kpl
d_r	~15 μm

Fig. 2-4 shows that the bearing capacitances calculated with Eq. (2-1) are similar to the results obtained with Eq. (2-2). Studying these relatively simple models for the bearing capacitance, it seems that Eq. (2-1) exaggerates the area of the capacitor plates by modeling them around the

bearing rollers, while Eq. (2-2) underestimates the capacitance by only taking into account the Hertzian contact area as the area of the capacitor plates. Studying the structure of a typical ball bearing, it can be assumed that the first one gives too large and the latter two small values for the bearing capacitance. For these reasons, it is assumed here that the "real" bearing capacitance is somewhere between the calculated values. It is important to remember that there can be no exact value for the bearing capacitance, because it is not a constant value but varies with the operating conditions. However, an approximation of the magnitude as carried out here is sufficient for the following study.

The bearing manufacturer has given a value of ~15 µm for the radial bearing clearance for the bearing type used in the experiments. Thus, the lubrication film thickness can be approximated to be ~1.5 µm for the bearings used in the test motor. This result in a bearing capacitance of ~127 pF calculated with Eq. (2-1) and ~26 pF calculated with Eq. (2-2). Taking into account what is measured and calculated for bearing capacitances in the references (Busse, 1997C) and (Muetze, 2007B) for somewhat similar size motors as the one used in this study, it is likely that the calculated bearing capacitance is in the right range.

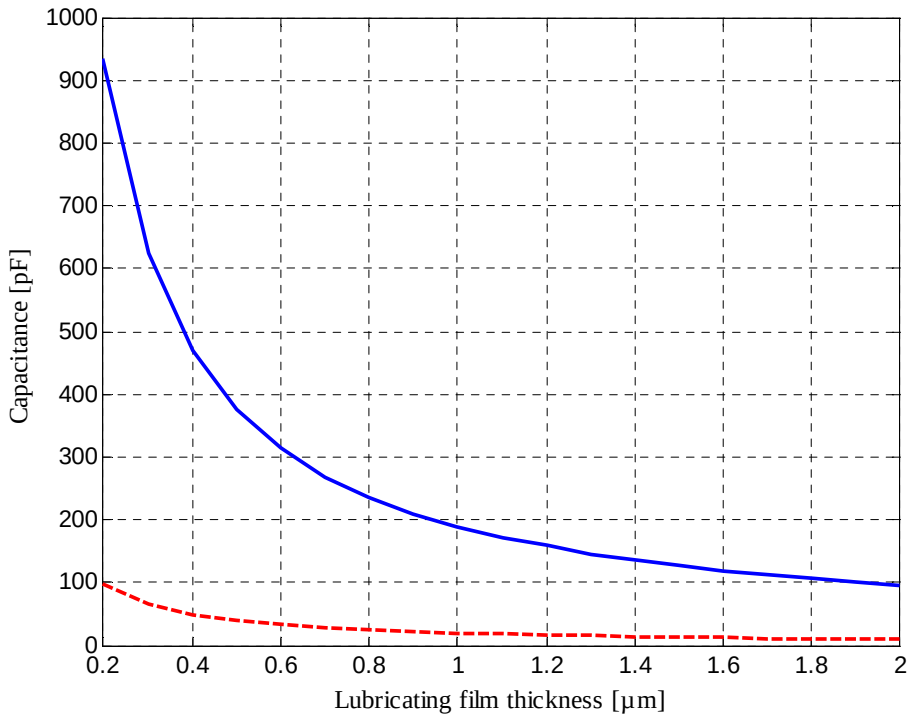

Fig. 2-4. Calculated bearing capacitances of a 15 kW test motor as a function of lubrication film thickness for both bearings. The capacitances are calculated with Eq. (2-1), indicated with a solid line, and Eq. (2-2), indicated with a dashed line. The bearing capacitance was calculated for the type 6209 bearing.

It was illustrated in the model given in Fig. 2-2 that the bearing capacitance is the main energy storage. However, according to (Muetze, 2007B) the bearing capacitance C_b is of about the same size as C_{wr}, which in turn is approximately 1/10–1/20 of C_{sr}. This would lead to the conclusion that the total energy storage owing to the parasitic capacitances is in the order of

nanofarads. For the following study, it is assumed that the capacitance storing the energy, still referred to as bearing capacitance, C_b is in the range of 1–10 nF, which is in good agreement with the calculated values and the values found in the literature. It should be remembered that even though energy is stored in different parasitic capacitances, all of it does not discharge instantaneously because there are inductances along the current paths.

The capacitance between the shaft and the frame of the test motor was also measured. Reliable measurement is difficult, because the capacitance varies constantly because of the rotation of the test motor and also because of temperature variation. The reasons are the asymmetries of the air gap and changing bearing parameters, such as lubrication thickness. A value of ~5 nF was measured for this capacitance. In this study, the capacitances of motors of other sizes were not measured or calculated. Some capacitance values for LV motors of different sizes can be found, for example, in (Muetze, 2007B). According to the values given in this reference, it can be assumed that the estimated energy storage of 1–10 nF can be used to estimate the energy stored and released during the discharge also in larger LV machines (FS160 and bigger).

2.3.2 Shaft voltage caused by common-mode voltage

Now that the energy storing capacitance is known, the maximum shaft voltage is investigated so that the energy stored in the capacitances can be estimated. It should be emphasized that the maximum shaft voltage is not necessarily limited by the breakdown voltage of the lubricant film. The reason for this is that the shaft voltage is mirrored from the common-mode voltage, and it may be less than the assumed breakdown voltage. In other words, the maximum shaft voltage is not necessarily limited by the breakdown voltage of the lubricant, but by the common-mode voltage and the BVR. For example, in the case of the test motor, it was noted with an adjustable voltage source that constant breakdowns took place when the shaft voltage exceeded 30 V (see Section 4.3). When the test motor was driven with a frequency converter, the shaft voltage did not reach anywhere close to this level. However, it should be remembered that far lower shaft voltages than 30 V can cause discharges too, because there are moments when the lubrication thickness is smaller at some points in the bearing races, and the threshold level of the lubricant is exceeded at these points. It was mentioned in Section 1.4 that shaft voltages exceeding 1 V can cause discharging bearing currents.

The shaft voltage is mirrored from the common-mode voltage at the motor terminals because of the parasitic capacitances that form the capacitive voltage divider as previously discussed in Section 1.3.2. If the common-mode voltage is known, the shaft voltage can be approximated with the BVR discussed in (Busse, 1997B). The equation to calculate the shaft voltage from the common-mode voltage has been given in Eq. (1-3). To calculate the BVR, the values of C_{sr} and C_{wr} are required in addition to the already known C_b. These can be either measured or calculated. A method to calculate an approximation of these capacitances is given in (Muetze, 2007B). These capacitances and the BVR are not calculated in this study, because more accurate results can be attained with directly measuring both the common-mode voltage and the shaft voltage of the test motor.

The shaft voltage can be measured with a brush connection as discussed in Section 1.5. The common-mode voltage was measured simultaneously with the shaft voltage from the terminals of the test motor. The motor windings were delta connected, and an artificial star point was formed with resistors for the common-mode voltage measurement. The common-mode voltage between this star point and the grounding connection was then measured. A short sample of the result is shown in Fig. 2-5. There are no discharges in the bearings of the test motor during this sample. It can be observed that the shaft voltage closely follows the common-mode voltage

multiplied by the BVR. The maximum shaft voltage magnitude of the test motor was found to be approximately 7 V when driven with a frequency converter at the nominal speed.

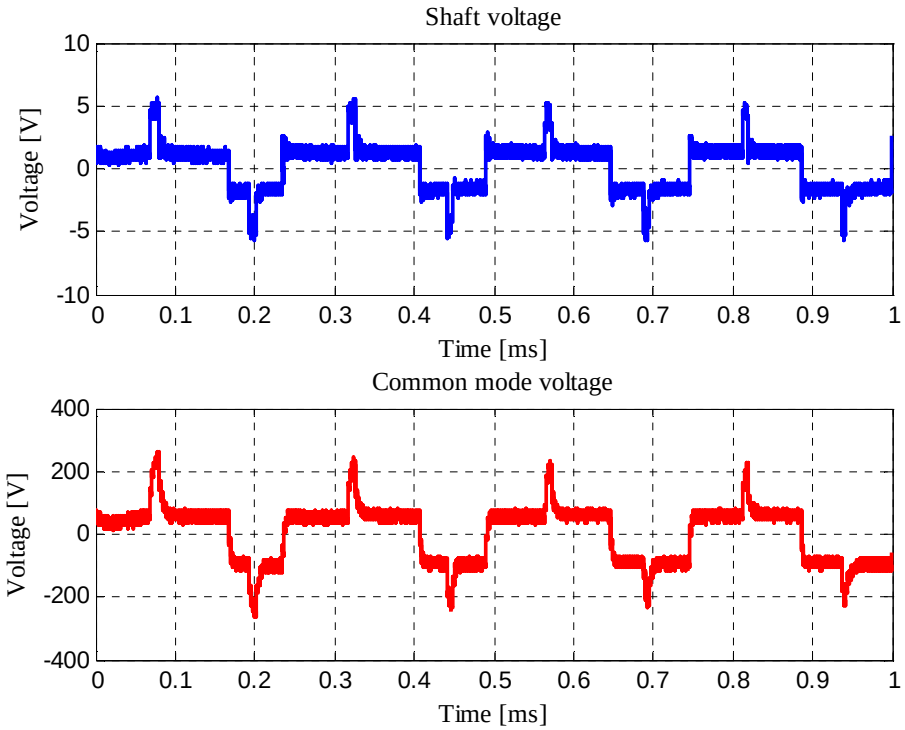

Fig. 2-5. Measured shaft voltage and common-mode voltage of the test motor. It can be observed how the shaft voltage is directly mirrored from the common-mode voltage. There are no discharges in the bearings during this sample.

The breakdown voltage of lubrication oil is 1–30 kV/mm (Busse, 1997B). If the oil film thickness varies between 0.2 and 2.0 µm, as previously mentioned, this means that shaft voltages of 0.2–60 V may cause discharges in the bearings. The authors of (Busse, 1997B) suggest that the breakdown voltage of 15 V/µm is well in line with the measurements they conducted. Based on this, shaft voltages of 3–30 V may cause discharges. This suggests that there can be bearing currents present in the test machine, because the shaft voltage exceeds the breakdown voltage. This was also verified with measurements; it was noticed that the shaft voltage of approximately 1.5–2 V was enough to occasionally cause a discharge through the bearings of the test motor.

Using the results presented in Fig. 2-5, the BVR of the test motor is calculated to ~2%. This means that the mirrored shaft voltage is two percent of the common-mode voltage measured at the motor terminals. According to (Muetze, 2007B), the BVR is typically in the range of 3–10%, as was mentioned previously in Section 1.3.2. This means that the shaft voltages present in the test machine when driven with a frequency converter represent the “best” case scenario. With different motors, higher shaft voltages can be expected. The test motor is also an LV (low-voltage) motor, and it can be assumed that with MV (medium-voltage) motors and HV (high-voltage) motors the shaft voltages encountered are far higher. Thus, if the following analysis

and the measurements presented in Chapter 4 indicate that it is possible to use the suggested RF method to detect bearing currents in the test machine used, then it can be assumed that the method works also with larger machines, where the shaft voltages and energies released are expected to be higher.

2.3.3 Energy stored in the bearing and parasitic capacitances

Now that the shaft voltage and the energy storing parasitic capacitances are known for the test motor, the energy stored in the capacitances can be calculated. As previously mentioned, the bearing capacitance is now assumed to contain all the energy as illustrated in Fig. 2-2. It should be remembered that the other parasitic capacitances are also included in the new "equivalent" bearing capacitance and are also part of the energy storage.

The energy in the capacitances can be calculated with Eq. (2-3), when the bearing capacitance C_b and the shaft voltage U_b are known. The energy charged in both bearing capacitances can reach values from 24.5 nJ up to 245 nJ when the shaft voltage is 7 V and the capacitance values are between 1-10 nF as previously assumed.

$$E_b = \frac{1}{2} C_b U_b^{\,2} \tag{2-3}$$

Even the maximum energy of 245 nJ can be considered quite small, which may lead to the conclusion that this is not enough to generate any damage to the bearing. This is however not true for the following reason: The energy is released in a very short time (a few nanoseconds) into a very small volume (the volume of micro craters is in the order of μm^3). A rough estimation can be made to analyze whether the energy released is high enough to melt a small crater in the bearing ring. First, it is assumed that the energy released during the discharge is concentrated on a small volume, and the discharge event is fast enough so that there is no significant heat conduction in the metal. In other words, all the energy goes into heating and melting of the metal. The mass that can be melted with the energy available can be calculated with Eq. (2-4). If the bearing material is assumed to be pure iron, then the specific heat capacity C is 0.45 KJ/(kg^{o}C), the heat of fusion S is 276 KJ/kg, and the temperature rise ΔT required to heat the iron is approximately 1500 degrees if it is approximated that the bearing temperature is 40 ^{o}C.

$$m = \frac{E_b}{\Delta TC + S} \tag{2-4}$$

With the energy E_b released during the discharge set to 245 nJ, which corresponds to the approximated bearing capacitance value of 10 nF and the shaft voltage of 7 V, the mass that is melted with this energy is estimated to be 0.258 ng. The density of iron being $7.87*10^3$ kg/m^3, the crater generated by a discharge is approximately 33 μm^3. This corresponds roughly to a crater having dimensions of 3.2*3.2*3.2 µm. The size of the calculated crater is somewhat larger than the size of the micro craters detected in the bearings. For example, in (Muetze, 2006) it is mentioned that the average crater size caused by EDM bearing currents is approximately 0.5 µm in diameter. However, in (Chmelik, 2007) it is stated that bearing-current-generated craters can be even an order of magnitude larger than this. The calculated

approximation is somewhere between, but it should be noted that it was now assumed that all the energy is released instantly in a very small area. In reality it is probable that the energy release is somewhat slower and some of the energy is just heating the bearing without melting it. It is also assumed that at least part of the energy radiates as electromagnetic waves. The radiated energy is probably only a fraction of the total energy. This is the interesting part when considering the applicability of the RF method presented in this thesis. As is the case in any of the transmitter/receiver pairs, the signal to noise ratio has to be large enough so that the transmitted signal can be correctly detected.

2.3.4 Radiated power from a discharge

It is of interest whether there is enough energy to radiate outside the motor so that it is possible to detect the radiation from the far field. It is assumed that not all the energy released by the discharge goes into melting of the bearing material, but some of it also radiates into the environment. It is however impossible to accurately predict the ratio of radiating energy. A rough approximation is made that only one-thousandth of all energy radiates. The discharge is approximated to last tens of nanoseconds at maximum, the rise time of a current pulse being nanoseconds (Kempski, 2001). Using this information, the radiated power as a function of discharge duration can be plotted. The radiated power is calculated and illustrated in Fig. 2-6 with pulse duration of 5–20 ns. The average power ranges between 12 and 49 mW, when the radiated energy is 0.245 nJ (this corresponds to 1/1000 of 245 nJ). The radiated power is in the same range as transmission power used in short-range radio devices such as ZigBee and Bluetooth.

To calculate the received power, the Friis equation, given in Eq. (2-5) can be used. In the equation P_r is the received power, P_t is the transmitted power and G_t and G_r are the gains of the transmission and receiving antenna with respect to isotropic antenna.

$$P_r = P_t G_t G_r \left(\frac{\lambda}{4\pi r} \right)^2 \tag{2-5}$$

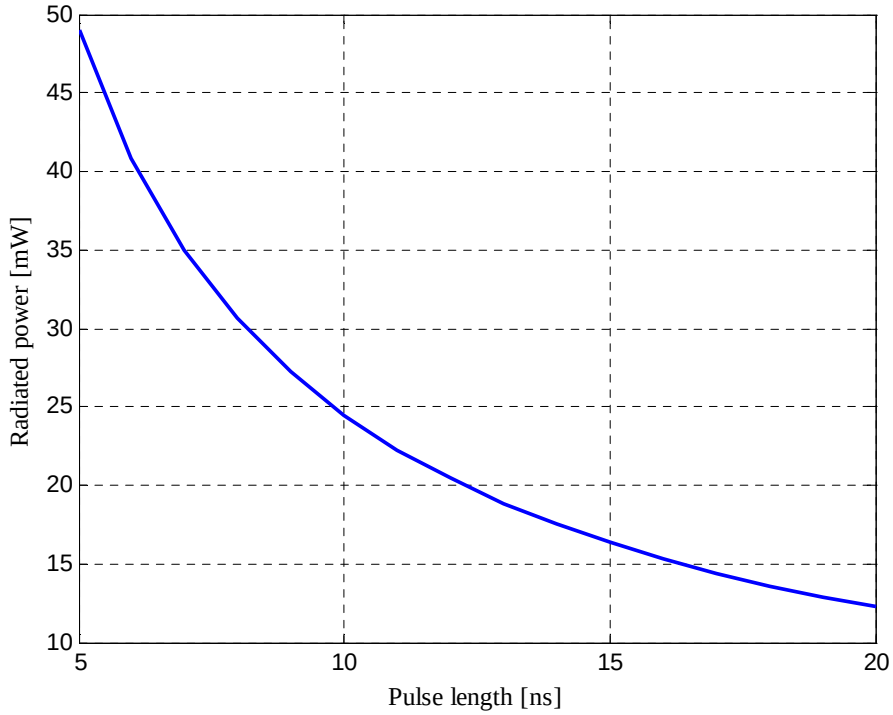

Fig. 2-6. Radiated power as a function of discharge pulse duration. According to the previous measurements, the total energy released during the discharge is estimated to be 245 nJ, but only very small amount of this energy radiates and the rest goes for heating the bearing.

In general, this equation is applicable only in free space, but can be used to approximate received power levels in indoors, where the transmission distance is short and there are no objects between the transmitter and the receiver. When predicting the received power with this equation, an issue arises: It has not been studied how an electric motor works as an antenna. This is discussed later in Section 2.5, but in this calculation, an electric motor is considered to have a gain G_t of 1.5. This corresponds to the gain of a dipole antenna, when the antenna length is short compared with the wavelength. The radiation pattern of this kind of a dipole antenna is close to omnidirectional. It is assumed that the receiving antenna is a similar log periodic antenna as the one used in the measurements in Chapter 4. The log periodic antenna has a gain G_r of 2–3 at a bandwidth of 200-400 MHz. It was discussed above that the discharge is short, hence generating wide bandwidth interference. For this study, the wavelength λ is chosen to be 1 m, which corresponds to 300 MHz. It is later shown that the spectrum of the emission ranges at least from 100 MHz to 400 MHz. The transmitted power attenuates faster with higher frequencies, so it is possible to achieve higher power levels of the measured signal if the emission is measured also at lower frequencies. For these calculations, the distance from the transmitter (the motor) to the receiving antenna was set to 1 meter, which is also used throughout the tests in Chapter 4. The received power was calculated to be in the range of P_r = 230–900 µW, with the transmitted power of P_t = 12–49 mW, respectively. As an example, if the distance is three meters, the received power drops to 25–100 µW.

Estimations given in this chapter, although being rough approximations, indicate that it is possible to detect emission from the discharge even one meter away from the motor. If these estimated values are compared with the ones obtained with the measurements, they are reasonably well in line: It is later shown in Chapter 4 that the signals measured have amplitudes of approximately 10–50 mV. The input impedance of the oscilloscope is 50 Ω. Hence, the received power is between 2–50 µW, which is somewhat less than the estimated values. However, as previously mentioned, it is not possible to predict what amount of the total energy radiates as electromagnetic waves, and the calculations were made assuming that the signal is transmitted with a fixed frequency of 300 MHz, whereas in reality the signal is broadband.

In general, the signal to noise ratio has to be high enough so that the signal can be detected. A specific value cannot be given, because it depends on the receiver sensitivity. It is later shown in this thesis that it is possible to detect the discharge emission signal with an oscilloscope. Furthermore, it is necessary that the signal can be detected despite other interference from the surroundings. The detection of the signal under interference is discussed in Chapter 3.

2.4 Spectrum of a discharge

It is well known that sparking generates high-frequency RF emission. This is known from experiments with spark gap transmitters. The frequency spectrum of discharge is analyzed in publications where partial discharge detection is studied. For instance, according to (Moore, 2005), the initial rise time of the current waveform produced by a partial discharge is high enough to generate interference that reaches high to radio frequency spectra yet remaining mostly below 1 GHz. Partial discharge detection is discussed in more detail in Section 3.1. In this section, the spectrum of a discharge pulse is analyzed. There are factors that affect the spectrum of the measured signal, most importantly the transmitter and receiving antenna parameters. It is worth recalling here that the transmitting antenna is now basically the whole frame of the motor, the bearing, and presumably also the shaft. This will be discussed in the next section, whereas in this section only the actual discharge pulse and the spectrum it generates are analyzed.

For several reasons, it is important to know the spectrum of the discharge pulse. The frequency band at which the emission from the discharge can be found has to be known so that it can be properly detected and measured. Interference is another issue, having a great impact on the measurements. There are various transmissions in different frequency bandwidths. If the discharge spectrum is known, it is possible to choose a bandwidth with less interference to facilitate the detection of the discharges. Interference is discussed in more detail in Section 3.3.

A discharge current pulse can be modeled in different ways. In (Boggs, 1982), a partial discharge current pulse is modeled as a Gauss function. This is presented in Eq. (2-6), where i_b is the amplitude of the current, and the pulse width at half of the maximum value is equal to 2.36σ. According to the measurements with the test motor, a value of ~2 ns at half maximum is close to the measured values. This corresponds to a value of σ = 0.9 ns. It is assumed that the discharge pulse is very similar to a partial discharge pulse, and thus the given model is used to approximate the spectrum of the radiated emission caused by the discharge in the bearings of an electric motor.

In (Sellars, 1995), the previous model is extended to include a dipole antenna. By modeling the transmitter antenna as a short dipole antenna, we can express the spectral content of a current pulse as given in Eq. (2-7), where l is the length of the dipole antenna and c is the speed of light ($\sim 3*10^8$ m/s). Fig. 2-7 illustrates the discharge current pulse in the time domain and the

estimated spectral content of the emission from the pulse when it is transmitted through the antenna. These are calculated with Eqs. (2-6) and (2-7). In an ideal case the antenna length has no effect on the spectral content, but only on the amplitude. The current pulse and power spectrum are normalized. As it can be seen, if the pulse is short (lasting only a few nanoseconds) and has a fast rise time, the spectral content can reach up to hundreds of megahertz. The peak power is around 200 MHz.

$$i(t) = i_{\mathrm{b}} \exp\left(-\frac{t^2}{2\sigma^2}\right) \tag{2-6}$$

$$P(\omega) = 40\pi\left(\frac{i_{\mathrm{b}} \cdot \sigma \cdot \omega \cdot l}{\mathrm{c}}\right)^2 \cdot \exp\left(-\omega^2 \cdot \sigma^2\right) \tag{2-7}$$

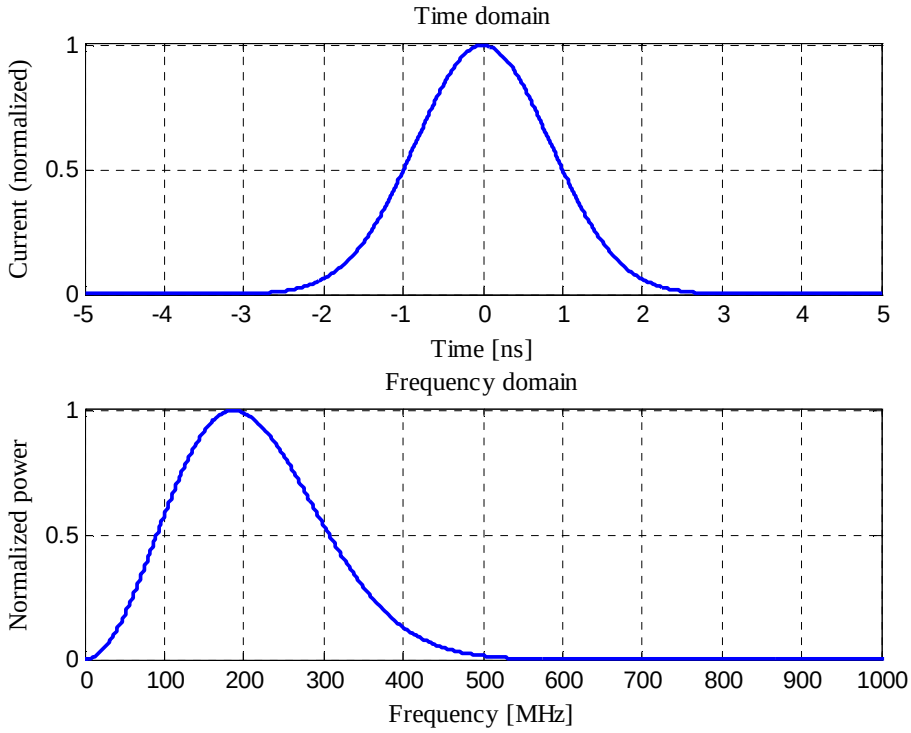

Fig. 2-7. Discharge current pulse in the time domain and the estimated frequency content when the pulse is transmitted through a short dipole antenna calculated with Eqs. (2-6) and (2-7) . It can be assumed that the spectral content of the radiated emission from the discharge pulse reaches up to several hundred megahertz.

A Fourier analysis was used to calculate the spectrum content of the pulse. Fourier analysis, and Discrete Fourier Transform (DFT) in particular, is a well-known tool and widely used in many

areas. The DFT is defined as given in Eq. (2-8) and allows us to transform a sequence of $\{x(n)\}$ into a sequence of frequency samples $\{X(k)\}$. In the equation N is the number of points of the DFT.

$$X(k)=\sum_{n=0}^{N-1} x(n)e^{-j2\pi kn/N} \text{ , } k=0,1,2,\ldots,N-1 \qquad (2\text{-}8)$$

There is no way to absolutely define the frequency content of the measured discharge pulse. However, there are signal processing techniques to estimate the frequency content of the measured discharge pulse. In this thesis, a periodogram is used to calculate a power spectrum estimate. The periodogram is only an estimate of the spectral density of the signal, and there may be more suitable techniques and estimates to achieve more accurate results, but these are also more complex. They were not studied, because the accuracy is not a very relevant issue here; it is possible to obtain a sufficient estimation of the frequency content of the discharge emission by using a periodogram. It also seems that the estimates are well in line with the theory. The periodogram is calculated with MATLAB as given in Eq. (2-9) when weighted with a window function $w(n)$. This is to be used in this thesis to estimate the spectrum content of the measured discharge pulses.

$$S(\omega)=\frac{\frac{1}{N}\left|\sum_{n=1}^{N} w(n)x(n)e^{-j\omega n}\right|^2}{\frac{1}{N}\sum_{n=1}^{N}|w(n)|^2} \qquad (2\text{-}9)$$

Frequencies below 1 GHz are low enough to be directly sampled without down-conversion with commonly available oscilloscopes. Next, the emission from sparking should be measured to validate the model. However, sparking inside a bearing is very difficult (if impossible) to detect visually. Thus, it is not possible to be certain if a detected emission actually originates from the sparking. Therefore, an electrical discharge machining (EDM) tool was used to generate a spark and a RF emission so that the sparking could also be verified by visual inspection. This way, it was possible to pinpoint the source of the emission and verify that the emission measured had really been caused by sparking.

Emission from the EDM tool was received with a wide-bandwidth antenna (200–2000 MHz) and recorded with a high-speed oscilloscope with an input impedance of 50 Ω. The details of the test equipment are given in Section 4.1 and Appendix I. The antenna was placed one meter away from the electrode tips. The spark was generated by moving the electrodes closer together until a discharge between them occurred. The result from an individual measurement is shown in Fig. 2-8. The emission from the spark is very short, lasting only about hundred nanoseconds. Oscillation observed in the measurement is due to electrical parameters of the electrical discharge machine, mechanical bouncing of the electrode tips, and multipath effect (discussed in Section 3.2). These factors cause the emission from sparking to last longer than it would be in an ideal case. The spectral density estimation with a periodogram, plotted also in Fig. 2-8, was calculated from the time-domain measurement as described above. It can be observed that the spectrum from the sparking is wideband reaching up to 700 MHz. The peak power occurs at

around 350 MHz. This differs from the calculated spectrum presented in Fig. 2-7 by 150 MHz, but it should be noted that the spark was generated with the EDM tool and not with the motor. When comparing the spectrum calculated from a discharge in the test motor, the results are more similar. An example of the spectrum from the discharge in a bearing of the test motor is presented in Fig. 4-4 on page 87. In this case, the peak power occurs at around 200 MHz, as estimated with the calculations.

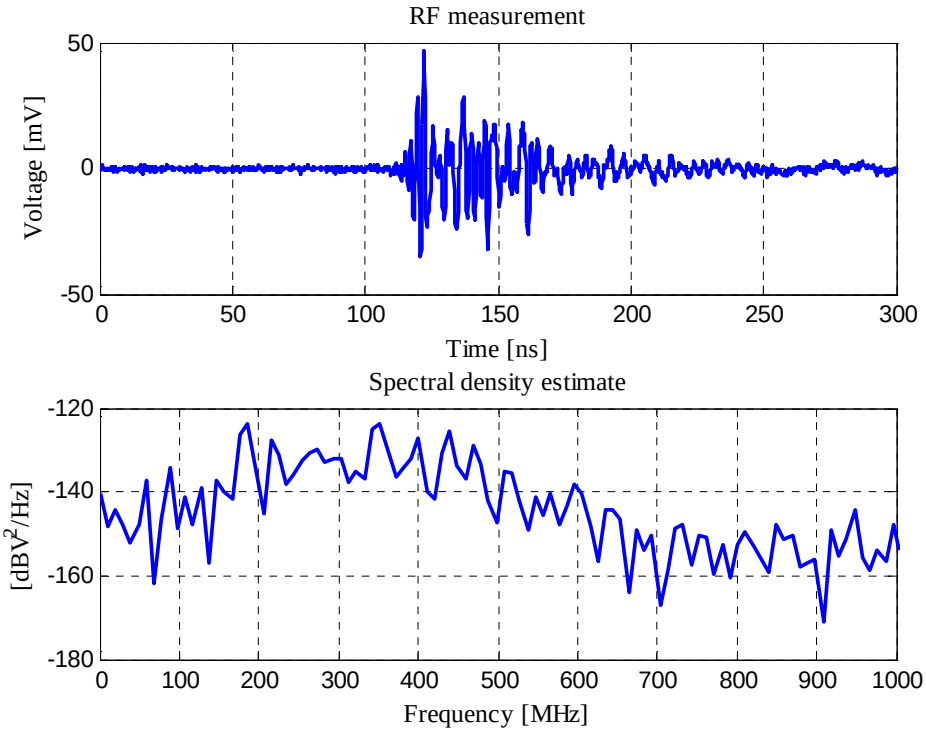

Fig. 2-8. Measured RF emission pulse from sparking generated with the EDM tool and measured with a wide-bandwidth antenna. The duration of the oscillating pulse is approximately 100 ns; however, the actual discharge is notably shorter being only a few nanoseconds. The input impedance of the oscilloscope is 50 Ω. The spectral density estimate obtained by a periodogram, calculated from the measurement, is also plotted. The discharge emission spectrum ranges up to 700 MHz.

There are certain factors that affect the frequency content of the discharge pulse from the bearings of a motor, so that it differs from that generated with the EDM tool. Firstly, the circuit parameters of the EDM tool and of the electric motor differ from each other. This has an effect for example on the pulse rise time and oscillation. Secondly, in the tests, the discharge in the EDM tool took place in air, whereas in a bearing of an electric motor it takes place in grease. Thirdly, the antenna structures differ significantly when comparing the electrodes of the EDM tool and the frame of an electric motor. This probably has a high impact on the spectrum of the discharge pulse and is therefore analyzed more closely in the following section.

2.5 Electric motor as an antenna

As discussed in Section 2.2, the motor frame should not be assumed to operate as a Faraday cage that blocks the emission from the sparking. Instead, it should be considered to be a part of the antenna structure. According to Maxwell's equations, electromagnetic waves are created when an oscillating electric field produces an oscillating magnetic field, which in turn generates an oscillating electric field, and so on. Now, when a discharge occurs, there is an alternating electric field inside the bearing, but also in the rotor and the frame of the electric motor. This is because the bearing current flows from the rotor to the frame through the bearings. For this reason, basically the whole motor and especially its frame have to be considered to be a transmitting antenna.

It should be noted that because of the high frequency of the discharging current, the skin effect causes the currents to flow near the surface of the frame. The frame of an electric motor is typically made of some alloy of cast iron or aluminum. The skin depth is calculated according to Eq. (2-10), where μ_0 is the permeability of free space, μ_r the relative permeability, ρ the resistivity, and f is the frequency. Skin depths for different frequencies are calculated and summarized in Table 2-2, both for aluminum and for iron. Based on these calculations, it can be observed that at the frequencies expected to be seen in the discharge pulses, the skin depths in an iron frame and in an aluminum frame are very small compared with the thickness of the frame, which is typically in the order of several millimeters. At high frequencies, the currents flow very close to the surface in both materials, and we may assume that the material of the frame makes no significant difference to how an electric motor works as an antenna.

$$\delta = \frac{1}{\sqrt{\pi \mu_0}} \sqrt{\frac{\rho}{\mu_r f}} \tag{2-10}$$

Table 2-2. Calculated skin depths for different materials at different frequencies.

Frequency	**Aluminum frame**	**Iron frame**
50 Hz	11.9 mm	2.4 mm
50 MHz	11.9 µm	2.37 µm
100 MHz	8.42 µm	1.68 µm
500 MHz	3.77 µm	0.75 µm

A transmitting antenna is a structure that can generate electromagnetic fields and allow them to propagate into space as an electromagnetic wave. Typically, antennas are reciprocal, which

means that they work similarly in both transmitting and receiving. There are several parameters that are important when studying antennas. Depending on the application in which they are to be used, these are for example: radiation pattern, gain, bandwidth, resonant frequency, impedance, aperture, polarization, and efficiency. The radiation pattern expresses graphically the intensity of radiation, or in other words, the field strength to different directions. For an ideal isotropic antenna the radiation pattern is a sphere, and thus, it radiates equally well in all directions. For any real antenna instead, there are always directions where the radiation is more intense than in other directions. This directionality is expressed as the gain of the antenna. The bandwidth of an antenna is the range of frequencies over which it is effective (Seybold, 2005).

The gain and bandwidth are of particular interest when considering the RF method studied in this thesis. The gain of the test motor is measured in Section 4.5. It is important to know where a receiving antenna should be placed to be able to measure the discharge pulse. The focus in this section is to show whether an electric motor can operate as an antenna. The bandwidth is very interesting, because it decides whether the motor is able to transmit a wide bandwidth discharge pulse or only a fraction of it.

Antenna parameters are typically calculated, simulated with a computer, or measured. In the previous sections, a dipole antenna was used as an approximation for the transmitting antenna. The reason was that there are equations that can be used to quite accurately calculate the gain and radiation pattern for a dipole antenna with different frequencies. However, the motor structure is far more complicated making the analysis more difficult, and a dipole antenna cannot be used to accurately model the motor as an antenna. None of the commonly used antenna structures are even close to an electric motor structure. So, it is not possible to calculate these antenna parameters with equations developed for known antenna structures. For accurate modeling, numerical techniques, such as FEM (Finite Element Method) could have been used. However, in this thesis, it was chosen to directly measure the motor parameters as an antenna. Parameters important for this study were measured for different sizes of motors.

The antenna parameters are commonly measured in a radio frequency anechoic chamber that is specially designed for the antenna measurements at a certain frequency bandwidth. The antenna to be measured is typically rotated around its axis to obtain the radiation pattern of the antenna. A proper anechoic chamber for the frequency range of 100–500 MHz was not available, and the larger electric motors analyzed were rather massive, which would have made the measuring setup complicated. For these reasons, the motors were analyzed in a typical laboratory environment. The motors were not running during the measurement. With the measurement conducted for the test motor, it was noted that there was no significant difference whether the motor was running or not, and it was easier to measure motors at standstill. The test motor measurements are presented and analyzed in Section 4.5.

Fig. 2-9 illustrates the absolute value of the measured S_{21} parameter of three different LV motors. The measurement was taken with a VNA (Vector Network Analyzer). The receiving antenna was set orthogonal to the motor axis, approximately one meter away from the motor under test. The test signal was injected at the NDE (Non Drive End) of the shaft and received with a wide bandwidth antenna using horizontal polarization. The test signal has constant power and its frequency is varied from 100 MHz to 500 MHz with steps of 1 MHz. Specifications and placement of the equipment used can be found in Appendix I. It can be seen from the results that an electric motor works as a wide bandwidth antenna. There are differences when comparing different motor sizes, but all of the motors seem to have the smallest power loss occurring around 200–300 MHz. This means that the transmitting antenna (the motor) is having higher gain at these frequencies.

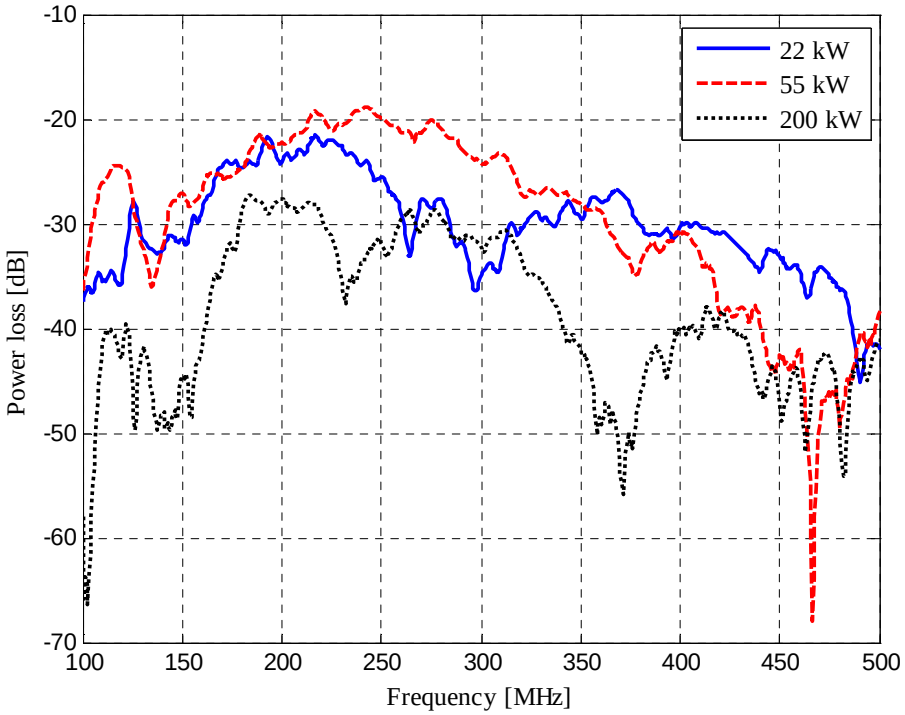

Fig. 2-9. S_{21} parameters measured with the VNA from electric motors of different sizes. Only the absolute value of S_{21} is shown. The direct distance between the motor frame and the receiving antenna was one meter. The receiving antenna was set orthogonal to the motor axis. The blue solid line shows the measurement obtained for a 22 kW motor (frame size 180), the dashed red line the one obtained for a 55 kW motor (frame size 250), and the dotted black line the one obtained for a 200 kW motor (frame size 315).

There are several issues that should be noted concerning these measurements. The measurements were not carried out in a radio anechoic chamber. However, even though this has an impact on the results, it can be neglected, because we are mainly interested to know whether a motor works as an antenna or not. The motors were not running during the measurement. With the test motor, it was tested whether there was a difference in the results if the motor was running or not. It was noted that at higher frequencies above 200 MHz the impact was small. At these frequencies, it can be expected that the electric impedance of the insulation resulting from the lubrication film is not significant. Consequently, it is possible to obtain adequate results by measuring the motors at standstill when there is no insulating oil/grease film between the bearings. Hence, it is possible to obtain reliable information on how a motor works as an antenna without complicated brush connections to the shaft, which could be required to inject the test signal if the motor was analyzed while running. A wide bandwidth antenna with a bandwidth of 200–2000 MHz was used. This means that the results below 200 MHz are not accurate. The antenna works also at frequencies below 200 MHz, but has not been specified by the manufacturer. It is later shown in Section 3.4.1 that it is feasible to detect a discharge pulse above 100 MHz because of the interference from the frequency converter. Another aspect to consider is the supply of the test signal to the motor. In these measurements, the signal has been supplied to the shaft of the motor, and there was an unavoidable impedance mismatch between the supply and the shaft. This greatly differs from the real case when a high-frequency signal is

generated by an electric discharge. These issues are discussed in more detail in Section 4.5, where more conclusive antenna measurements with the test motor are presented and analyzed.

3 DETECTION OF DISCHARGES IN THE BEARINGS OF AN ELECTRIC MOTOR

In radio technology, development basically started with the invention of the spark gap transmitter, and has gone a long way to UWB data transmission, where short wideband pulses are transmitted at very high frequencies. Something still remains the same: Interference is a very important issue when dealing with RF transmission, where the channel is often occupied by more than one transmitter. In this chapter, RF interference from various sources and its effect on the detection of the discharge emission is discussed. A short introduction to radio wave propagation is given as a background for the measurements presented in Chapter 4.

Techniques that can be used to detect the source of emission (sparking) and distinguish this from interference in measurements are also discussed. The emission from sparking is a short decaying pulse, which is easily detectable with a time-domain measurement if similar impulsive interference is not present. However, the strength of the discharge signal can be significantly lower than the interference from the frequency converter or from some other source, thus making the detection impossible without application of a proper signal analysis. The methods discussed in this chapter are filtering, Fourier analysis, and different location techniques.

3.1 Partial discharge detection in transformers

Detecting incipient faults by measuring high-frequency emission from sparking is not a new idea. It has been used for example to detect PDs (partial discharge) in the insulation of power transformers, electric motors, and power cabling (Stone, 1995). Partial discharge occurs when the electric field exceeds the local dielectric strength of the insulation. The reasons for this can be for example damage caused by overvoltage or lightning strikes, manufacturing defects, and deterioration as a result of natural aging (Judd, 2005).

Some studies in the field of the radio frequency PD detection in power transformers in gas-insulated substations are for instance (Judd, 2005, 2005B) and (Moore, 2005, 2006). The measurements are typically referred to as VHF (Very High Frequency) or UHF (Ultra High Frequency) detection of PDs, depending on the frequency band used in the measurements. VHF designates a frequency band ranging from 30 to 300 MHz, whereas UHF designates a frequency band ranging from 300 MHz to 3 GHz. Typically, a VHF/UHF signal generated by the PD inside a transformer is received with an antenna, and it is amplified and/or filtered and sampled with a high-speed oscilloscope or an A/D converter and a computer. This is similar to the measurements carried out in this thesis, with the exception that in the PD detection of power transformers the antenna is typically mounted inside the power transformer. Another possibility is to equip the transformer tanks with dielectric windows to allow the signals from PDs to reach the antenna outside the transformer tank (Judd, 2005B). It should be noted however that this differs from the discharge in a bearing, where the emission is measurable outside of the motor, even though in both cases the discharge is surrounded by a metal casing. The reason for this is that in the case of PD, the current does not necessarily flow through the transformer tank. Instead, bearing currents always flow through the frame of the motor as was discussed in the previous chapter. In other words, the transformer tank is a Faraday cage that blocks emission quite effectively, whereas in the electric motor case the frame is a part of the antenna structure.

It is mentioned in (Judd, 2005) that the signal from the PD is radiated all around the power transformer through a multitude of paths. The signal oscillates and the receiver is subject to heavy fading because of the multipath effect. The frequency spectrum of the emission is wide because of the short nature of the PD current pulse and its fast rise and fall times. Individual

pulses can have a duration of less than <1 ns, but at the receiver they are recorded as an oscillating and decaying pulse lasting typically less than 100 ns (Judd, 2005). Because of the shortness of the pulse, it is possible to achieve transmitting powers of several hundred nanowatts, even though the total amount of energy released is very small. Similar values were obtained in the previous chapter, when the power of discharge inside a bearing was estimated. In (Moore, 2005), it is reminded that the initial rise time of a PD current pulse depends on the insulation material. If oil is used, the rise time is faster because of the higher dielectric constant of oil compared with air, thus widening the spectrum of the PD towards higher frequencies.

One of the targets in PD detection is to be able to pinpoint the exact location of PD. This is one of the reasons why higher frequencies are more interesting, because the wavelengths are shorter than the dimensions of the transformer. In this case, higher frequencies can mean for example moving from the VHF to the UHF region. By using two or more antennas or sensors, it is possible to calculate the location of the source from signal arrival times. In (Judd, 2005), it is suggested that the PD source can be located within 20 cm by sampling it with an oscilloscope with a bandwidth of 500 MHz or more. In their setup, they have received the signal with two or more antennas. The cumulative energy of each pulse is calculated from the received signals. By observing the energy diagram, it is possible to calculate the time difference of the signal arrival times for each of the receiving antennas. Knowing the location of the antennas, it is possible to calculate the location of the PD source. The location of PD is discussed also in (Moore, 2005). A multiple antenna system to detect the source of PD has been developed. This is also based on calculating the signal arrival time differences. Individual signals are first detected by thresholding; this means that if the signal exceeds a certain threshold, it is detected. The arrival time differences are then calculated by cross-correlating the signals from different antennas (Moore, 2005).

3.2 Propagation of radio waves

Terms such as ‘multipath effect’ and ‘fading’ have been previously used in this study, but they have not been fully explained yet. In this section, a short introduction to the propagation of radio waves is provided as background information to support the thesis. The effects of the surroundings have to be taken into account when measuring RF signals. A discharge signal also differs from commonly used continuous carrier wave transmissions by being impulsive by nature. This has to be taken into account when discussing the propagation of radio waves and the equipment used to capture these radio waves. The most important difference is probably due to the steep current pulse rise time during the discharge as the radiated RF signal has a high frequency content reaching up to hundreds of megahertz. In the time domain, the radiated signal is a very short impulse differing radically from the continuous carrier wave transmissions.

The space surrounding a transmitting antenna is usually divided into two different regions. These are the near field and the far field. The borders between these different fields are only vaguely defined, and no certain border can be specified. There are different ways to approximate where the near field ends and where the far field begins. It can be roughly assumed that the near field is the region with the radius $r << \lambda$ and the far field is the region where $r >> \lambda$, where λ is the wavelength of the transmitted wave. It is well known that in the near field the magnetic field and the electric field fall off rapidly and, for example, current measurements with a magnetic probe have to be made close to the source. However, in the far field the radiated power is proportional to $1/r^2$ (Rappaport, 2002). In practice, this means that it is possible to measure the emission at some distance away from the motor. This distance depends for example on the transmission power, which however is unknown. In this thesis, the tests showed that it was possible to successfully measure a discharge at least three meters away from

the test motor. Of course stronger discharges can be detected even further away, but it is possible that weaker discharges are then not correctly detected.

Multipath effect and fast fading are phenomena that definitely influence the measurements if the RF method presented in this thesis is used outside a radio anechoic chamber. This means that all practical measurements suffer from these effects. The multipath effect and the signal distortion caused by it are easily understandable: If the motor radiates the discharge signal around itself and the receiving antenna is omnidirectional. Further, if the receiving antenna was placed close to the motor and there were no obstacles between them, the RF emission from the discharge could travel along a direct line-of-sight path to the receiving antenna. However, in practical applications, there are probably obstacles around the motor, and the antenna may be somewhat further away. Typical obstacles are for example floors, walls, and different metal structures that are common in industrial environments and that act as reflectors. Thus, the radiating emission that leaves the motor into all directions reflects from these obstacles and travels to the receiving antenna along a path longer than the direct one. The received RF emission from the discharge, as seen at the receiving antenna, is the sum of all these reflected emissions delayed depending on the distance they have traveled before reaching the receiving antenna (Rappaport, 2002). Note also that it is assumed here that the discharge generates a single impulse that radiates from the motor. Because of the multipath effect, the received signal will look like a series of impulses or a rapidly decaying oscillation. The multipath effect depends on the surroundings, and the received signal is different for instance if the motor or the receiving antenna is moved to a different place while the transmitted signal remains the same. Similarly, variations in the surroundings during the transmission of the signal (for example, the machines are moving) cause fluctuations in the received signal. This is called fast fading. This basically means that the amplitude of the received signal may vary even if the transmitted signal amplitude stays constant.

Noise can be divided into two groups, viz. received noise and noise caused by the receiving equipment. The latter depends on the hardware used to measure RF signals, and can be reduced with the choice of proper hardware. Noise from the surroundings together with the receiver sensitivity determines the lowest possible transmission level at which the signal can be detected. Typically this is white noise that is eventually distributed on all channels, but there can be other transmissions going on that can overlap the measured signal. These other transmissions are handled as interference, and they are addressed in greater detail in next section.

3.3 Interference

In radio applications, a common problem is interference from various sources that can distort the received signal. Interference can be some random bursts from machinery or more continuous transmission from the cellular network. The spectrum from the sparking may span up to several hundred megahertz, and thus other transmissions in this frequency band can be considered as interference, because the interest is only in the discharge emission. Fig. 3-1 illustrates different types of transmissions that are allocated in this frequency band in Finland. The illustration is only an approximation based on the information of frequency allocation in Finland given by FICORA (Finnish Communications Regulatory Authority). Even though there are some country-specific allocations, this can be used to estimate the frequency allocation also in other parts of Europe. SRD in the figure is an acronym for a short-range device. These are, as the term implies, short-range wireless devices that are used, for example, in sensor networks and RFID (Radio Frequency Identification) applications. It can be seen from Fig. 3-1 that the frequency band from 150 MHz to 450 MHz is more suitable for spark detection than for example the 500 MHz–1GHz range, because there are fewer continuous transmissions and thus

less interference. It should be noted that the frequency band from 150 MHz to 450 MHz is allocated for example to military, TV, and amateur radio use; nevertheless, for the time being, there is no TV transmission at these frequencies in Finland. However, the situation can be different in other countries. It can also be assumed that military and amateur radio transmissions are less continuous and more local than for example TV transmission, which is basically continuous and the coverage of which is wide.

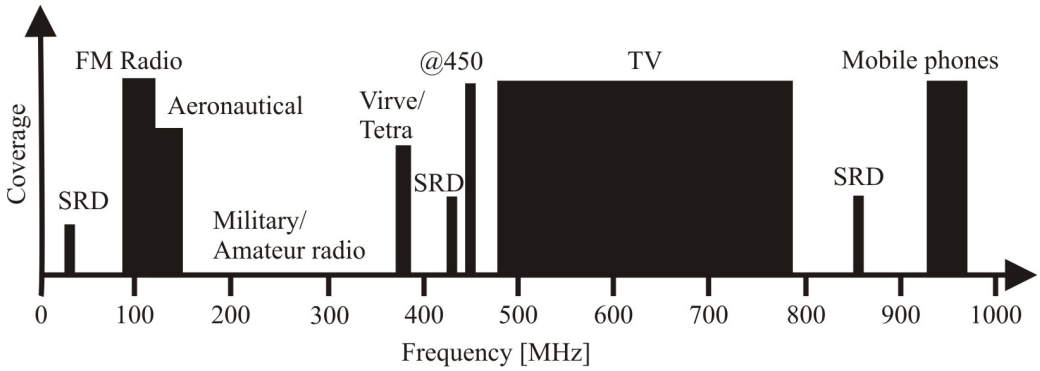

Fig. 3-1. Illustration of frequency allocation in Finland. There are no specific allocations for continuous transmissions in the bandwidth from 150 MHz to 450 MHz at the time being. This bandwidth is allocated mostly to military and amateur radio use, and thus transmission in this band may vary with location and time.

The environment where sparking measurements are taken can vary significantly, and it is not possible to predict all the various sources of interference. For example, a motor drive can be located underground in a mine where practically all the interference from outside is minimized because of attenuation. There can also be strong sources of interference caused for example by welding equipment or other machinery that generates sparking. Furthermore, there is one source of interference that is always present in a motor drive if there are bearing currents. It is the inverter, which is known to be a strong source of EMI.

3.3.1 Frequency converter as a source of interference

The initial measurements carried out in the frame of this thesis showed that interference from a frequency converter has to be studied more closely, because it has such a strong effect on detection of discharges and thus bearing currents. EMI from the frequency converter can be divided into conducted and radiated EMI. The two major sources of EMI in the frequency converter are the rectifier unit and the inverter stage. There are other minor sources such as power supplies for the control electronics, pulse transformers, and clock sources. From these, especially the inverter stage has the highest importance, because the interference it generates has a high amplitude and is similar to the discharge emission.

According to (Silventoinen, 2001), the inverter stage is the main source of EMI in DC voltage link converters. The reasons for this EMI are the high switching frequency including harmonics and noise from switching and commutation phenomena. Hence, the emission from the switching is impulsive, and depending on the type of the inverter and modulation, it can be either periodic or nonperiodic. It is difficult to predict what kind of interference is present in a certain system. A guideline could be that higher switching times and higher voltages are more likely to interfere with discharge signals. Poor grounding and long motor cables also increase the likelihood of radiating emissions (Skibinski, 1999). According to (Silventoinen, 2001), hard

switching inverters are more problematic with respect to EMI than soft switching inverters, because the frequency content is higher. Measurements of inverter-generated EMI has been presented in (Ogasawara, 1997) and (Revol, 2004).

In this work, the interference from the inverter was analyzed experimentally. The inverter used in the measurements was a standard PWM inverter. The measurements were conducted in a shielded laboratory, where interference from other sources was blocked. Detailed information on the equipment and the measurement setup is given in Section 4.1 and in Appendix I. Fig. 3-2 depicts the RF measurement of the interference generated by the inverter switching instances with the common-mode voltage measurement. The radiating emission was measured with a wide-bandwidth (200–2000 MHz) antenna. The common-mode voltage was simultaneously measured at the terminals of the test motor. The emission voltage was measured over a 50 Ω input impedance of the oscilloscope. The common-mode voltage was measured from the virtual star point composed of resistors at the motor terminals as described in Section 1.5. In this measurement, the antenna was located one meter away at the side of the test motor. The inverter was located three meters away from the antenna. When comparing the RF measurement and the common-mode voltage measurement, it is obvious that the interference was caused by the switching of the inverter. All RF pulses coincide with the switching instant of the inverter as can be seen from the common-mode voltage waveform.

The interference activity is directly related to the switching frequency of the inverter. Most importantly, there is additional interference whenever the frequency converter is turned on. A method has to be found to be able to detect sparking in presence of inverter-generated interference. One method could be to measure the common-mode voltage simultaneously with the RF measurement so that the interference pulses and discharge pulses could be separated. However, this is not very practical, because it requires simultaneous measurement of phase voltages or the common-mode voltage, and reliable detection of discharge pulses cannot be guaranteed. A far better way is to filter the interference, which is a commonly used technique, for example, in radio communications. To be able to do this, detailed information about the frequency content of the inverter interference is needed.

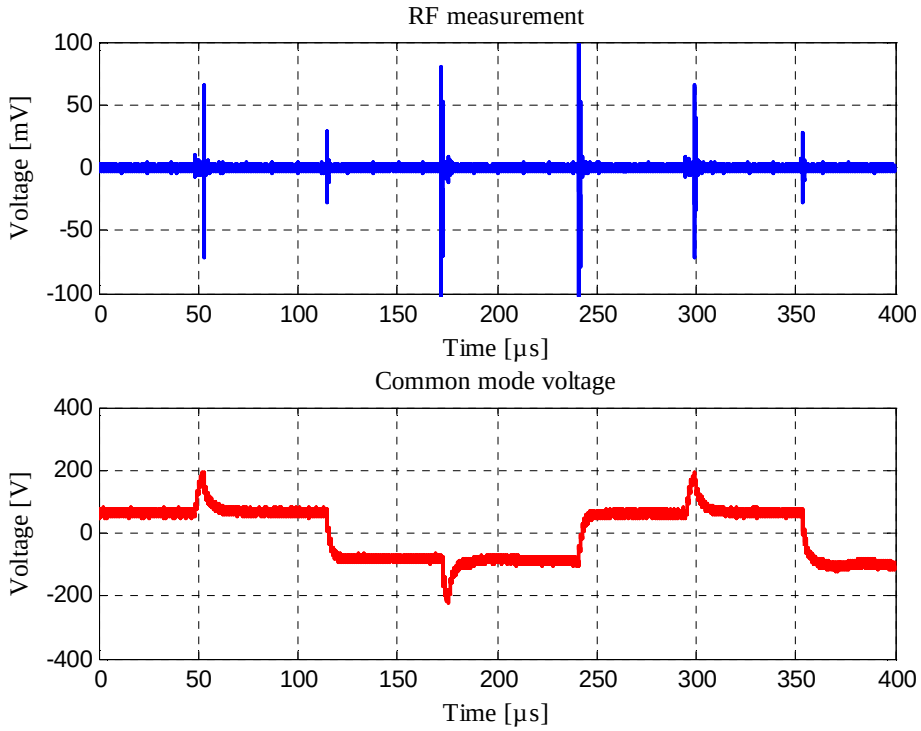

Fig. 3-2. RF measurement of interference generated by the inverter switching instants, measured with a wide-bandwidth antenna. The common-mode voltage is simultaneously measured at the terminals of the motor. When comparing these two measurements, it is obvious that the interference is due to the inverter switching. The input impedance in the RF measurement is 50 Ω.

The RF measurement of an individual interference pulse generated by a switching instant is plotted in Fig. 3-3 together with the spectral density estimation by a periodogram calculated from the RF measurement. The emission is very similar to a discharge pulse presented in Fig. 2-8 generated with the EDM tool. Both are short oscillating and decaying pulses. There is a difference in the length of the pulses, the interference being at least twice as long as the discharge emission. Also, the rise time is shorter and oscillation frequency of the discharge emission is higher when compared to the interference emission. If the spectrum is studied, it becomes obvious that the frequency content of the inverter pulse is well below 100 MHz. It should be noted that the amplitude of the result is not very accurate because of the limited bandwidth of the antenna used in the measurements (the bandwidth of the antenna is 200–2000 MHz). However, the amplitude of the interference is still considerably stronger than the amplitude of the discharge pulses, and thus makes it practically impossible to detect electric discharges if inverter-induced interference is present.

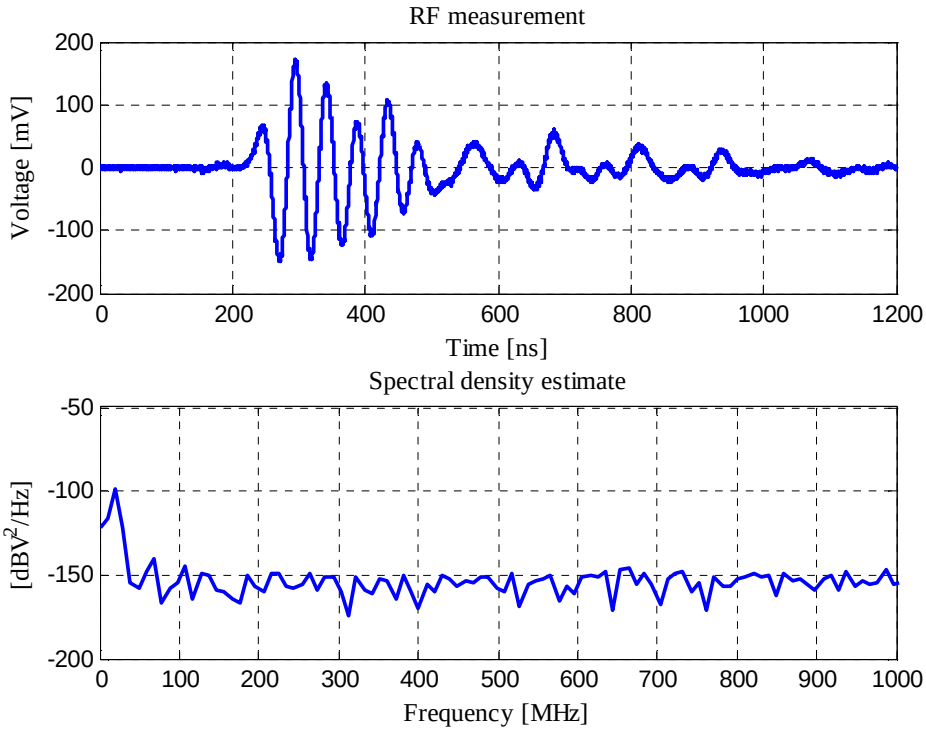

Fig. 3-3. RF measurement illustrating the emission from the inverter. The emission is measured with an antenna having a bandwidth of 200–2000 MHz. A spectral density estimate by a periodogram is calculated from the RF measurement. It is obvious that the spectrum of the inverter-generated interference is at much lower frequencies compared with the spectrum of the discharge pulse generated with the EDM tool and shown in Fig. 2-8. It can be said that the interference caused by inverter switching is mainly concentrated below 100 MHz.

It is obvious that because of the switching of the inverter, interference from an inverter is inevitable in the bearing sparking measurements. In general, discharge detection from a time-domain measurement is not possible in practice without additional signal processing. The reason is that the inverter interference is also impulsive, but stronger in amplitude than the emission from the discharge. The interference is also repetitive in the sense that there is a pulse every time when there is a switching instant. For these reasons, it is not directly possible to distinguish between an emission from the discharge and from the inverter. Basically, the interference from the inverter overlaps the discharge emission. Consequently, a method to distinguish discharge signals and/or eliminate the interference in the measurements has to be found. Different ways to process the measured data are proposed in the following section; the most important of which being interference mitigation with filtering.

3.4 Signal analysis methods for discharge detection in the bearings of an electric motor

It has been discussed above in Section 2.4 that the discharge inside the bearing generates a short current pulse, which lasts only a few nanoseconds. The radiated emission pulse from the discharge is somewhat longer (tens of nanoseconds) because of the oscillation caused by the multipath effect, but has also a very high rise time. Thus, the frequency content of the radiating emission from the discharge can reach up to hundreds of megahertz. These pulses differ from

typical continuous carrier wave transmission used in communication, and are easily detectable in the time domain. The simplest method to detect individual pulses is to set some threshold level above the background noise level and then detect each pulse that crosses the threshold level. However, because of interference from the environment and especially from the inverter, distinguishing the inverter-switching-generated pulses from the discharge pulses is not possible without additional signal processing. In this section, signal processing techniques used later in the analysis of the discharges are introduced. In all the measurements presented in this thesis, data are first captured with an oscilloscope and then processed with a PC and MATLAB. This method facilitates testing of different methods to detect discharging, but does not allow real-time detection. Requirements for real-time discharge detection are discussed in Section 3.6.

3.4.1 Interference mitigation with high-pass filtering

The simplest method to eliminate unwanted interference is the filtering of data. This can be partially done even before digitizing the signal. Antennas have a certain optimum bandwidth at which they operate best, and frequencies outside this bandwidth are usually strongly attenuated. Basically, the antenna operates as a band-pass filter. The same applies to other measurement equipment used, such as cabling, connectors, amplifiers, and A/D converters, which all have limited bandwidths. Additional filters can be implemented between the antenna and the oscilloscope, or filtering can be applied later to the digitized data.

Previously it was stated that there are various transmitters and transmissions generating unwanted interference in the frequency range from 1 MHz to 1 GHz. This is the bandwidth where emission from the discharge can be found. Continuous transmissions in a certain band can be rejected by a means of a band reject filter. However, the measurements in this thesis are conducted in a laboratory that is well protected against outside interference, and therefore this kind of continuous interference at a certain frequency was not studied extensively. In Section 3.4.2 the difference of continuous transmission and electric discharge emission is briefly discussed. On the other hand, the interference generated by the inverter is more problematic and different from normal RF transmissions. Interference caused by inverter switching is always present in bearing current measurements; the magnitude of the interference is far stronger compared with the emission from the discharge; furthermore, the interference is impulsive and similar to discharge pulses in the time domain. This section takes a closer look at how to mitigate the effect of the inverter interference by filtering.

The measurements show that radiating interference from the inverter occurs mainly well below 100 MHz as previously shown in Fig. 3-3, while the emission from the discharge is expected to reach from 100 MHz up to several hundred megahertz according to the results presented in Section 2.4. Fig. 3-4 shows a combined spectrum of the discharge pulse generated with an EDM tool (dashed red line) and interference from the inverter switching (solid blue line) plotted in the same figure. These are taken from the measurements presented in Fig. 2-8 and Fig. 3-3. One can clearly see that even though interference from the inverter and emission from the discharge generated with the EDM tool partially overlap, it is possible to distinguish them from each other by comparing the differences in the frequencies that they allocate. Interference from the inverter is mainly below 50 MHz, while the emission from the discharge generated by the EDM tool is mainly above 50 MHz. This suggests that a low-pass filter can be used to eliminate the interference from the inverter and leave the emission from the sparking mainly untouched. This can also be explained as follows: A signal can be detected if it has a positive SNR (signal to noise ratio). In this case, the EDM discharge signal has a positive SNR between 50–650 MHz, as shown in Fig. 3-4.

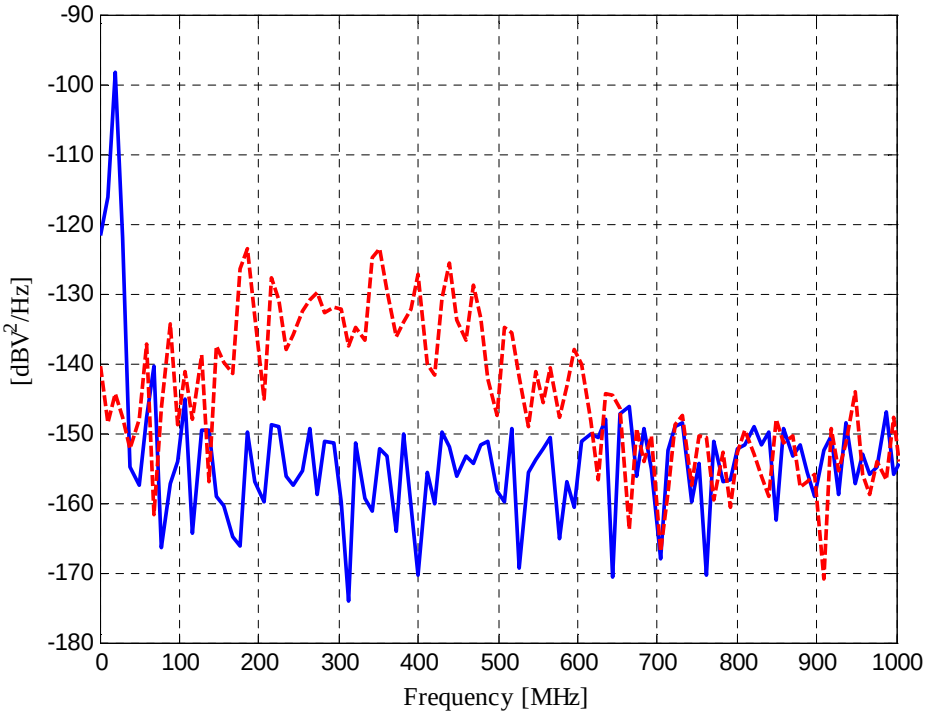

Fig. 3-4. Measured radiated emissions from the inverter switching (solid blue line) and from the discharge generated with an EDM tool (dashed red line). This is a combination of the previous measurements presented in Fig. 2-8 and Fig. 3-3. The discharge signal has a positive SNR between 50 and 650 MHz. This information suggests that the discharge signal is detectable even if there is inverter-generated interference present.

The filtering of inverter-switching-generated interference was first verified with MATLAB. This means that filtering was applied to the previously recorded data: The measurement data were recorded with an oscilloscope and transferred to a PC and then processed with MATLAB. The design criteria for the filter were that it should be a high-pass or a band-pass one with a lower stop band between 50–100 MHz. According to this, several different filters were composed and applied to the recorded data. These varied, for example, by having a different stop band, response, and complexity. After testing series of different designs with trial and error, it was found that a fourth-order high-pass filter with a Butterworth response and a cutoff frequency of 50 MHz is suitable for mitigating the inverter-switching-generated interference. Low-order design eases possible implementation for external hardware, such as discussed later in Section 3.6. Butterworth design was chosen only to get a flat frequency response in the passband. This filter is used in the following example and the filter coefficients are given in Appendix II.

Fig. 3-5 illustrates an unfiltered RF measurement showing two similar pulses. This was recorded with a high-bandwidth antenna placed on the side of the test motor, one meter away. The motor was driven with a frequency converter, which was placed three meters away from the antenna. The test setup is introduced in more detail in Section 4.1 and Appendix I. The current measurement is taken simultaneously from the jumper cable, which is used to short the

insulation between the bearing and the frame of the test motor, using the technique described in Section 1.5. When comparing the RF and the current measurements, the first pulse (at 0.7 µs) results from the discharge in the bearing, because at the same time there is a current pulse flowing through the bearing. This current pulse being close to 400 mA at the maximum amplitude can be considered harmful, because it will probably generate a micro crater, including removal of some material from the bearing race. This is the starting point of the bearing failure as discussed in Section 1.4. During the latter inverter-generated interference pulse (at 2.2 µs) there is only a small fluctuation in the current. This fluctuation is probably due to the HF capacitive currents that flow through the bearing without a discharge, or more specifically, without generating a spark. As discussed in Section 1.3.1, these capacitive currents can be considered harmless. It should be noted that the amplitude of the interference pulse is significantly higher than the discharge pulse in the RF measurement.

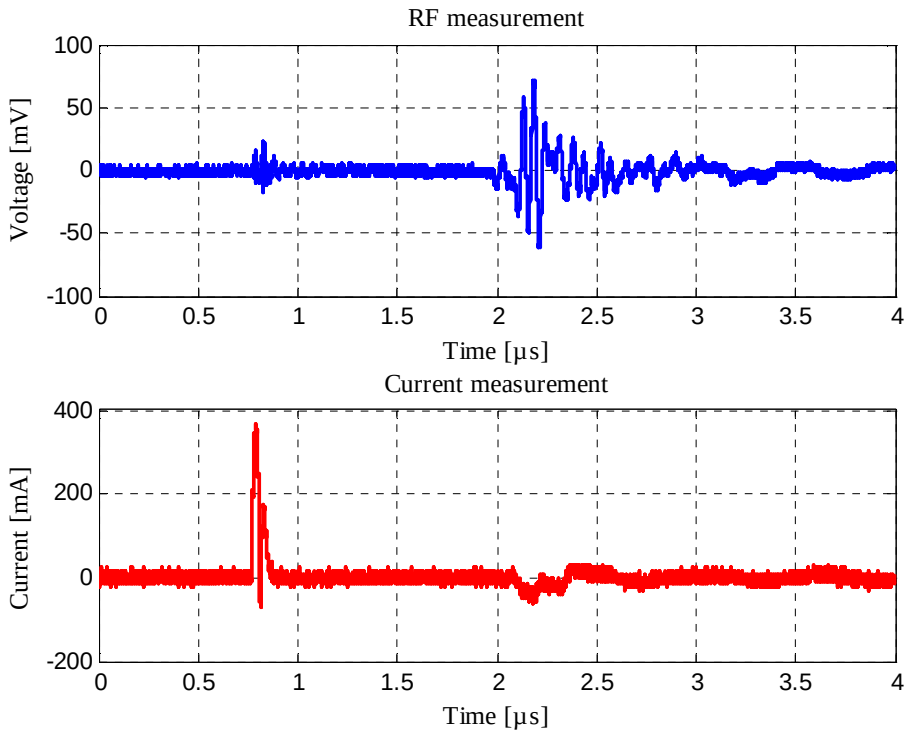

Fig. 3-5. RF measurement showing the discharge pulse and the inverter-generated interference pulse. The bearing current is simultaneously measured from the test machine. It can be seen that the inverter switching interference is far stronger in amplitude than the discharge pulse. During the inverter switching pulse, at approximately 2.2 µs, only a capacitive current flows through the bearing, which can be considered harmless. When the discharge pulse occurs at approximately 0.7 µs, there is a current pulse peaking almost 400 mA flowing through the bearing of the test motor. This has potential to be harmful to the bearing and may generate a micro crater.

It is obvious that it is impossible to predict the origin of an individual detected pulse without a current measurement because of the similarity of the discharge pulse and the inverter-switching-generated interference pulse. It is worth mentioning that even though there is a significant difference in the amplitudes in this example, the magnitudes of both pulses vary and it is not possible to say anything certain of their amplitudes. Further, the pulses can partially overlap,

which makes the detection of the discharge pulse practically impossible without additional signal processing. To detect the discharge pulse from the time-domain representation, the previously designed high-pass digital filter was applied to the measurement, and the results are shown in Fig. 3-6. It can be seen that the interference caused by the inverter switching is eliminated and the pulse from the discharge is mainly unchanged. There is some phase shift caused by the filter, and also some low-frequency oscillation has been filtered from the discharge pulse. From the time-domain representation of the measurement, it is now possible to detect the instant at which a discharge occurs in the bearing of the test machine. This indicates that there are bearing currents in the test motor. The current measurement is the same as before and it is presented here only to clarify the results.

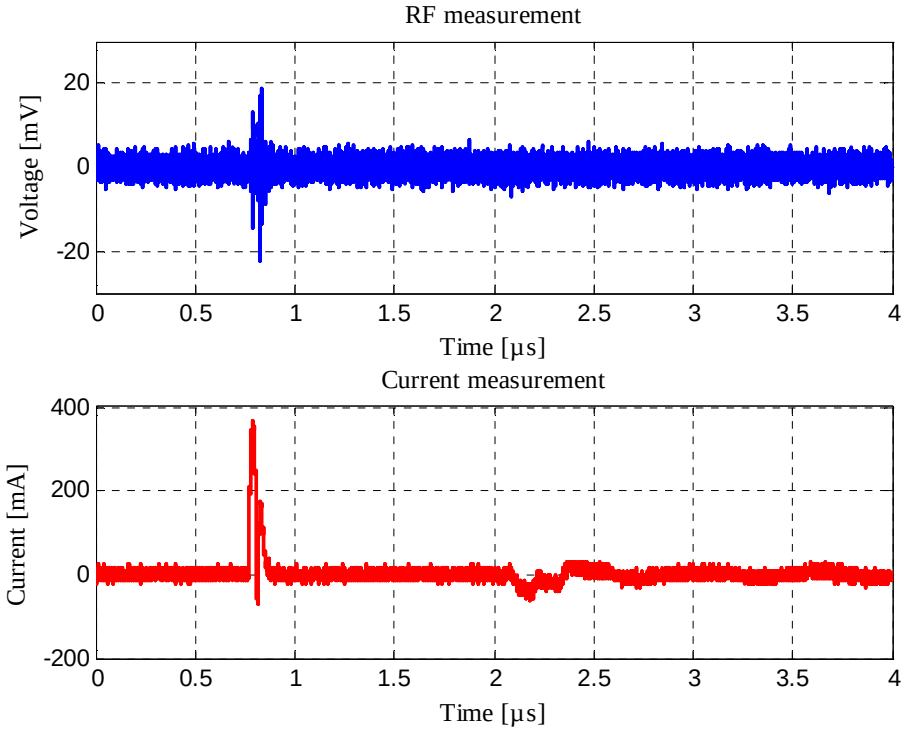

Fig. 3-6. Same measurement as in Fig. 3-5, but filtered with a fourth-order digital high-pass filter with a cutoff frequency of 50 MHz. The inverter-switching-generated interference is completely eliminated from the signal measured with the antenna, and emission caused by the discharge is clearly seen. The current measurement is the same as before, and the capacitive current flow indicates the moment at which the inverter-generated interference, that has been filtered away, occurred.

It may be difficult to filter the recorded data at a later time with a PC. The reason for this is that the amplitude of the inverter-generated interference may be significantly stronger than one of the discharge pulses. If the oscilloscope scale is chosen so that there is no clipping, it is possible that the resolution becomes too small to properly detect the RF signal from a discharge. This means that some amount of filtering before the A/D conversion is required. For this reason, various passive filters were evaluated. Based on the results obtained from the previous design of the digital filter, it is clear that a high-pass or band-pass filter with a pass band of approximately 100–1000 MHz is suitable. Three different commercially available high-pass passive filters

with passbands of 41–800 MHz, 90–400 MHz, and 133–1000 MHz were investigated. These are illustrated in Fig. 3-7.

Based on the measurements, the first analog filter does not effectively filter the inverter switching interference, and therefore additional digital filtering was required to properly detect the discharges. The two latter analog filters were found to mitigate most of the interference from the inverter, and no additional filtering was required. The BHP-100+ high-pass filter with a passband of 90–400 MHz was found to be better of these two. It filters most of the unwanted interference and preserves the signals from the discharges in the bearings. This is the filter that is used in the measurements presented in Chapter 4.

Fig. 3-7. Three tested passive high-pass filters. The passbands of the filters from bottom to top: 41–800 MHz, 90–400 MHz, and 133–1000 MHz. The middle one (BHP-100+) was found to be the most suitable for filtering the interference from the inverter, and it has been used in the measurements presented in Chapter 4.

These passive filters are inexpensive and easy to use. They are sold with most commonly used connectors and are very suitable for mitigating the unwanted interference generated by the inverter switching. It should be pointed out that because they are passive, they do also attenuate the measurement signal. For the BHP-100+ attenuation in the passband is <1 dB, in the stopband between 40–55 MHz >20 dB and between DC-40 MHz >40 dB. In the measurements presented in this thesis, this was not found to be problematic, because the discharge signals are still detectable. However, in certain cases when a discharge is measured further away from a motor, or for some other reason the emitted RF signal is of low power, it may be impossible to properly detect the discharge signal after filtering. In this case, additional amplification will be required before or after the filtering to amplify the discharge signal.

3.4.2 Discharge detection using short-time Fourier transform

The RF pulses from discharges in the bearings of an electric motor may be difficult to detect in the time domain if inverter-generated interference is present, as was shown in Fig. 3-5. This was solved with filtering, which made the detection possible. However, there may be other random pulses from other interference sources that are random in amplitude, but still very similar to discharge pulses if observed only in the time domain. In this section, a method is studied that combines time and frequency information. Previously, Fourier transform has been used to identify the frequency content of a signal in the form of a periodogram as discussed in Section 2.4. Unfortunately, in this case no time information is preserved, because it is assumed that the frequency content remains the same over the whole sample period. The method that can be used to show both time and frequency information simultaneously is called STFT (short-time Fourier transform). STFT can be used to analyze the frequency spectrum of signals that evolve with time, making it very suitable for studying discharge signals that are impulsive.

The STFT can be calculated as given in Eq. (3-1), where $x(n)$ is the signal, w is the window function and k is the location on the time axis. The Fourier transform is calculated from smaller frames that are segmented from the original signal with windowing function.

$$X(k,\omega) = \sum_{n=-\infty}^{\infty} x(n)w(n-k)e^{-j\omega n} \tag{3-1}$$

An example how STFT can be used is given in Fig. 3-8, where a spectrogram is shown. The spectrogram is calculated from the previous unfiltered measurement that is shown in the time domain in Fig. 3-5. The advantages of the time/frequency presentation are obvious. Both the discharge emission and the inverter switching interference are easily distinguishable in the spectrogram. The discharge pulse starts at approximately 0.7 µs and is very short, but reaches above 300 MHz in the frequency domain. The opposite is the emission pulse from the inverter, which starts at approximately 2 µs. The duration of this pulse is longer compared with the discharge pulse, but it is far lower in the frequency domain. The amplitude of the inverter interference is also higher, which is shown by the darker colors. It should be noted that, in this case, the signals are also easily distinguished by their durations. However, pulse lengths may vary, making detection more difficult when comparing the pulse lengths. In this case, the comparison using also the frequency information is advisable.

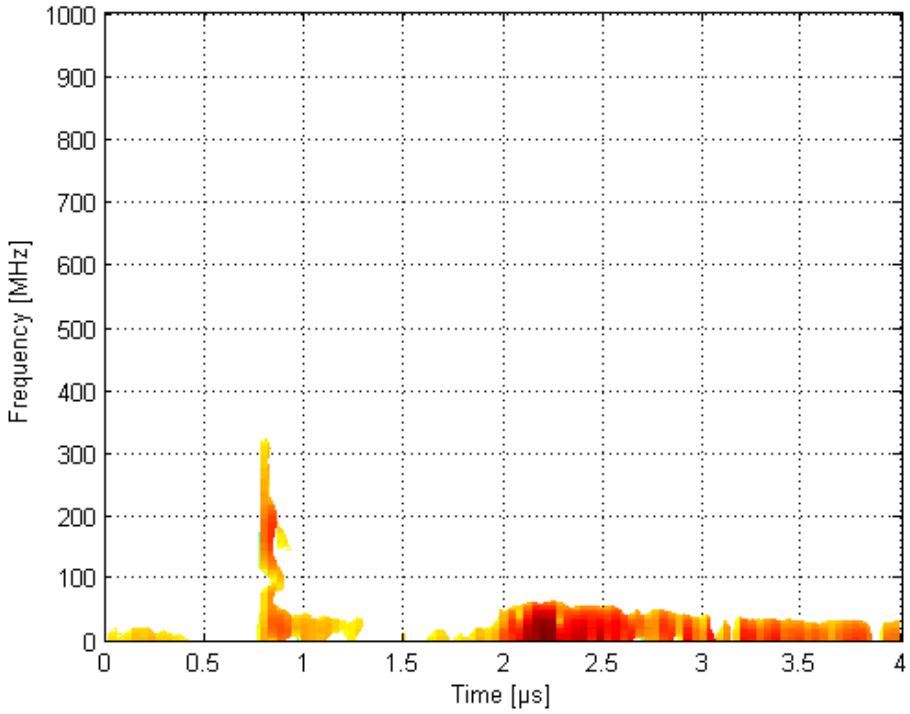

Fig. 3-8. Spectrogram calculated with STFT from the RF measurement presented previously in Fig. 3-5. A discharge pulse (at ~0.7 µs) can be distinguished from an inverter-generated pulse (starting at ~2 µs) by observing the spectral content of each pulse. The discharge pulse has a spectral content reaching up to 300 MHz, while the interference pulse is only close to 50 MHz. The inverter-generated pulse is also longer lasting and stronger in amplitude.

In the laboratory environment, there is no other significant interference source beside the inverter, because the laboratory is shielded against radio frequency interference from the outside. For this reason, filtering with the passive high pass filter introduced in previous section was found to be sufficient to mitigate the only source of interference present in the measurements. A typical interference source, in addition to the inverter-switching-generated interference, could be continuous transmission at a certain frequency or frequencies. This was not measured, but continuous transmission can be simulated to show how it differs from the transmission of impulses. The same measurement (see Fig. 3-5 and Fig. 3-8) is used, but a continuous transmission with a carrier frequency of 600 MHz is added. Depending on the amplitude of the continuous carrier wave transmission, it can overlap the discharge pulse and the inverter interference making them undetectable in the time domain. However, using STFT a spectrogram can be plotted to distinguish between the different signals. The spectrogram is shown in Fig. 3-9. The continuous signal can be seen at 600 MHz continuing over the whole sample, and it can be easily distinguished from the signals of the pulses.

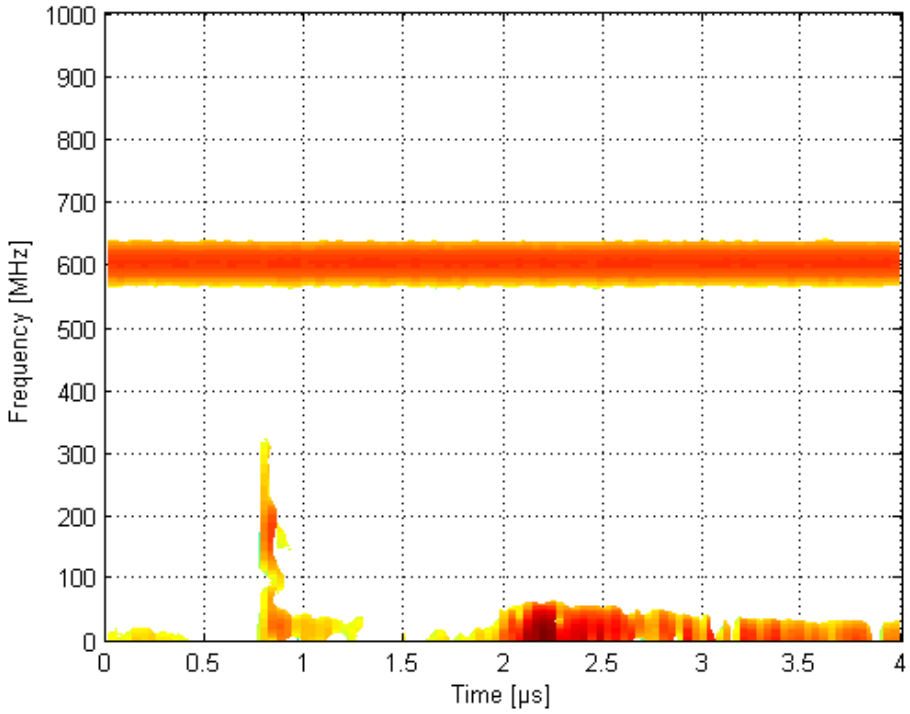

Fig. 3-9. Spectrogram calculated with STFT showing a continuous transmission at 600 MHz, a discharge in the bearing, and interference from the inverter switching. The continuous carrier wave transmission can be distinguished from the signals of the pulses as the transmission continues over the whole sample period.

3.4.3 Discharge activity calculation with envelope detection and pulse counting

It is now assumed that the filtered measurement contains only the signal from one discharge or multiple signals from multiple discharges. It is known that these signals are very short oscillating and decaying pulses, as was shown previously. Each pulse represents an individual discharge inside a bearing of an electric motor. In other words, each of the discharge pulses carries information on the bearing current flow. If there is a discharge in the bearing, there is also a flow of bearing current from the shaft to the frame. This is the case with EDM bearing currents, whereas other bearing currents can also flow in a different direction. As previously discussed in Section 1.4, it is likely that material is removed from the bearing races as a result of each of these discharge events. This suggests that it could be useful to detect and calculate the number of discharges to estimate harmfulness of the bearing currents. This approach is similar to electrical bearing stress discussed in (Muetze, 2006) and given in Eq. (1-6).

It has been noted that the pulse duration and the amplitude of the discharge signal vary considerably between different discharges. The reason for this is that the factors affecting the discharge are random and nonconstant. These include for example the lubrication film thickness, common-mode voltage, and temperature. The circuit parameters are dependent on the motor type and the length of the supply cables, as well as on the grounding arrangement. In

addition, the impact of the environment on radio wave propagation has been discussed above, and also multipath effect, which causes signal distortion, has been pointed out. A series of experiments showed that it is not possible to directly link the shaft voltage and the individual discharge emission amplitude together. This can be seen in the measurements presented in Section 4.3, where a constant shaft voltage is applied to the shaft of the test motor. For example, in Fig. 4-9 the shaft voltage is kept at 5 V, but the measured RF signal amplitude varies between the discharge events. The same applies to the bearing current. It is only certain that there is a bearing current if there is a discharge, but the peak amplitude of the bearing current remains unknown. The oscillation and the pulse duration of the received signal is affected by so many factors that it cannot be used as a good indicator of the shaft voltage or the bearing current amplitude.

A conclusion can be made that the exact moment at which a discharge occurs in a bearing can be detected with good accuracy, but it is difficult to say anything certain about the shaft voltage or the bearing current amplitude based on the RF emission amplitude, duration, or oscillation. However, it is obvious that the knowledge that there are sparking and bearing currents in the motor is useful, even though it is not possible to say anything about their magnitudes. By measuring the discharge activity during some time period, it is possible to know whether there are discharging bearing currents in the system. If bearing current mitigation techniques are to be applied, it is possible to compare discharge activity before and after installation to see whether there has been any change in discharge activity.

Discharge activity measurements are presented in Chapter 4. Some signal processing techniques are proposed in this section. It is assumed that the input signal only contains the discharge pulses after filtering. It is recommended that an envelope of the measurement signal is then taken. This can be achieved by first taking a square of the input signal. If necessary, some low-pass filtering can be applied. The threshold level can then be set to some specified value or just above the noise level. Pulses crossing this threshold level are then detected and counted. Because of the pulse distortion and oscillation there has to be a hold off period after each detection. If pulse length is considered, a hold off time between 50–250 ns is suitable to detect most of the pulses correctly. The idea is illustrated in the example shown in Fig. 3-10. The threshold level is now set to 10 mV. An enlarged version reveals that there are actually two discharges very close to each other.

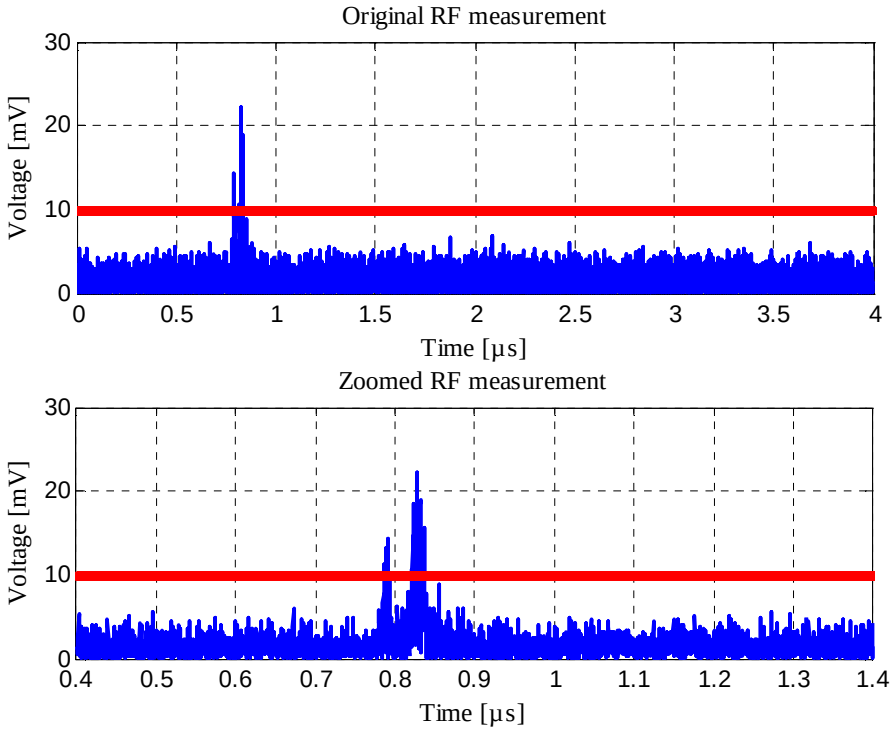

Fig. 3-10. Discharge activity can be measured by recording those pulses that are over some predefined threshold level. The enlarged version reveals that there are actually two discharges very close together, and therefore the hold off time has to be correctly set to detect all discharges.

3.5 Locating the sources of discharges

If multiple electric motors are in the same space, this raises difficulties in detecting the bearing currents when using the proposed method. The source can be any of the many motors, because if only one antenna is used, there is no easy way to identify where the emission is coming from. One possibility is to subsequently operate only a single motor at a time during the measurements. This is not desirable and in many cases not possible. A better option is to apply methods such as directive antennas and multiple antennas, which can be used to detect the source of radiation. Almost all available antennas are more or less directional. However, dipole and monopole antennas can be considered omnidirectional, while for example Yagi and horn antennas are more directional. The directivity of antennas can be improved with a reflector, which is typical in antennas used for satellite communication.

To achieve reliable detection, for example, to be able to identify the radiating motors out of the group of several motors would require an accuracy of approximately one meter. The frequencies from the emission are mainly below 1 GHz, meaning that the shortest wavelengths are ~30 cm. This would suggest that it is possible to detect the source of radiation with required precision. Directional antennas can also be used to decrease the interference from other sources, if the sources of interference are located in different directions than the electric motor under

inspection. Directional antennas also have a higher gain, and thus they could help to pick up weak emissions better than omnidirectional antennas.

According to (Vossiek, 2003), there are three different measurement principles for location detection: Angle-of-Arrival, Received-Signal Strength, and propagation-time-based systems. These are now considered in turn, when taking into account the nature of the discharge signals.

In the Angle-of-Arrival method, the position is calculated via goniometry (Vossiek, 2003). Detection of the radiating source can be carried out by using directional antennas or antenna arrays. The location of the measuring antennas is fixed and only the direction is varied. The direction to the radiating source is then evaluated from the receiving antennas. The location of the radiation source is at the intersection of several measured direction pointers acquired from different measurement points. The accuracy is limited by the directivity of the measuring antennas and the number of antennas or measurement points used for location. Multipath propagation can make the localization even more difficult, which has a greater impact with indoor measurements. Problems may also arise if the direction of the transmission source is to be located by determining the direction in which the signal strength is strongest. This would require a constant power and the transmitted signal to be continuous. Neither is true in the case of emission because of discharges in bearings. For these reasons, the practicability of the Angle-of-Arrival method can be questioned.

The Received-Signal Strength method is based on propagation-loss equations (Vossiek, 2003). In the simplest version of the method, knowing that the far field transmission loss is equal to $1/r^2$, the distance r can be calculated if the transmitted and the received power are known. Probably the simplest propagation-loss equation is Frii's equation that has been presented in Eq. (2-5). However, in indoor applications, the calculation of attenuation is more complicated because of multipath propagation and fast fading, as has been discussed in Section 3.2. To be specific, when detecting bearing sparking, the Received-Signal Strength method cannot be applied, because the transmitted discharge emission from sparking varies and is not known. With this method, it is possible to obtain some kind of indication about the location of the source, but it is impossible to say anything about the accuracy of the information.

Propagation-time-based techniques, such as the Time-of-Arrival method, estimate the distance of the source based on a calculation of the signal propagation delay between the transmitter and the receiver (Pahlavan, 2002). It is well known that radio waves travel in a free space at the speed of light, and in air only slightly slower than that. The time of arrival is measured from the phase of a carrier signal or directly from the arrival time of a wideband narrow pulse. The latter can be thought to be very similar to a pulse generated by a discharge in the bearings of a motor. In this case, the resolution is determined by the signal bandwidth (Pahlavan, 2002); and it also depends on how well the arrival time of the impulse can be estimated.

The applicability of the above-discussed methods for locating the discharges caused by bearing currents depends on several issues. Taking into account what was previously mentioned about the problems related to the Angle-of-Arrival and Received-Signal Strength methods, the only plausible method would be the Time-of-Arrival method. This of course depends highly on the required accuracy. The required resolution for the locating can be thought to be at least one meter, but in many cases a resolution of several meters is adequate. Basically, this means that the source of emission can be targeted at a single motor. This differs from partial discharge detection and sensor network location in that in the bearing current detection the source is known prior to locating, or there is at least an approximate of a possible source. In the case of bearing current (discharge) detection, it is possibly to obtain confirmation of the source of the

emission. In this case, the Time-Difference-of-Arrival method is very suitable. Two or more omnidirectional antennas can be placed around the expected source of radiation, each at an equal distance away from the source. It is recommended that there are no obstacles between the antennas and the source motor. Thus, the first pulse arriving at the antenna has propagated the shortest line-of-sight path. If the emission is detected at the exact same time at each of the antennas, it can be said that the source of emission is in the middle of the antennas.

The time-Difference-of-Arrival method was tested in a laboratory environment. Two similar omnidirectional antennas were used, and they were connected to the oscilloscope with cables of equal length. The specification of the equipment used is given in Appendix I. The distance between the antennas was kept constant at two meters, while their distances to the motor were varied. The oscilloscope channels were sampled simultaneously to detect the difference of the arrival times of a discharge pulse at each of the antennas. In the first measurement, both antennas were located at each end of the test motor one meter from the centre of the motor and two meters from each other. In the second measurement, the distance between the antennas was the same two meters as previously, but the antennas were moved so that the other one was 0.3 meters to the test motor, while the other one was 1.7 meters. The distances were measured from the centre of the motor shaft. These two test setups are illustrated in Fig. 3-11.

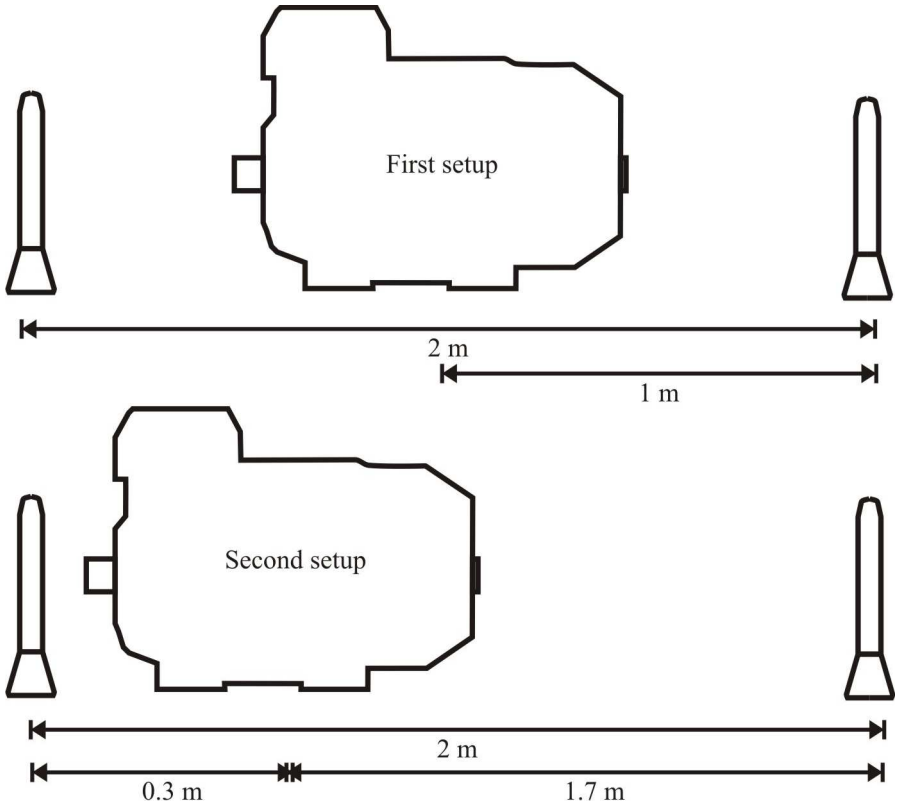

Fig. 3-11. Test setups for testing the applicability of the time-difference-of-arrival method. In the first setup, the measurement antennas were placed two meters apart from each other. The test motor was placed in the middle of the two antennas, and the distance to a single antenna was one meter. In the second setup, the antennas were moved so that the test motor was 0.3 meters to one antenna, while the distance to the other one was 1.7 meters. The distances were measured from the centre of the motor shaft.

The result from the first measurement is illustrated in Fig. 3-12. In this measurement, the distance to the centre of the test motor was the same for both antennas. It is clear from Fig. 3-12 that there is a significant difference in the pulse shapes and amplitudes detected with the two antennas even though they come from the same source and similar antennas were used. This is mostly due to the multipath effect, where the emission reflects from the nearby objects and, depending on the phase, increases or decreases with other reflections as was discussed in Section 3.2. This means that it is important to use only the first pulse that has propagated through a direct path to the antenna in the time-difference-of-arrival calculation. It is not clear from the original RF measurement what is the time-difference of the signals, and therefore some additional signal processing is required. In this case the signals were rectified and normalized. The processed measurement shows the beginning of the discharge emission enlarged. The received signals are also rectified to neglect phase differences, and the amplitudes are normalized to facilitate the comparison of the two signals. It can be seen that the first pulses arrive almost at the same time. The arrival time difference is approximately 1 ns. In distance this is about 30 centimeters, which is the same as the wavelength of the highest frequencies present in the discharge emission. In other words, the time difference of 1 ns is well between the limits of the accuracy that is possible to obtain with the frequencies present in the discharge emission. Taking this into account, it can be concluded that the source of emission is at an equal distance from each of the antennas, meaning that the source is the test motor between the antennas as expected. There is yet another possibility for the small time difference in the pulse arrival times. The antennas were placed equally away from the centre of the test motor. However, the discharge occurs in the DE bearing, which is somewhat closer to the one antenna than the other.

A series of other measurements was made, in which the location of the antennas was varied. The second measurement illustrated in Fig. 3-13 is an example of one of these. In this second measurement, one antenna was placed at the side of the motor, approximately 30 centimeters from the centre of the test motor. The other antenna was approximately 1.7 meters from the source motor, because the distance between the antennas was kept at a constant of two meters. This second test setup is also illustrated in Fig. 3-11. Again, the impact of the multipath effect is clear in the measurement plotted in Fig. 3-13. In the processed measurement, the received signal is rectified and normalized to facilitate the detection of the arrival time of the discharge pulse at each of the antennas. The time difference of arrival is now approximately 6 ns. This corresponds to the propagation difference of ~1.8 meters in distance. Taking the accuracy into account, this result is well in line with the information that the distance that the signal has to travel is 1.4 meters longer to the one antenna than to the other.

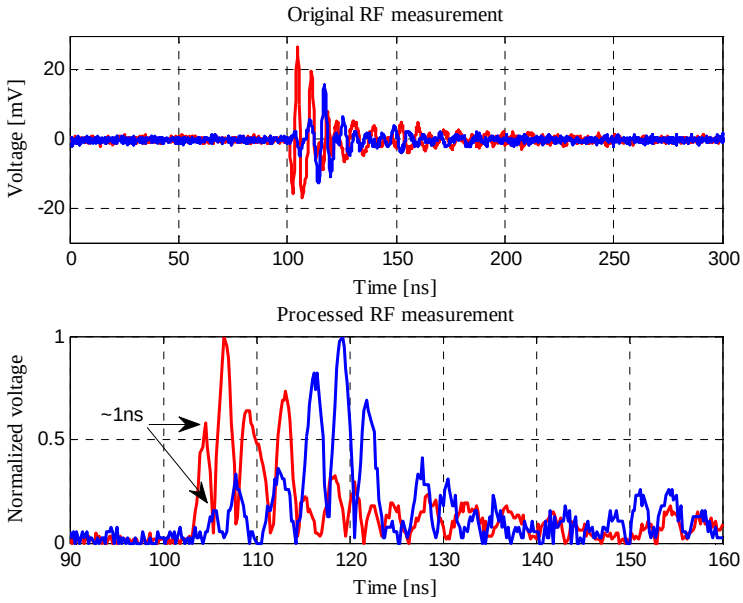

Fig. 3-12. In the first measurement, both antennas are placed at an equal distance from the centre of the test motor. The original RF measurement shows both signals as they are received at the antennas. The pulse arrives almost at the same time at both antennas. The time-difference-of-arrival between the signals is ~1 ns, which is within the range of accuracy.

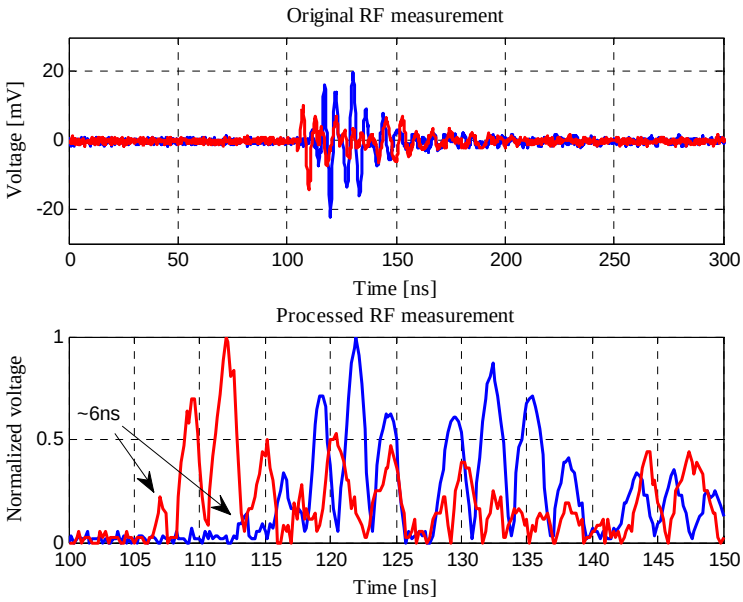

Fig. 3-13. In the second measurement, one antenna is placed next to the motor and the other antenna further away. The distance between antennas is kept at two meters, as in the previous measurement. There is now a significant difference in the arrival times between the two antennas. The time-difference-of-arrival between the signals is ~6 ns, which corresponds to the propagation distance of ~1.8 meters.

This example proves that it is possible to locate the source of the discharge within the required accuracy. The accuracy can be enhanced by adding more antennas or measuring from multiple locations. The challenge with this method is the determination of the arrival time of the impulse. The transmitted signal is not known, and as can be seen from this example, the distortion of the received signal caused by the multipath effect makes it hard to use techniques such as cross-correlation. There are more advanced signal processing techniques available, but these were not studied, because an in-depth analysis of the source location aspects was beyond the scope of this thesis. For a human being, it is relatively easy to determine the arrival time of the impulse, but automatic detection would require a more detailed investigation before being implemented into hardware. It might be possible to obtain reasonable accuracy if similar threshold detection were implemented as discussed previously in Section 3.4.3. However, it might be problematic to correctly set the threshold level so that it is always correctly triggered to the first impulse.

This example also proves that the source of the discharge is the test motor and not some unexpected other source. In this example, the shaft voltage was supplied to the test motor with an adjustable voltage source to avoid all possible interference from the inverter. However, similar measurements were carried out with a frequency-converter-driven test motor, and according to these it can be said that the source location is also possible in this case. More importantly, it is obvious that the source of the emission from the discharge is the test motor and not the frequency converter. The dimensions of the test motor are not large enough to determine the bearing in which the discharge takes place. For this reason, it is also uncertain whether this would even be possible, because it should be remembered that the frame of the motor is also part of the transmitting antenna.

3.6 Suggestions for real-time discharge detection

In this section, the possibility for real-time sparking detection is considered. The advantages are discussed and requirements for suitable hardware are given. The idea is to give some design suggestions for a measurement device to detect bearing currents using the method discussed in this thesis. The measurement data presented here have first been captured with an oscilloscope and processed with a computer. It is clear that this kind of an approach clearly limits the applicability of the presented method for several reasons: The activity of discharges can be calculated only from rather short periods of time that are limited by the memory of the oscilloscope or other data-recording devices. At higher sampling rates of a few gigasamples per second, the maximum sample lengths can be only several milliseconds with commonly available oscilloscopes. Short samples may not give a very good indication of the problem, because the dynamics of the system are presumably far longer in most cases. However, they are a sufficient to measure whether there are sparking and thereby bearing currents occurring in the system. If the RF method presented in this thesis is to be further studied, there is certainly a need for real-time discharge detection so that it is possible to monitor the discharge activity over longer periods of time.

Different approaches can be taken when designing a system for real-time sparking detection. The one chosen in this consideration is based on modularity, and lessons learned from measurements. The system can be roughly divided into the following sections, viz. signal capture, filtering/amplification, digitalization, additional signal processing, and detection. Each of these sections will be discussed subsequently. An overall layout of the proposed system is given in Fig. 3-14.

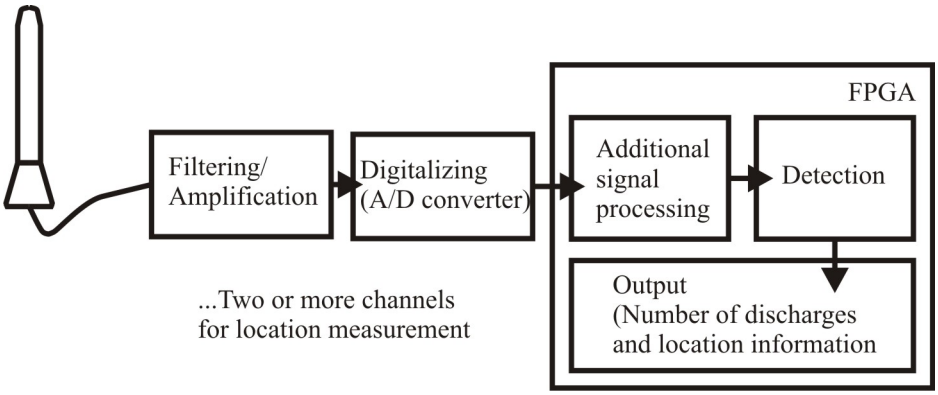

Fig. 3-14. Proposed layout of a real-time discharge detection hardware. It may consist of two or more directional antennas. Filtering and/or amplification are required before digitalization of the signal. An FPGA or alternatively a DSP can be used for real-time signal processing. The additional data processing includes more filtering, signal detection, and time difference of arrival calculation for signal source detection. The user obtains information of the source location and discharge activity.

An important part of the system is a sensor for signal capturing. Based on the results of this thesis, it is suggested that a highly directional antenna with a bandwidth of 50–500 MHz should be used. If accurate source locating is needed, then two or more antennas are required. The source for emission is typically known, and with a directional antenna it is possible to mitigate interference from other sources. Directional antennas also have a higher gain that helps to detect weak discharge signals. Multiple antennas and thus multiple channels will be required if location techniques are going to be applied.

It is possible to filter the data after sampling, but some filtering is basically mandatory before digitalizing the signal. The reason for this is that a discharge pulse can be significantly weaker than for example interference from an inverter. This can lead to poor resolution at analog to digital conversion, and most of the discharge pulse can be lost. A passive high-pass filter is highly recommended for this reason. A band-pass filter can be even a better choice to prevent anti-aliasing. According to the measurements, amplification before the digitalization is not mandatory. The discharge pulse is strong enough to be detected in a close proximity even without amplification. However, adjustable amplification can be useful to obtain maximum resolution when digitalizing the signal.

Conversion of the received analog signal to a digital signal is carried out with an analog to digital converter. Nowadays it is possible to acquire suitable A/D converters with a bandwidth of 400–500 MHz and a sampling rate of 0.8–1 gigasamples or more. An FPGA (Field Programmable Gate Array) is probably the most suitable choice for fast signal processing, where one or more channels are simultaneously processed. Another possibility is a fast DSP (digital signal processor). The requirements for the digital processing unit are that the unit has to be able to do the required signal processing in real time.

It is suggested that the operator of the device can adjust the threshold level as of which the discharge signal is detected. The same applies to the detection time, which should be adjustable. The operator may require feedback on the number of discharges detected, their levels, and possible location information. Additional signal processing such as different kinds of filters should be available to be chosen as preferred.

An alternative method for real-time detection of sparking is also proposed. Some commonly available fast oscilloscopes provide programmable trigger settings. Such an oscilloscope could be programmed so that it is triggering to the sparking, counting each individual discharge and then continuing after some holding time. The holding time has to be short enough to capture all of the discharges, preferably around 50–250 ns. This way the amount of data required can be kept low, because only the number of pulses is saved. It might be also possible to direct the trigger information to an auxiliary output where it can be recorded with a proper hardware.

4 MEASUREMENTS AND ANALYSIS OF DISCHARGES IN THE BEARINGS OF AN ELECTRIC MOTOR

In this chapter, a description of the equipment used in the measurements is given together with the measurements and their analysis. The test equipment is listed in Appendix I. The measurements are divided into three sections: Measurements with an adjustable voltage source, measurements with a frequency converter, and antenna analysis of the test motor with a network analyzer. The analysis of the measurements is given along with each measurement. The signal processing methods described in Chapter 3 are used to eliminate interference in order to detect the emission from the discharges. The main source of interference in these measurements is the frequency converter.

The objective of these measurements is to show that the RF method presented in this thesis works as the theory presented in Chapter 2 indicates. It is also studied how the method applies to the bearing current detection. Different parameters are studied; for example, the impact of the shaft voltage on the discharge emission is analyzed. The applicability of the method is shown with the test motor having insulated bearings to enable the bearing current measurement. This way, it is possible to compare the bearing current measurements with the results obtained with the RF method. Finally, it is shown that the RF method can successfully detect emission from the discharges from an unmodified motor, hence revealing whether bearing currents occur in the system or not.

4.1 Test system and measurement setups

For practical reasons, the thesis and measurements concentrated mainly on EDM bearing currents. This means that LV <20 kW motors were chosen for the tests. All the measurements were carried out at Lappeenranta University of Technology. The laboratory where the measurements were realized is shielded with copper plates built into the laboratory walls thus forming a Faraday gage, so that RF interference from outside is effectively blocked. The measurements are not performed in a radio anechoic chamber, and a strong multipath effect is present. This naturally has an effect on the results as was discussed in Section 3.2. However, this is closer to a real situation in which motors are located in an industrial environment typically full of steel structures that act as reflectors. The multipath effect has a high impact on the measurements, distorting the received signal. However, the multipath effect does not influence the detection of discharges caused by bearing currents. For these reasons, the results presented in this chapter can be used to prove the applicability of the RF method for detecting bearing currents from electric motors.

The test setup consists of a three-phase delta-connected 15 kW 4-pole LV induction motor that is used as a primary test motor in most of the measurements throughout this chapter. Another similar motor is used to drive the test motor in the measurements with an adjustable voltage source presented in Section 4.3. The drive motor is unmodified, and it is used as a test motor in the measurements presented in Section 4.4.2. The motors are electrically isolated from the ground and from each other. Thereby, it is easier to control and measure different voltages and currents in the motors this way. The driving motor is directly connected to the mains, if not otherwise mentioned. The primary test motor has well-insulated bearings. The insulation consists of a one centimeter thick Polyethylene (PE) plastic ring between the outer ring of the bearing and the frame of the motor. The insulation can be bypassed with a jumper cable to measure the bearing current. Both bearings have similar insulation and jumper attachments. An adjustable DC (direct current) power source and a copper brush are used to charge the shaft and the bearing capacitances by injecting electrical charges onto the shaft of the motor. To reduce

the effect of the power source, a ballast resistor with a value of 3.3 kΩ is installed between the brush and the power source. In the measurements presented in Section 4.4, a frequency converter (ABB ACS400 series) is used. In these measurements shaft voltage is generated as discussed in Section 1.3.2.

The main part of test setup is illustrated in Fig. 4-1 without the measurement equipment or the frequency converter. The test setup is based on the setup presented in (Stack, 2005), in which a similar system was successfully used to generate accelerated bearing faults. An external power supply was used to generate the shaft voltage, and the bearing condition was monitored with vibration measurements (Stack, 2005).

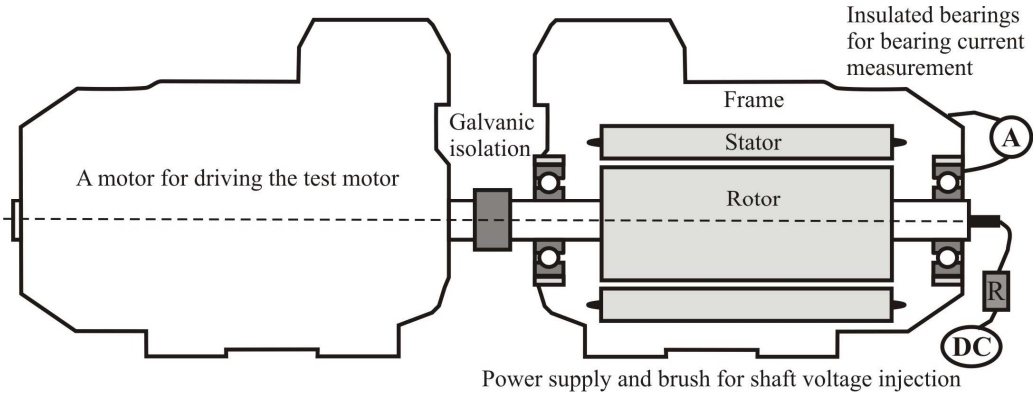

Fig. 4-1 Test setup consisting of two similar three-phase delta-connected 15kW 4-pole LV induction motors. The shaft voltage is generated either with an adjustable DC power source and supplied to the shaft with a brush through a ballast resistor, or a frequency converter is used. The bearings of the primary test motor are insulated with PE plastic rings. The insulations can be bypassed with a jumper for bearing current measurements. The test rig is electrically isolated from the ground, and the motors are isolated from each other.

An image of the test setup is shown in Fig. 4-2. With the test setup, it is possible to measure the shaft voltage and the bearing currents with variable shaft voltages and with the frequency converter operation. The common-mode voltage was measured via an artificial star point as described in Section 1.5. The common-mode voltage can be measured between this point and the ground connection. In most of the measurements presented in this thesis, a wide-bandwidth log periodic antenna has been used. This can also be seen in Fig. 4-2. In all of the measurements, except in the measurements presented in Section 3.5, the antenna is located at the side of the test bench directly perpendicular to it. This differs from Fig. 4-2, where the antenna is placed at the end of the test bench to fit the whole setup in the image. In the measurements presented in Section 4.5, the location of the antenna is varied in order to measure the radiation pattern of the motor.

The distance from the test bench to the antenna is kept constant at one meter in all of the measurements presented in this thesis except for localization measurements presented in Section 3.5. The distance was chosen based on the assumption that the discharge emission is mainly concentrated above 100 MHz. At these and higher frequencies it can be assumed that measurements at distance of one meter are mainly measured in the far field region. The method was verified as far away as three meters and was found to be working at this distance as well. However, at these distances the signal levels are weaker and additional amplification would have been required. For these reasons, the measurements presented in this thesis are performed

one meter away, measured from the centre of the motor to the tip of the antenna. The distance to the frequency converter from the test bench is three meters and approximately four meters to the antenna. The cable connecting the motor and the frequency converter is four meters long, symmetric, and shielded.

Fig. 4-2. Image of the test setup showing the motors used in the measurements and the wide-bandwidth log periodic antenna.

The log periodic antenna is used in all measurements, except for the location measurements presented in Section 3.5, where two similar monopole antennas were used. The log periodic antenna has a bandwidth of 200–2000 MHz. The antenna works also at lower frequencies, but the manufacturer has not given any specifications for frequencies below 200 MHz. The interest in most of the measurements is in the bandwidth of approximately 100–500 MHz. Hence, this is in line with the antenna-specified range. The size of the antenna is moderate (maximum length 85 cm and weight 2 kg), and it can be easily moved to different locations. The antenna is also highly directional and has an average gain of 5 dB to the direction of the main lobe. It should be mentioned that a two-meter coaxial cable with a characteristic impedance of 50 Ω was used between the antenna and the oscilloscope, both matched to 50 Ω. The voltage is measured over this input impedance.

List of the equipment used in the tests is given in Appendix I.

4.2 Challenges when measuring discharges

The frequency range of the emissions generated by the sparking is wide, reaching from a few megahertz to several hundred megahertz. The pulses from the bearing sparking are short, lasting only tens of nanoseconds. Interference from an inverter can have a far stronger maximum amplitude than the emission from the sparking. These are issues that have to be considered

when requirements for the measuring equipment are set. It is possible to use a spectrum analyzer to detect high-frequency emissions that indicate possible sparking and bearing currents. However, random nonperiodic processes may be difficult to capture correctly with certain types of spectrum analyzers. Therefore, real-time spectrum analyzers are needed for accurate detection instead of traditional frequency-sweep-based spectrum analyzers. High-sampling-rate oscilloscopes, which can be used to capture the signal, are commercially available, and the spectrum can then be calculated with FFT from the recorded data. With time-domain measurement, it is possible to detect discharge pulses and calculate their number of occurrence within a certain time to obtain an indication of the activity of bearing currents, as was discussed in Section 3.4.3. With the oscilloscope measurement, special attention has to be paid to the sampling rate required to fully capture the discharge emission, which leads to large amounts of data. Memory limits the length of samples to a few milliseconds with sampling rates of 1 Gsamples/s or above. Furthermore, handling large datasets, for example digital filtering with a computer takes time, and for real-time signal processing a different hardware is required. Suggestions for such of hardware have been discussed in Section 3.6.

There are some issues that have to be taken into account when discussing the repeatability of the measurements. Most importantly, a discharge in a bearing is a random phenomenon, which depends on multiple issues, such as common-mode voltage, shaft voltage, lubrication thickness, parasitic capacitances, the position of the bearing rollers, dynamics of the load, and temperature, just to name a few. With an adjustable voltage source, the shaft voltage can be kept constant. This is done in the measurements presented in Section 4.3, but because of the rolling bearings, the lubrication thickness varies constantly and discharges occur randomly. With a frequency converter, the situation is more complicated, because the charging of the shaft voltage cannot be predicted. The discharges occur randomly and each discharge is different from the previous one. For this reason, the transmitted emissions from the discharges vary in amplitude and length. The received emission at the receiving antenna is even more distorted because of multipath propagation as was discussed in Section 3.2.

In addition, yet another issue influencing the measurement results is the effect of the environment. In a real situation, there is always some kind of interference present, as was discussed in Section 3.3. In these measurements, there is no additional external interference, because the laboratory is well protected against RF interference from the outside. There is only interference from the frequency converter, which has been previously discussed, and interference from the measurement equipment, which can be considered negligible. The multipath effect caused by the surroundings is probably the main reason for the variation and distortion in the received signals.

In the measurements with an adjustable voltage supply, a brush connection is used to inject the voltage to the shaft of the test motor. This is shown in Fig. 4-3. A ballast resistor is used to reduce the effect of the voltage source on a discharge event. However, it should be noted that the impedances of the brush connection, cabling, and the voltage source will have an effect on the bearing current and on the shaft voltage at the instant of a discharge. It can be assumed that part of the bearing current oscillation during the discharge is due to these impedances. The brush connection is designed to be free of sparking that would interfere with the RF measurements. The cabling to the brush is a coaxial cable to decrease the radiation from the cable. Similarly, the jumper used to short the insulation was made as short as possible to decrease its effect as an antenna. The length of the jumper was five centimeters long including the connectors.

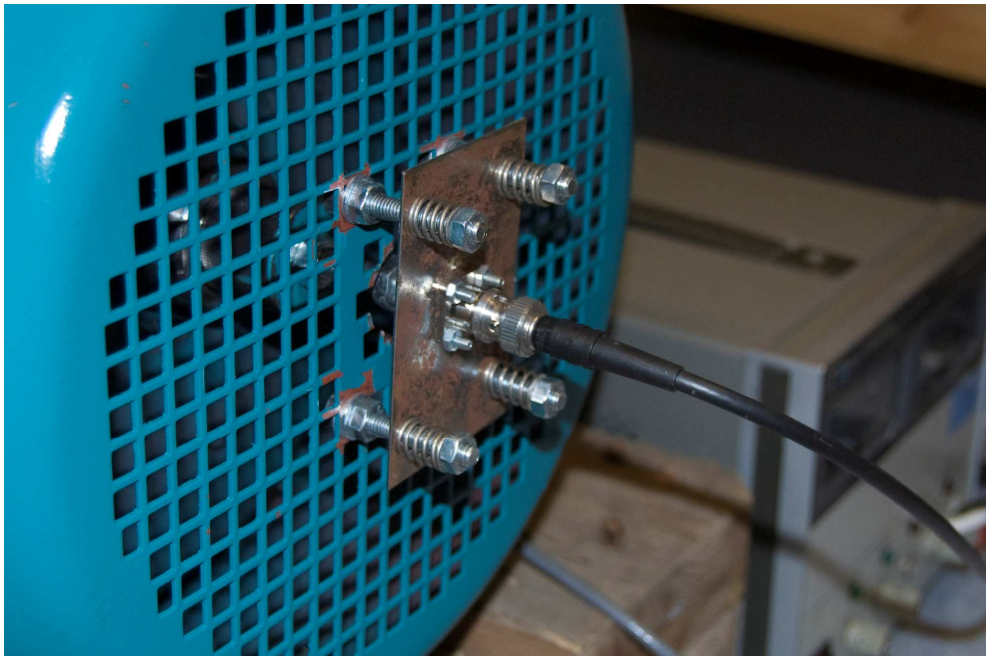

Fig. 4-3. Spring-loaded brush connection for injecting shaft voltage to the shaft of the test motor with an adjustable voltage source. The coaxial cable is used to decrease radiation from the supply wire. There is also a ballast resistor between the brush connection and the voltage source to reduce the effect of the voltage source on a discharge event.

In most of the measurements, only the insulation at the bearing at the DE was shorted, while the other end remains insulated. This was done for several reasons: The number of simultaneous measurements is reduced, because the current has to be measured only at one end. This leads to less data to be handled. The effect of shorting the insulation only at one end is that the bearing currents can then only flow through this bearing. It is then known that the discharge always occurs in this bearing. It is possible that the total number of discharges is reduced, because the discharge can occur only at the shorted bearing. In addition, circulating currents in the motor are eliminated. There cannot be any rotor ground currents either, because the motors are grounded only out one point and there is an insulated coupling between them.

It was stated earlier that the focus in this thesis is on EDM bearing currents. The reason for this is that it is assumed that the method studied here is applicable to all kinds of bearing currents if they also generate sparking, meaning that there are electrical discharges in bearings that cause arcing and thus melt the bearing races. So it is sufficient to prove the applicability of the method in the case of EDM bearing currents. Another reason is that according to previous studies (Binder, 2008), EDM currents are the main bearing current type occurring in LV motors of the frame/motor size used in the tests. High-frequency circular bearing currents are mainly problematic in machines larger than the test motor and especially MV and HV machines. Rotor ground currents depend on how grounding issues are taken into account, and with a good grounding, they can be avoided. Capacitive currents are generally considered harmless, and they are therefore not discussed further here. Even if the second bearing is insulated, it is possible that there are capacitive bearing currents in the shorted bearing. This was previously shown for example in Fig. 3-5.

4.3 Measurements with an adjustable DC voltage source

In this section, measurements with the test motor and an adjustable voltage source are presented. The emission radiated from the motor when different voltages are applied to the shaft of the test motor is shown. The shaft voltage and bearing currents are also measured during a discharge, and their behavior is analyzed. The activity of discharges (bearing currents) is investigated with different shaft voltages. The reason why these tests are carried out without a frequency converter is that it is thereby possible to measure discharges without filtering and to vary the shaft voltage and study its effect on the bearing currents and on the received emission.

The target of the first series of measurements with the test setup was to identify whether the emission from the discharge inside the bearing in an electric motor is similar to the one predicted in Chapter 2. The log periodic antenna was located one meter away at the side of the electric motor under test. The bearing insulation at the drive end was short circuited with a wire loop, and the other end was left open. A voltage of 5 V was applied to the shaft with an adjustable DC source and a brush connection (see Fig. 4-3). The test motor was running at nominal speed during the measurements and driven by the line-driven motor.

In Fig. 4-4, one result from the measurements is illustrated, showing the discharge emission captured with the antenna and the calculated spectrum. The recorded RF emission from the discharge in the bearing of the test motor is very similar to the emission recorded from the EDM tool shown previously in Fig. 2-8. The pulse lasts approximately 100 ns, but this can be assumed to be mostly due to multipath propagation. The actual discharge can be approximated to be no longer than 5 ns. A spectral density estimate with a periodogram was calculated from the measured data to obtain an approximation of the frequency content of the discharge emission. The estimated spectrum is also plotted in Fig. 4-4. The frequencies reach up to 300 MHz, and the signal power is mostly concentrated between 100–300 MHz. The highest power density is around 200 MHz. This result is very similar to the estimation presented in Chapter 2. Later, in the measurements with the frequency converter, a high-pass filter is used to filter frequencies below 90 MHz, and therefore these frequencies can be neglected.

When these results are compared with the results obtained with the EDM tool and previously shown in Fig. 2-8, it can be observed that there are some differences. The frequency content of the discharge pulse from the EDM tool is significantly higher, reaching up to 700 MHz, while the frequency content of the discharge pulse in the case of the test motor reaches only up to 300 MHz. There are three significant differences between these two pieces of hardware. Firstly, in the case of the EDM tool, the medium where the discharge occurs is air, whereas in the bearings of the electric motor it is oil/grease. The permittivity of oil is 2–5, while that of air is 1. However, in this case, the rise time of the current pulse should be higher in the oil because of the higher permittivity, meaning that the frequencies are higher in the case of a discharge in the bearing. Secondly, the inner electric circuitry of the EDM tool and the motor are very different. This means that parasitic capacitances and inductances of the electric motor have an impact on the rise and fall times of the bearing current pulse. This also includes the impact of modifications made to be able to measure the current from the bearing of the motor. Thirdly, the motor is a very different kind of antenna compared with the EDM tool. The motor antenna parameters are studied and measured in Sections 2.5 and 4.5, but it is not studied how the EDM tool works as an antenna. It is possible that the EDM tool transmits high frequencies better than the motor frame. For these above three reasons, it seems that the spectrum of the discharge is mostly limited by the electrical parameters of the motor and the motor parameters as an antenna.

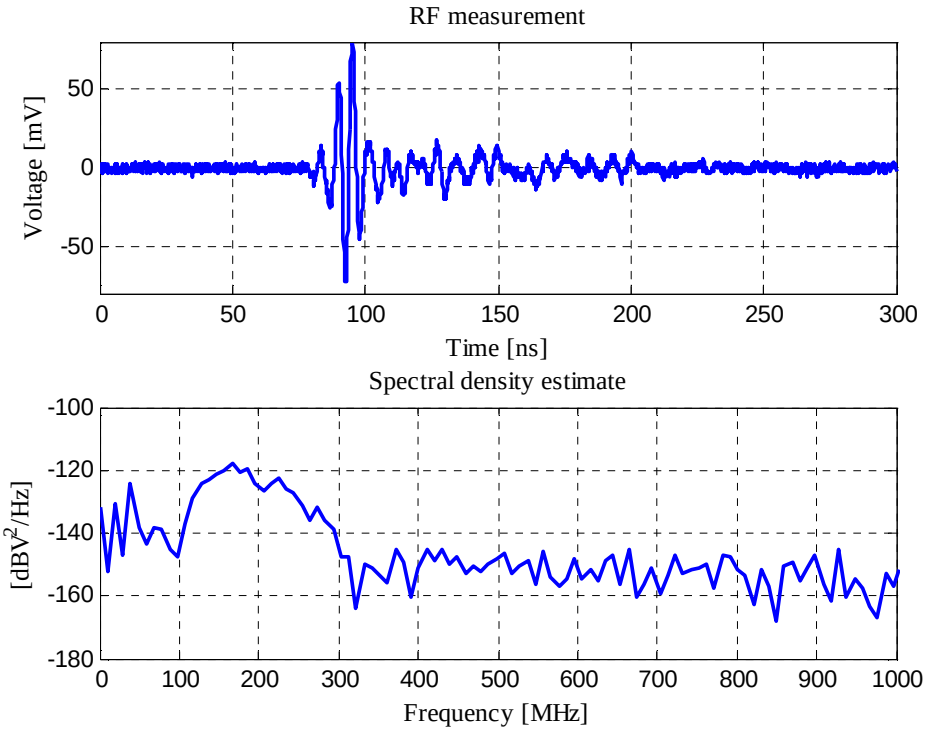

Fig. 4-4. Single discharge inside a bearing of the test motor measured with an antenna that is located one meter away from the motor. The discharge quickly generates a decaying oscillating pulse that lasts approximately 100 ns. A spectral density estimate by a periodogram is calculated from the measurement to determine the frequency content of the signal. Most of the signal power is concentrated between 100 and 300 MHz.

It is not possible to detect visually the spark inside a bearing of the test motor. Hence, the origin of the emission plotted in Fig. 4-4 remains still somewhat unknown. For this reason, a current measurement was added to the jumper shorting the bearing insulation at the DE bearing of the motor. The current probe TCP202 was used to measure the current through this jumper as shown in Fig. 4-5. The insulation at the NDE bearing was left open so that all bearing currents flow through the jumper at the DE bearing. Five volts was applied to the shaft and the motor was running at nominal speed. The result of the measurement is shown in Fig. 4-6. At the moment when the shaft voltage discharges, the current pulse reaches 170 mA and then quickly decays. The current strongly oscillates, which is probably mostly due to the impedances of the adjustable power source, cabling, and the brush. The somewhat limited bandwidth (DC–50 MHz) of the current probe may have some effect on the results by attenuating the highest frequencies. However, according to these results, it can be said that the bearing current and the discharge constitute the source of the emission received with the antenna. It should be also pointed out that this measured current gives only some indication of the actual current flowing inside the bearing. In (Muetze, 2007) it is shown with help of model the difference between the detected current and the actual current inside the bearing.

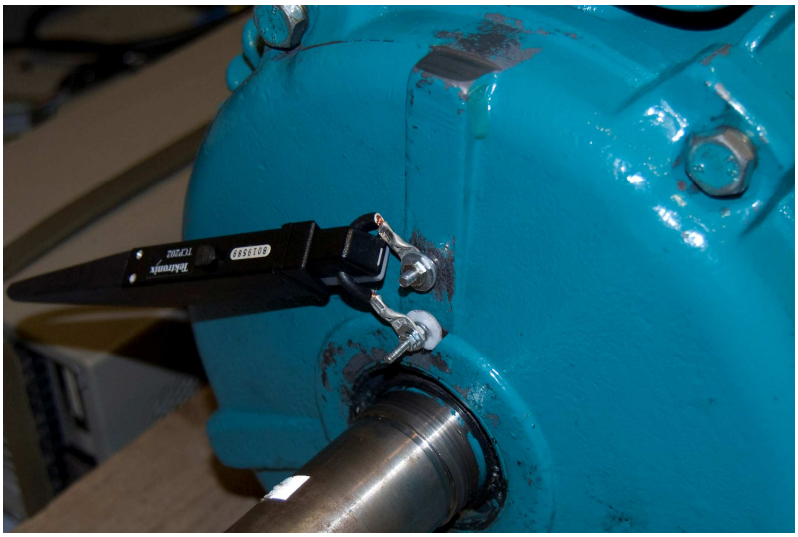

Fig. 4-5. TCP202 current probe is used to measure the bearing currents through the jumper cable that is used to short the bearing insulation at the DE bearing of the motor.

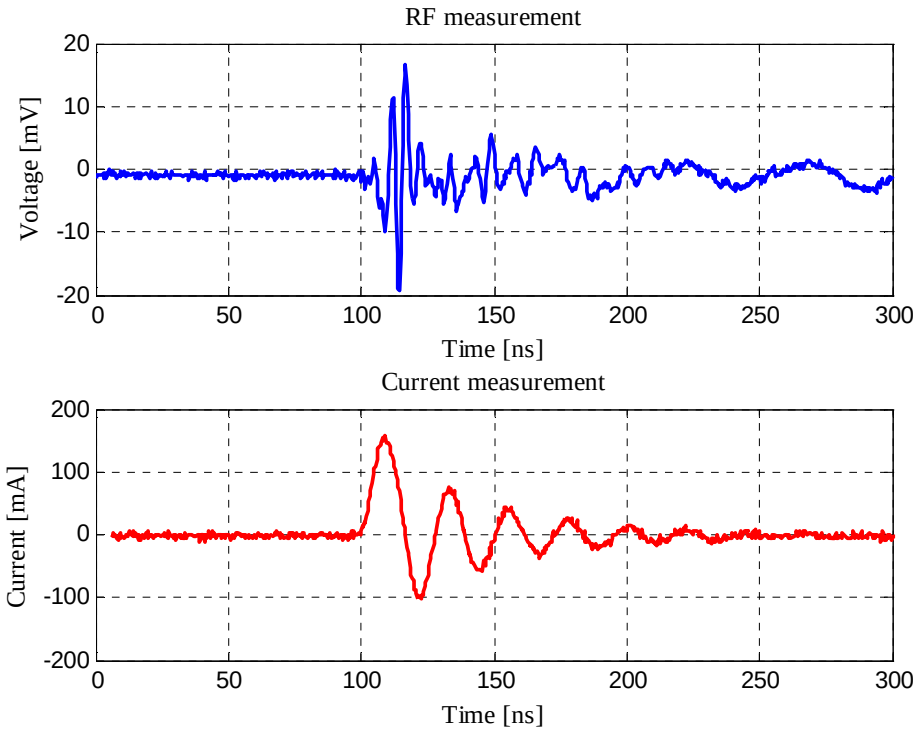

Fig. 4-6. RF emission from the discharge measured with an antenna and the simultaneously measured bearing current are obviously linked together. With a shaft voltage of 5 V, the bearing current reaches 170 mA. The current oscillates, which is probably due to the internal impedances of the motor, the brush connection, the jumper cable and the voltage source.

For the next tests, a shaft voltage measurement was added to monitor also the shaft voltage during the discharge. As mentioned above, the shaft voltage was generated with a DC power source and supplied to the shaft through a 3.3 kΩ ballast resistor and a brush connection. The shaft voltage was measured from the brush connection. The voltage applied to the shaft was kept at a constant of 5 V, and the motor was running at nominal speed during the measurements. Two similar measurements are presented in Fig. 4-7 and Fig. 4-8. At first sight, it seems that a discharge can be recognized from the shaft voltage. For example, in Fig. 4-8 both discharges coincide with a clear drop in the shaft voltage. However, in Fig. 4-7 approximately at 78 ms a discharge occurs, but there is only a minor drop in the shaft voltage. According to these results, it seems that the shaft voltage cannot be used as a reliable indicator of bearing currents and discharges. However, the voltage source together with connections needed for voltage and current measurements certainly has an impact on these results.

The situation becomes even more complicated when the source of shaft voltage is a frequency converter, which generates a nonconstant shaft voltage. The shaft voltage varies according to the common-mode voltage and it is determined by the capacitive voltage divider as discussed in Section 1.3.2. For example, it was shown in Fig. 2-5 how the shaft voltage mirrors from the stator common-mode voltage. It is also possible to obtain some indication of the EDM bearing currents by simultaneously measuring the common-mode voltage and the shaft voltage. Typically, the shaft voltage follows the common-mode voltage, but if there is a strong discharge, such as in Fig. 4-7 at 20 ms, the shaft voltage differs from the common-mode voltage waveform. Of course, there is not necessarily a discharge, but there can be a momentary contact between the rollers and the rings of a bearing, which grounds the shaft. This would discharge the shaft, but without generating sparking and high frequency emission. It should be kept in mind that this method is applicable only to detect EDM bearing currents. Circulating currents and rotor ground currents are practically impossible to detect this way, because in their case the common-mode voltage and the shaft voltage are not similarly linked together.

In these measurements (Fig. 4-7 and Fig. 4-8), the bearing current is also measured. At the supply voltage of 5 V for the shaft, the largest currents measured had amplitudes close to a half ampere. It was also noted from several measurements conducted, that the amplitude of the emission recorded and the amplitude of the current pulse do not necessarily correlate. For example, the bearing current pulse with a high magnitude can generate a discharge emission that is low in amplitude or vice versa. This can be seen from Fig. 4-7. However, in Fig. 4-8, the situation is different, the discharge emission with a higher amplitude correlates with a current with a higher magnitude. There can be different reasons for different bearing current amplitudes; one of them is the fact that the distance between the rollers and the races vary, and thus the current channel during the discharge varies. It is probable that also the roughness of the bearing races has an impact on the current amplitude. The conclusion is that the bearing current amplitude is random during the discharge. There is an upper limit to the bearing current that is determined by the maximum shaft voltage and parasitic capacitances. For these reasons, this limit for bearing current is individual for different motors and also depends on the frequency converter.

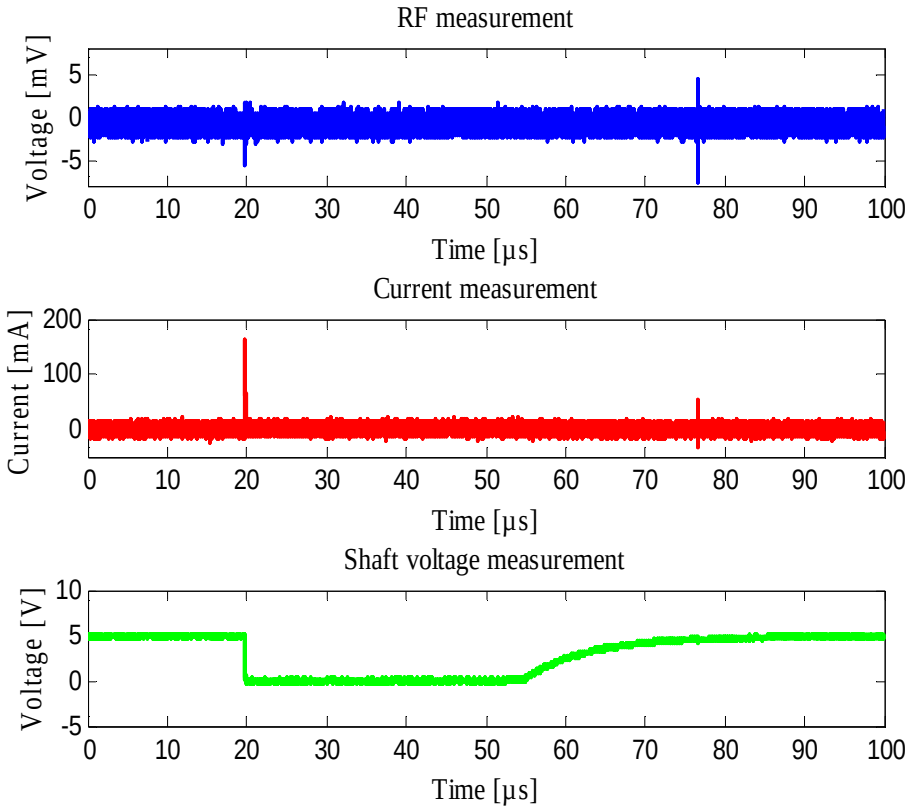

Fig. 4-7. Two discharges measured with an antenna, but only during the first one the shaft voltage drops to zero. The radiated emission is stronger, but the bearing current through the bearing is weaker during the latter discharge than during the first one.

It is important to remember that it is not possible to make any comparison between different motors based on the discharge emission magnitude only, because it is no information how well the different motors radiate the discharge signal. The situation is even more complicated because of the multipath effect that distorts the emission signal. Some comparison can be made between different discharges from the same motor if the receiving antenna is kept at the same place and there are no obstacles between the motor and the antenna. For a better accuracy, reference measurements, such as voltage and current measurements, are needed. However, it is shown in Fig. 4-9 that even if the shaft voltage remains constant, there is a lot of variation in the discharge amplitude. The reasons for this are also partly unknown as is the case with the bearing current amplitude. The breakdown voltage of the lubricant film probably has a high impact on this behavior, because it is not constant; when the threshold level is lower, a smaller shaft voltage is required to discharge through the lubricant film, which causes a smaller discharge emission and vice versa.

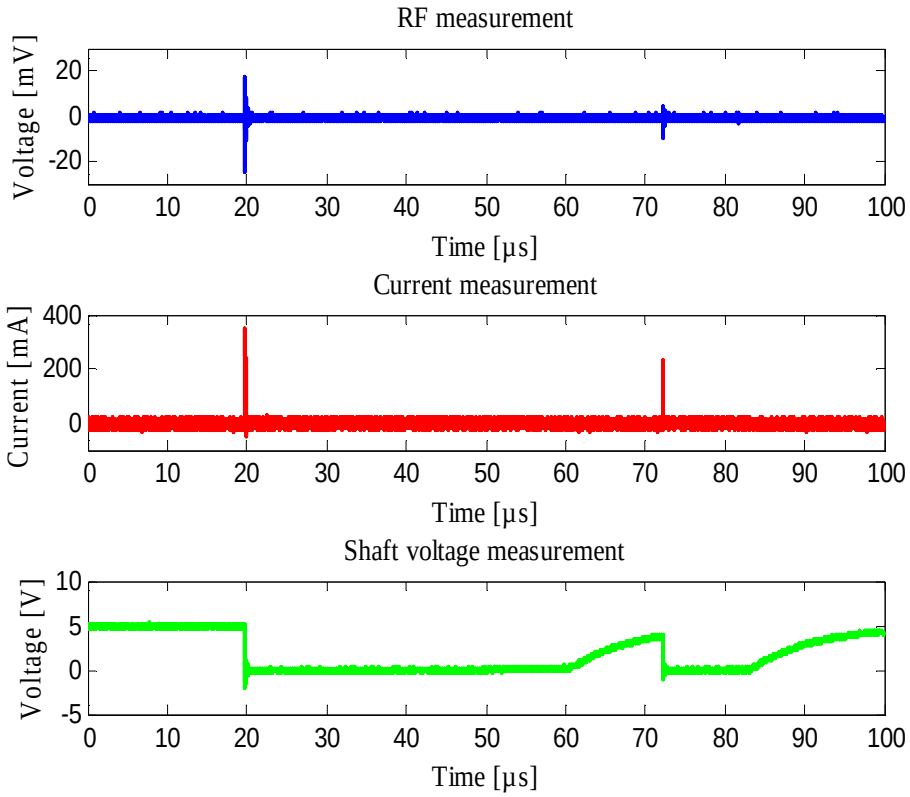

Fig. 4-8. Two discharges measured with an antenna. The shaft voltage drops to zero during both discharges. The radiated emission and also the bearing current are stronger in the first discharge than in the latter one.

The previous measurements have shown only one or two discharges, and thus they do not give any indication of how often discharges occur inside a bearing. Fig. 4-9 shows a 10 ms measurement, with the shaft voltage adjusted to 5 V. It can be seen that multiple discharges occur within a short period. This raises a question whether it is possible to obtain an indication of how harmless the bearing currents are by calculating the amount of discharge pulses during some time period, as was discussed in Section 3.4.3. This was not elaborately tested in this study, but in the next measurement the effect of the shaft voltage on the discharge activity was measured and analyzed. In order to be able to verify the relationship between a bearing damage and discharge activity, a series of considerably longer measurements would be required. This would require running the motor several days/weeks or preferably till the bearings fail, which can take much longer time. The number of discharges should be calculated over this whole period, and the bearings should then be opened and investigated. However, this was not realized in this thesis because there was no suitable measurement device available to continuously measure discharges for such a long time (see Section 3.6).

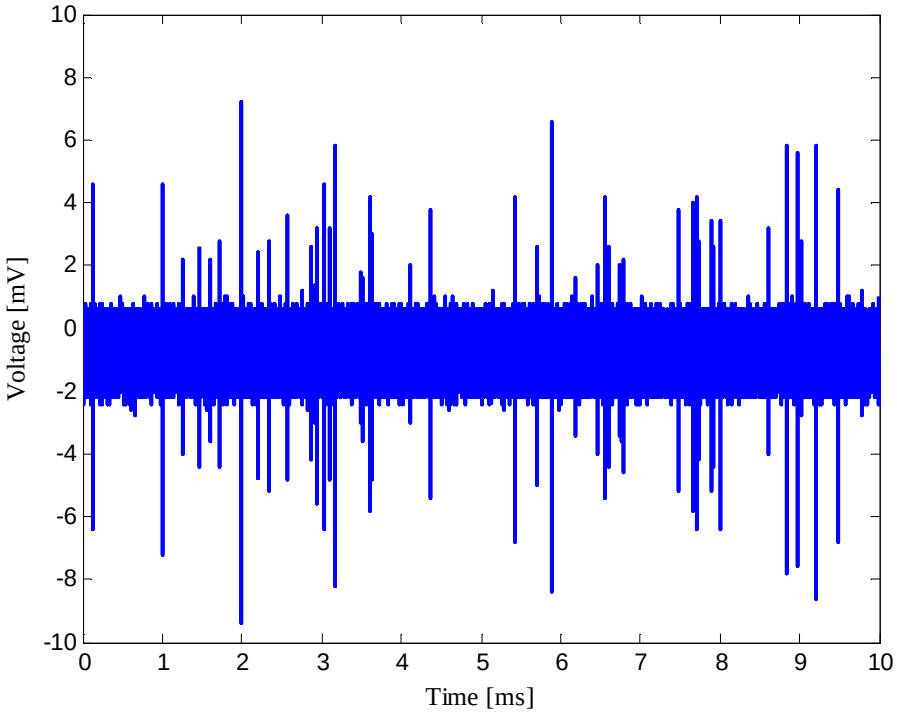

Fig. 4-9. 10 ms measurement showing high discharge activity at a constant shaft voltage of 5 V. Every peak above the noise level indicates an electrical discharge through the bearing of the test motor.

In (Muetze, 2006), it is stated that if the bearing current amplitude, or more specifically, the calculated local bearing current density exceeds a certain value, the bearing current can be considered harmful. As indicated by the previous measurements, it is not possible to accurately predict the amplitude of the bearing current by measuring the amplitude of emission from the discharge. It can be seen, for example, from the previous measurements presented in Fig. 4-7 and Fig. 4-8 that there is no direct relation between the current pulse amplitudes and the measured emission amplitudes. Even if the current amplitude can be measured, it has not been possible to predict the available lifetime of the bearing based on current measurements. The estimated bearing current densities can be used only to indicate the harmfulness of the bearing currents. The same applies to the shaft voltage. As the previous measurements have shown, it is not possible to accurately predict the shaft voltage amplitude by measuring the RF emission from the discharge. Furthermore, it is not possible to predict the bearing lifetime even if the shaft voltage is known. Basically, the only thing that can be said about the shaft voltage is whether it is above a certain threshold that might cause bearing currents in the system. As low shaft voltages as 200 mV are proposed for this threshold level (Prashad, 2001). If the shaft voltage exceeds this, there is an increased risk for bearing currents in a motor. The measurements with different shaft voltages have shown that if the shaft voltage of the test motor is over 2 V, measurable discharge emissions and bearing currents constantly occur in the bearings of the test motor. The threshold level is not very accurate. It was noted that when the shaft voltage was between 1.5–2 V, sometimes, discharges occurred in a bearing as well. At lower shaft voltages, no discharges were detected with the RF method or current measurement.

According to (Muetze, 2006) and (Preisinger, 2001), a discharge inside a bearing can melt a micro crater into the bearing race. Eventually, multiple craters and the dynamic effect caused by the movement of the rollers can lead to a bearing failure. This leads to the conclusion that every discharge can form a micro crater and can be considered potentially harmful as was discussed in Section 1.4. However, it is not yet sure whether all the discharges have enough energy to melt a crater in the bearing ring. An assumption can be made that it is maybe more important to record the occurrence of discharges than the shaft voltage or the bearing current amplitude. This approach is similar to electrical bearing stress discussed in (Muetze, 2006) and given in Eq. (1-6) and was discussed previously in Section 3.4.3

To further analyze the relationship of shaft voltage, current amplitude, and activity of discharge pulses, a series of measurements was conducted. In these measurements, the bearing at the DE was shorted with a jumper, and the bearing current measured using the current probe. The limited memory of the oscilloscope and the high sampling rate limited the length of samples to 3.2 ms. The shaft voltage was varied with an adjustable voltage supply. Shaft voltages between 0–50 V were investigated. The measured data were processed afterwards, and the number of discharges detected with the signal processing techniques discussed in Section 3.4.3. From the current measurement, peaks over 20 mA and 100 mA were detected. The results are presented in Table 4-1. Note that current pulses with amplitudes over 100 mA are also included in the column with the number of current pulses over 20 mA.

According to these results, it seems that the shaft voltage does not have a significant effect on the discharge activity between 2.5–30 V. When the shaft voltages exceeded 30 V (measured with 40 V and 50 V), the number of discharges grew exponentially. The number of discharges at these higher voltages was over hundred, and these are not included in the table. It seems that the threshold level of the lubricant film was constantly exceeded. At shaft voltages below 1.5 V, no discharges were detected. The voltage level at which discharges were starting to occur was approximately between 1.5–2.5 V. It is important to note that even though the threshold level was set just above the noise level, more bearing current pulses were detected with the current measurement than with the antenna measurement. The reason for this is that some of the discharges were too weak to be correctly detected. With higher shaft voltages, the case is different, and more impulses were detected with the antenna than with the current probe. In this case it is probable that there are also discharges that are too short/weak to be detected with the current probe.

The short sample lengths are problematic and might have an effect on the accuracy of the results, but it seems that the position of the rollers of the bearings and the lubrication thickness at a certain moment has a stronger effect on the discharge activity than the shaft voltage. It was noted that when raising the shaft voltage, the emissions from the discharges were generally stronger. With a higher shaft voltage, currents with a higher amplitude were recorded. It can be assumed that higher shaft voltages are more harmful, because more energy is released, but the discharge activity is not necessarily directly dependent on the shaft voltage. This applies as long as the shaft voltage stays within certain limits. This means that there is probably some upper limit at which the shaft voltage is all the time over the breakdown voltage level of the lubricant. For the bearings of the test motor, this level is approximately between 30–40 V. It should be recalled here that with the frequency converter, the maximum shaft voltage measured was approximately 7 V.

Table 4-1. Measured discharge activity with different shaft voltages. The discharge activity is recorded for a time period of 3.2 ms.

DC supply voltage to the shaft	Number of discharges detected with the antenna (The threshold level was set just above the noise level.)	Number of current pulses with the measured maximum amplitude over 20 mA	Number of current pulses with measured maximum amplitude over 100 mA
2.5 V	1 (~0.3 disch./ms)	2 (~0.6 disch./ms)	0
5 V	4 (~1.25 disch./ms)	5 (~1.6 disch./ms)	1 (~0.3 disch./ms)
10 V	7 (~2.2 disch./ms)	9 (~2.8 disch./ms)	3 (~0.9 disch./ms)
20 V	5 (~1.6 disch./ms)	4 (~1.25 disch./ms)	1 (~0.3 disch./ms)
30 V	4 (~1.25 disch./ms)	3 (~0.9 disch./ms)	0

4.4 Measurements with the frequency converter

In this section, the measurements carried out with the frequency-converter-driven test motor are discussed and the results of the tests are analyzed. The measurements were conducted in such a way that they would closely resemble an actual operating situation. In the previous measurements with an adjustable voltage source, the supply voltage to the shaft stayed constant, and the test motor was rotated with the line-driven motor. This differs from the variable-frequency drive, in which the common-mode voltage changes constantly, and the shaft voltage varies accordingly. Further, in the series of the measurements with the adjustable voltage source the brush connection to the shaft and the voltage source are a part of the bearing current circuitry, which may have an effect on the bearing current and thus on the radiated emission. In these measurements, with the motor driven by a frequency converter, the brush connection is only used to measure the shaft voltage. The effect of the PE insulation ring around the bearings can be considered insignificant, because it is shorted with a jumper. In Section 4.4.2, additional measurements with the motor without insulated bearings are presented continuing the results obtained with the modified motor. The main target of these measurements is to show that the RF method can be used to detect discharges in the bearings of the frequency-converter-driven motor.

4.4.1 Measurements with the motor having insulated bearings

Where possible, the measurement setup was kept similar to the one used in the measurements presented in the previous section and described in Section 4.1. In this case, both bearings are well insulated, and depending on the measurement, they can be individually short circuited with jumpers so that the bearing current can be measured with a current probe.

In the previous measurements with the adjustable voltage source, the emission caused by the bearing currents was easy to detect, because all the RF emission pulses were corresponding to discharges inside the bearing of the test motor. However, as discussed in Section 3.3, the inverter is a strong source of electromagnetic interference. In the time domain, the interference from the inverter switching resembles the emission from the discharges as shown in Fig. 3-3. A 100 µs measurement was taken to analyze the signal activity when the supply frequency of the motor is set to 50 Hz and the motor is running at nominal speed without load. The unfiltered measurement is shown in Fig. 4-10. Multiple short pulses appear randomly with different amplitudes. The pulse inside the ellipse is due to a discharge inside the bearing, and the others are due to inverter switching and can be considered as interference. It is practically impossible to distinguish the discharge induced pulse from the inverter-switching-generated pulses without additional measurements or signal processing. In this measurement, the bearing insulation at the drive end was short circuited and the current through the jumper was measured with a current probe. This way, it was possible to differentiate the pulses caused by a discharge inside the bearing of the test motor.

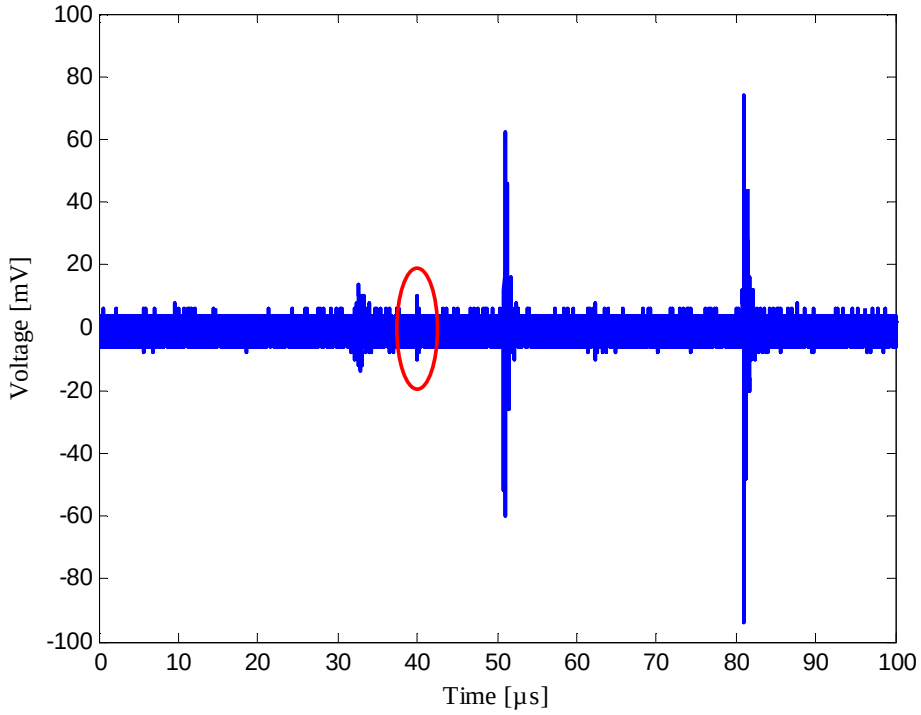

Fig. 4-10. Measurement showing strong interference from the inverter and one pulse resulting from sparking. The pulse from the sparking is indicated with an ellipse.

Considering the bearing discharge pulse plotted in Fig. 4-11, its shape and frequency content are very similar to the one of the discharge pulse generated with the EDM tool (see Fig. 2-8), and even more similar to the one generated with the adjustable voltage source (see Fig. 4-4). The spectral density estimation by a periodogram calculated from the RF measurement further supports this conclusion. Most of the discharge signal power occurs at between 100–300 MHz. Because of the high-amplitude interference from the inverter, the measurement shown in Fig. 4-11 was triggered to a current measurement, which is also shown in the figure. The oscilloscope trigger was used to find the maximum amplitude bearing current with the test motor and the frequency converter combination. The maximum bearing current amplitude recorded was ~650 mA. According to (Muetze, 2006), if the bearing current density exceeds 0.1 A/mm^2, the currents can be considered harmful, and they can significantly shorten the lifetime of the bearings. The measured value exceeds the recommended value almost three times, and it can be assumed that the lifetime of the bearings of the test motor is significantly reduced because of the bearing currents that are present in the test motor with the current motor/frequency converter combination.

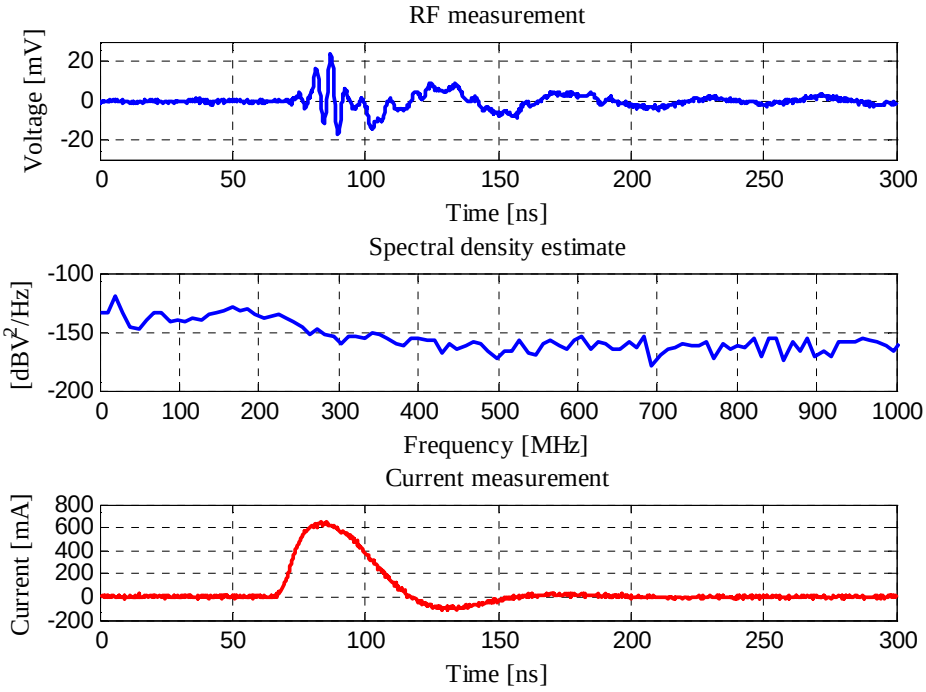

Fig. 4-11. RF measurement of emission of the discharge pulse from the bearings of the inverter-driven motor recorded with the antenna. The bearing current is simultaneously measured via the jumper that shorts the bearing insulation. The maximum measured current amplitude is ~650 mA, which can be considered to be harmful. A spectral density estimate by a periodogram calculated from the RF measurement is also plotted. Most of the discharge signal power occurs at between 100 and 300 MHz, which is similar to the results obtained with the adjustable voltage source.

It is obvious from Fig. 4-10 that it is impossible to detect the discharge from the time-domain measurement without signal processing or some other measurement, such as a current measurement, because of the interference caused by the inverter switching. The filtering of the

inverter-generated interference has been discussed in Section 3.4.1. In the following measurements, a passive high-pass filter BHP-100+ was used. The filter has a passband of 90–400 MHz, which should preserve most of the discharge signal energy while it filters the inverter-generated interference. A measurement similar to the one shown in Fig. 4-10, but this time filtered with the filter, is shown in Fig. 4-12. In this measurement, the supply frequency of the frequency converter is again 50 Hz. All the inverter-switching-generated interference has been eliminated. The bearing currents were measured simultaneously to verify that the discharge pulse shown in Fig. 4-12 is due to the bearing currents. However, the current measurement used to verify the result is not shown in the figure.

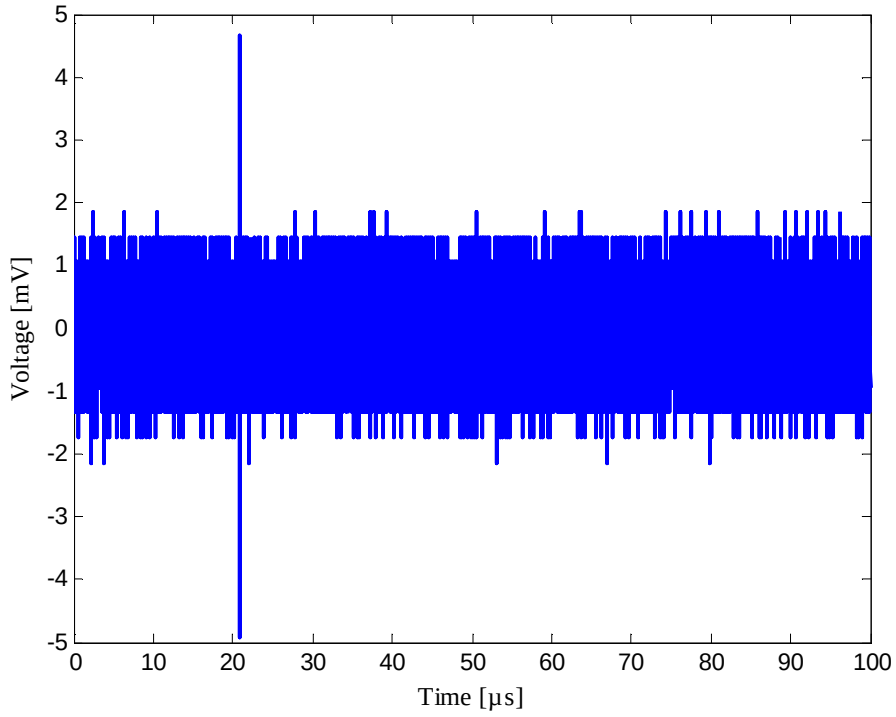

Fig. 4-12. Filtered RF measurement showing only the discharge pulse caused by bearing currents. The inverter-generated interference has been eliminated with a high-pass filter. It was verified with a simultaneous current measurement that the origin of the emitted pulse truly was a discharge in the bearing.

It was shown in Fig. 2-5 that the shaft voltage mirrors from the stator common-mode voltage. Here, we also take into account that the previous measurements with different shaft voltages (Section 4.3) showed that if the shaft voltage was above 2 V, the discharge activity was higher. The above-mentioned suggests that there should be more discharges in the bearings of the motor when the common-mode voltage has its highest amplitude. The motor windings of the test motor were delta connected, and an artificial star point was formed with resistors for common-mode voltage measurement. The common-mode voltage between this star point and the grounding point was then measured. The RF emission from the discharges was simultaneously measured, and the results are shown in Fig. 4-13. It seems obvious that most discharges occur when the common-mode voltage (and thus the shaft voltage) reaches its maximum value. However, there is also discharge activity between these local maxima. The

reason for this is that the bearings are constantly moving, and the lubrication thickness can momentarily be so small that discharges can occur even at lower shaft voltages.

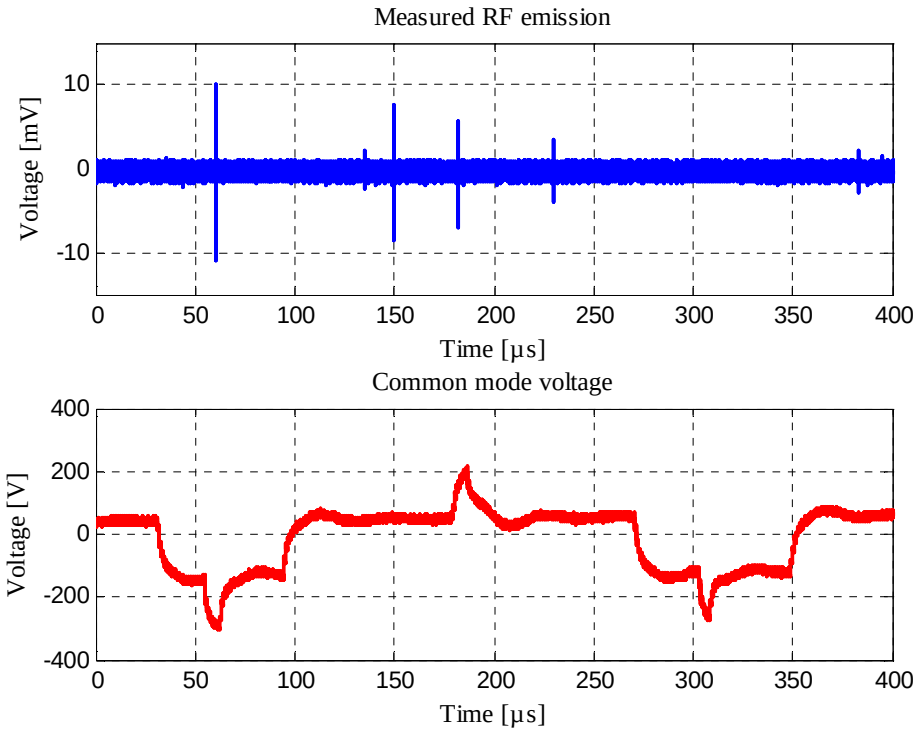

Fig. 4-13. Common-mode voltage at the motor terminals and discharge activity measured with an antenna. Discharges also occur between the instances when the common-mode voltage (and the shaft voltage) reaches its local maxima.

4.4.2 Measurements with the unmodified motor

The test motor used in all the previous measurements had electrically insulated bearings. If the insulation had not been shorted with the jumper, no bearing currents would have occurred in the motor. To be able to measure bearing currents with a current probe, at least the other bearing was short circuited with a jumper. For this reason, a question arises whether the jumper has affected the RF measurements. There is a possibility that it might have worked as an antenna making the RF method plausible. The jumper is only five centimeters long and should not significantly affect the radiated emission below 500 MHz. The antenna measurements with unmodified motors presented in Fig. 2-9 also suggest that motors can work as an antenna even without any modifications. To be certain whether discharges in bearings and hence bearing currents can be detected with the RF method, measurements with an unmodified motor are required.

To eliminate all uncertainties about what might influence the results with the modified test motors, a series of measurements with an unmodified motor was carried out. The motor used in

the test is the same type to the motor used in the previous measurement, but this time without insulated bearings. The same frequency converter was used as in the measurements presented in Section 4.4, and the supply frequency was set to 50 Hz. The motor was running without a load. The BHP-100+ high-pass filter was used between the antenna and the oscilloscope to eliminate interference from the frequency converter. Fig. 4-14 shows that the results are well in line with the previous measurements. The interference from the frequency converter is eliminated by the filtering, and only discharge pulses are recorded. The effect of filtering can also be seen from the spectral density estimation by a periodogram, which is calculated from the RF measurement. Frequencies below 90 MHz are almost completely filtered. Even though the filter used is described as a high-pass filter, it has a limited passband of 90–400 MHz. For this reason, also the higher frequencies above 400 MHz are filtered. The results confirm that the discharges in the bearing of an unmodified motor can be detected with the RF method described in this thesis.

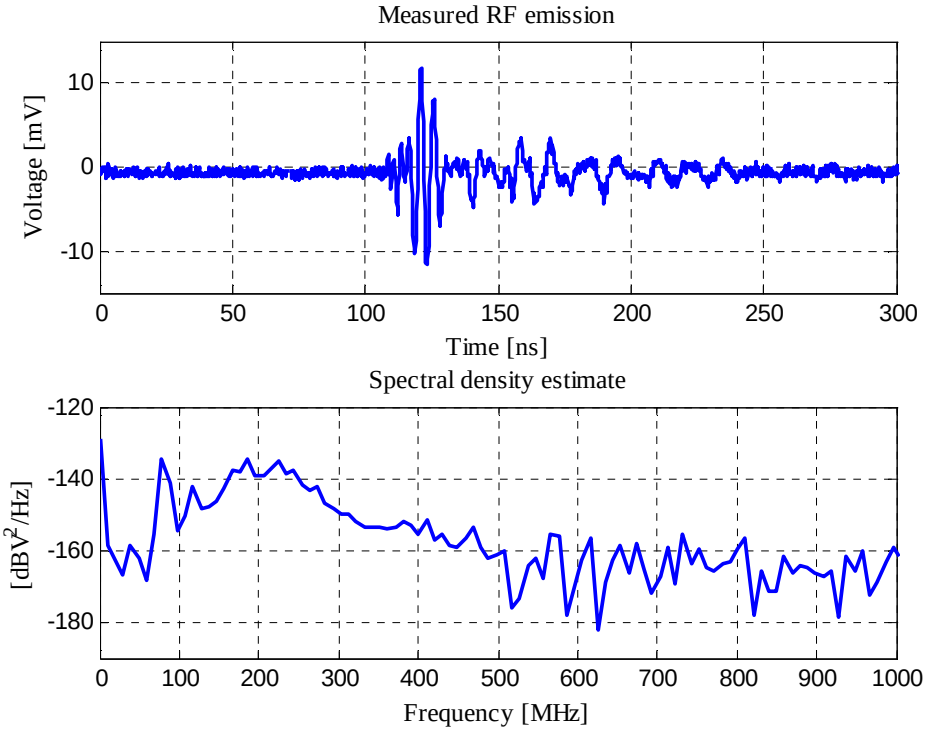

Fig. 4-14. RF measurement showing the detected discharge pulse from the unmodified motor. The spectral density estimate by a periodogram is calculated from the discharge pulse. The effect of high-pass filtering is seen from the strong attenuation below 90 MHz. There is attenuation also above 400 MHz, because the passband of the filter is 90–400 MHz.

Finally, a series of RF measurement showing discharge activity in the unmodified test motor were taken. Exemplary results are presented in Fig. 4-15. This figure is similar to the one presented in Fig. 4-9, where a constant voltage was supplied to the shaft with the voltage source. It is important to note that the discharge activity presented in Fig. 4-9 includes a lot more discharges in the same time period than the one presented in Fig. 4-15. In the first one, the shaft voltage was constant at 5 V during the measurement. In the latter, the maximum shaft

voltage reaches 7 V with the current motor/frequency converter combination. However, the average common-mode voltage and thereby the shaft voltage is well below 5 V, and therefore the discharge activity is lower.

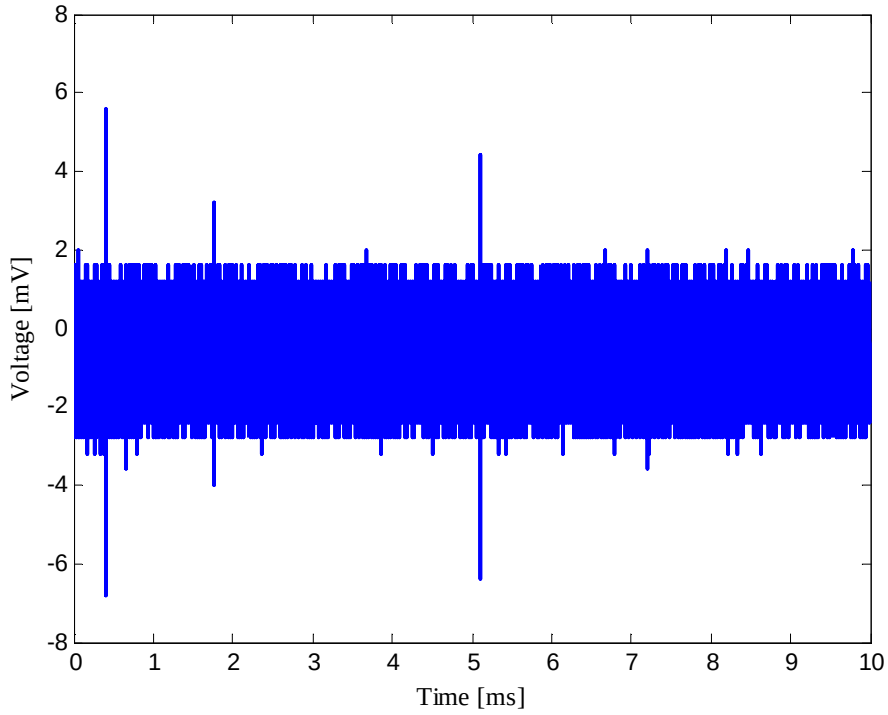

Fig. 4-15. RF measurement showing discharge activity in the bearings of the unmodified test motor when driven with the frequency converter. At least three discharge pulses from the bearings of the test motor can be detected.

According to the measurements presented in Sections 4.3 and 4.4, it seems that the test setup and the results obtained with it can be used to show the applicability of the method during "real" operating conditions. The RF method for detecting discharges and hence discharge bearing currents has proved its applicability in all setups and operating situations analyzed. It is difficult to say anything certain about the discharge activity, because the sample times are rather short. However, it is clear that there were constantly discharges in the bearings of the test motor when it was operated with the frequency converter. A special hardware, such as described in Section 3.6, would be required for more conclusive measurements about the discharge activity and its effects on the bearings of an electric motor.

4.5 Measurements of an induction motor as an antenna

In Section 2.5, measurements of three different motors with the VNA have been presented to show how an electric motor operates as antenna (Fig. 2-9). In this section, more conclusive measurements are reported, and the focus is on the same motor that was used in the measurements presented in Sections 4.3 and 4.4. Furthermore, the challenges with measuring the motor parameters as an antenna are discussed. To avoid confusion, from now on, the motor

is referred to as AUT (Antenna Under Test) to make clear that its properties as an antenna are studied.

These measurements only give some indication of how the motor works as an antenna. The results are not very accurate, for reasons explained below, but they certainly give some insight on the operability. The most important reason for the inaccuracy of the measurements is that it is not possible to properly supply a measurement signal to the AUT. There is probably a high impedance mismatch between the supply and the shaft. Practically, the only solution is to use the brush connection to the shaft that was used in the previous measurements to measure or to supply the shaft voltage. The measured signal is transmitted at different frequencies and measured with the receiving antenna. This differs considerably from the actual situation where the high frequency emission is generated as a result of rapid discharge of voltage. A passive antenna is reciprocal, and thus in general it is possible to either use the antenna under measurement as a transmitting antenna or as a receiving antenna. In these measurements, however, the AUT was only used as a transmitting antenna. There is also some measurement error caused by the environment, the multipath effect, and the limited bandwidth of the receiving antenna. These issues have been discussed in Section 4.2.

The basic radiation pattern measurement can be performed by placing the AUT on a rotational platform and rotating it to obtain a two-dimensional polar pattern. This is not very practical with the motor because of its size and weight. It was decided to move the measurement antenna around the AUT and take measurements at certain points. The AUT is symmetrical, and thus only one side was measured and mirrored to the other side. Typically, a radiation pattern is given in dBi, which means decibels relative to an isotropic antenna. Therefore, the gain is the increase in the signal received from the antenna compared with that which would be received from an isotropic radiator with the same source power. This would require two identical antennas for range calibration, which was not possible. In these measurements, the general interest is not in the performance of the AUT, but the aim is to obtain some indication where the receiving antenna should be placed when measuring RF pulses caused by discharges in the bearings. For these reasons, the absolute values of the gain are not given in the measurements.

The motor radiation patterns at different frequencies are given in Fig. 4-16 for horizontal polarization and in Fig. 4-17 for vertical polarization. The NDE is at 0 degrees and DE is at 180 degrees. An illustration of the test setup is given in Appendix I. In these measurements, the insulation from both bearings was short circuited and the motor (AUT) was running at nominal speed. More specifically, the motor to be measured was driven with the drive motor during the measurements. This represents the actual operation as closely as possible. The receiving antenna was moved to different locations as previously discussed, and the distance to the AUT was one meter. The measurements show that the AUT is quite omnidirectional if horizontal polarization is observed. In the case of vertical polarization, there is more directivity towards the ends of the motor. The conclusion from these measurements is that the location of the measuring antenna is not critical if bearing currents are to be measured by detecting the emission generated by the discharges in the bearings. This is a very good result, because it can be assumed that in any industrial environment, the placement of the measuring antenna can be very restricted. For example, the space can be very limited, and there can be various structures blocking the way, so there is probably no possibility to choose where to place the measuring antenna.

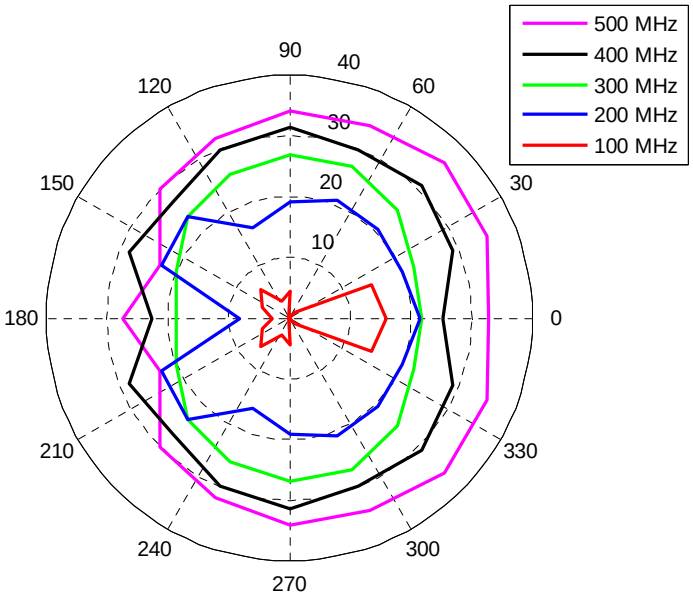

Fig. 4-16. Motor radiation patterns shown with frequencies from 100 to 500 MHz. Horizontal polarization.

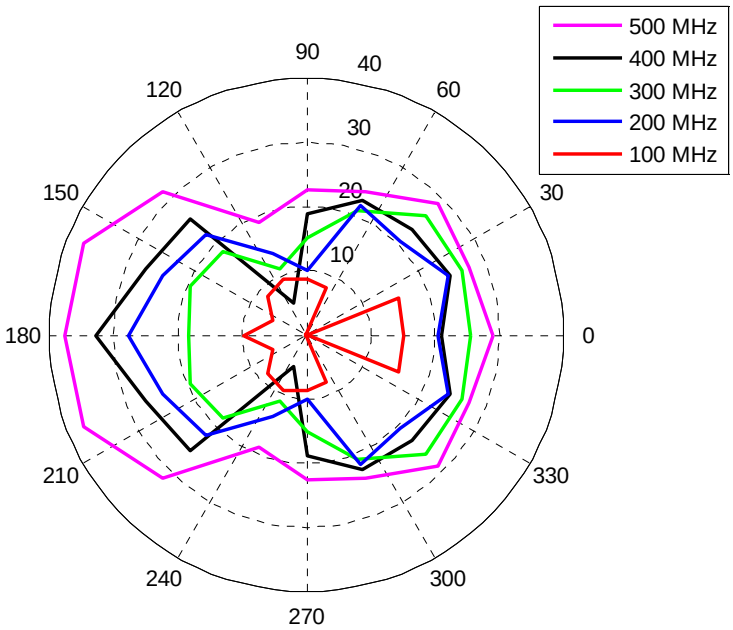

Fig. 4-17. Motor radiation patterns shown with frequencies from 100 to 500 MHz. Vertical polarization.

If not otherwise mentioned, most of the measurements presented in this thesis are measured at the side of the motor. This means that the receiving antenna was placed one meter away normal to the motor, which corresponds to the 90 degree point in Fig. 4-16 and Fig. 4-17. An absolute value of S_{21} parameter is measured as a function of frequency at this point and shown for both polarizations in Fig. 4-18 to better illustrate the frequency dependency. Power loss at horizontal polarization is 10–20 dB less compared with vertical polarization.

Measurements with different size motors were presented in Section 2.5 and the results are plotted in Fig. 2-9. The motors were not running during these measurements. It is shown that at frequencies above 100 MHz, which are relevant in this study, it does not make significant difference whether a motor is running or not. The reason for this may be that the insulation caused by the lubrication film at higher frequencies looks more like a short circuit, in which case the situation is the same as if the motor is at standstill and there is an ohmic connection between the bearing rollers and the rings. Fig. 4-19 shows the difference in the power loss when the test motor is running and when it is at a standstill. There are some differences below 200 MHz, but above this, the values are very close. Based on these results, we may state that it is possible to get a fairly good indication of how a motor works as an antenna even if the motor is not running. This is a very good result, because it is far easier to supply the signal to the shaft when the motor is not running.

As it was mentioned above, these antenna measurements are rough approximations and probably not very accurate. For example, comparing the results plotted in Fig. 2-9 and in Fig. 4-18, some differences can be seen. The results in Fig. 2-9 are quite similar between motors of different sizes, but if these are compared with the results presented in Fig. 4-18, there is a noticeable difference at higher frequencies. The reason for this is probably the impedance mismatch between the VNA output supply and the shaft of the motors. In the test motor, the brush connection shown in Fig. 4-3 was used to supply the test signal to the shaft. However, in the measurements presented in Section 2.5 and the results plotted in Fig. 2-9, the test signal was supplied to the shaft of the motors without brush connection. It is very likely that this is the reason for the difference in the results. It is not possible to say whether the results in Fig. 2-9 or in Fig. 4-18 are closer to a real situation, because both cases differ considerably from the real situation where the high-frequency pulse is generated by a discharge. Nevertheless, even if there is an impedance mismatch in the supply, there is power radiated from the motor to the receiving antenna. This was verified by carrying out the measurements without a proper connection to the shaft of the motor. In this case, the attenuation was far stronger compared with the results plotted in Fig. 4-18. Furthermore, all the results presented in Sections 4.3 and 4.4 indicate that the motor works as an antenna and can transmit frequencies between 100–400 MHz.

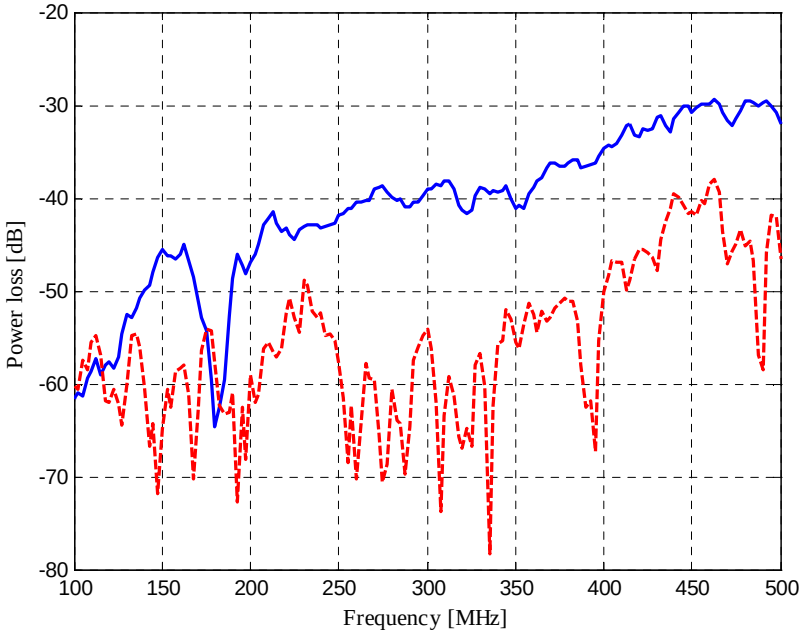

Fig. 4-18. Absolute value of S_{21} parameter measured from one meter away normal to the motor. Horizontal polarization (solid blue line) and vertical polarization (dashed red line) are both measured and plotted.

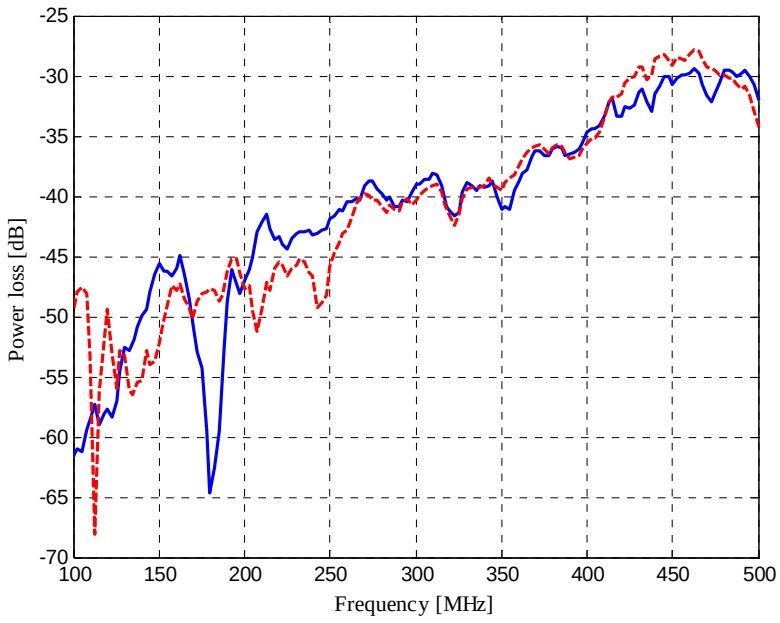

Fig. 4-19. Absolute value of the S_{21} parameter plotted when the motor is running (solid blue line) and when the motor is at standstill (dashed red line). Some differences occur at lower frequencies, but above 200 MHz the values are very close.

5 SUMMARY AND CONCLUSIONS

In this chapter, the main results of this work are summarized. The main objective of this thesis was to study the presented radio frequency method and its applicability to detect discharge bearing currents in frequency-converter-driven induction motors. The usability of the results is discussed and some suggestions for future work are given.

5.1 Key results of the work

It is assumed that the most important reason for bearing damage caused by bearing currents is the electrical discharges in the bearing. These discharges take place through the lubricant film between the raceways of the inner and the outer ring and the rolling elements of a bearing. This phenomenon can be considered similar to the one of electrical discharge machining, where material is removed by a series of rapidly recurring electrical arcing discharges between an electrode and a workpiece.

A radio frequency (RF) method has been studied that can be used for nonintrusive detection of bearing currents from an induction motor. The method is based on the measurement of the radio frequency emission caused by the discharges (sparking) in a bearing of the motor. It is theoretically shown how an electric motor can work as a "spark gap" transmitter. The theory is then verified by measurements.

The theoretical discussion includes a model of a motor as a spark gap transmitter. The following points are discussed: The energy charged in parasitic capacitances, which is released during a discharge, is estimated. It is shown with calculations that this energy is enough to cause micro-cratering in the bearings of the motor and generate detectable RF emission. The frame, the bearings, and the rotor of an electric motor together comprise a transmitting antenna that determines how the emission spreads into the environment. This is shown with measurements, and it is verified that different sizes of LV (low-voltage) motors work as antennas.

The RF method is highly subjected to external interference. A general discussion about radio wave propagation and about various interference sources is given. Frequency converters are extensively used to drive induction motors. Therefore, they require special attention as a source of interference. The frequency converter is identified as a source of an impulsive interference transmitter that has a high impact on the applicability of the RF method presented. The reason for the interference is the switching instances of the IGBTs. For this reason, different techniques are studied and proposed to mitigate the inverter-generated interference and to make detection of discharges possible. One suitable technique is high-pass filtering, where low-frequency switching interference is filtered and high-frequency discharge emission is preserved. To further analyze the applicability of the RF method, various localization techniques are proposed, and one method is verified with measurements. It is shown that the source of discharges and thereby the motor in which bearing currents are suspected can be located with a reasonable accuracy.

Most importantly, the applicability of the RF method is studied with a series of measurements. For this reason, a test bench has been constructed that allows shaft voltage variation, bearing current measurement, and operation with or without a frequency converter. The applicability of the method is verified also with an unmodified motor. These measurements give valuable information on how different parameters, such as shaft voltage and the frequency converter affect the discharge emission. It is also analyzed which phenomena can be detected with the RF method studied. For example, it is not possible to determine the magnitude of the current

flowing through the bearing or the magnitude of the shaft voltage by measuring only the discharge emission.

It is possible to detect the discharges with an oscilloscope and an antenna that are capable of measuring short nanosecond pulses with a frequency content of close to one gigahertz. High-pass filtering is required because of the inverter switching interference. The radiation pattern of the test motor is measured to find the best spot for the receiving antenna. It was found out that it is not critical how the receiving antenna is placed according to motor position. Some design suggestions for a specific discharge (bearing current) detector are also given.

5.2 Usability of the results

Discharge activity measurement: Discharge activity measurements carried out in this thesis were limited to short samples of 3.2 ms. It was shown that there is a certain shaft voltage level, above which EDM bearing currents start to occur, and these currents can be detected with the RF method. For the test motor this was around 1.5–2.5 V. When the shaft voltage was raised, there was no significant increase in the number of the discharges, until a threshold level was exceeded and the discharging was practically continuous. For the test motor this happened near 30 V. Based on this information, it is suggested that the RF method can be used to detect discharges and thereby EDM bearing currents in the motor bearings. The RF method was successfully applied for detecting the discharges at a distance of three meters from the motor, and it can be assumed that distances above this are possible with a proper antenna and amplifier. This combined with the location techniques discussed opens new opportunities for nonintrusive continuous detection of discharge bearing currents. There is no need to measure each motor individually, but with two or more antennas a larger area can be easily covered and motors with high discharge activity can be targeted.

Verification of bearing current mitigation techniques: There is no best solution to mitigate bearing currents. It is often proposed to insulate both bearings and/or use a shaft grounding brush. Basically, either of these should work in an ideal case if also proper grounding of the motor is ensured. Insulating the bearings blocks the path for the current, but this requires that the insulation is adequate. This may also shift the problem to the bearings of the load machine. A shaft brush eliminates the voltage, but may require maintenance to keep the brush impedance low enough. Common for all these techniques is that they raise the overall cost of the system. Thus, it is necessary to know whether the problems encountered are really caused by bearing currents. Further, regardless of the chosen mitigation technique, it is useful to know if the countermeasures taken are effective. To this end, the method studied in this thesis offers a nonintrusive method to detect discharge bearing currents in a motor. Comparison before and after installation of mitigation techniques can be done relatively easy with the RF method.

Scope of the bearing current detection method: This thesis focuses on inverter-induced bearing currents in induction motors, with a particular reference to EDM type bearing currents. However, there is no reason why the method studied in this thesis could not be applied to different types of bearing currents and motors/generators. An assumption of the occurrence of sparking is a precondition for application of this method. Thus, other bearing currents can be detected only if they also cause discharges. Whether this happens in the case of different types of bearing currents remains uncertain. Furthermore, bearing currents are not limited only to induction motors, but occur also in PM (Permanent Magnet) motors/generators. PM machines have gained more interest during the last years as a result of improvements in magnetic materials; this has made PM machines rivals for more common induction machines. There is currently very little information available on bearing current problems in permanent magnet

motors. However, there is no reason to believe that PM machines are not subject to this phenomenon. It can be assumed that the method presented in this thesis can also be applied to study bearing currents in PM motors as well as other type of synchronous motors.

5.3 Suggestions for future work

The RF method has proven to be a viable tool to investigate the occurrence of bearing currents. There is also an opportunity to use the method to predict the lifetime of a bearing in a similar manner as electrical bearing stress introduced in (Muetze, 2006) and given in Eq. (1-6). In this case, the apparent current density and switching frequency would be replaced with discharge activity. There are some important questions regarding to these issues that remain unanswered and are given as suggestions for future work. These questions that require more research are listed below:

- Is it possible to use discharge activity information to predict the available lifetime of the bearing?
- Is it possible to set specific discharge activity limits that would indicate when the bearing currents significantly affect the bearing lifetime?
- Is there a limit for discharge activity that can be considered “safe”?
- Does the discharge activity increase when a bearing is further damaged?
- Does the measurement of discharges and/or discharge activity provide some additional information that was not addressed in this study? This information could be assessed by comparing it with other measurements associated with the topic.

REFERENCES

(ABB, 2005) ABB Motors, *The motor guide*, 2nd edition, ABB Automation power products, LV Motors, Vaasa, 2005.

(Akagi, 2004) Akagi H. and Doumoto T., An Approach to Eliminating High-Frequency Shaft Voltage and Ground Leakage Current From an Inverter-Driven Motor, *IEEE Transactions on Industry Applications*, Vol. 40, No. 4, July/Aug. 2004, pp. 1162–1169.

(Akagi, 2006) Akagi H. and Tamura S., A Passive EMI Filter for Eliminating Both Bearing Current and Ground Leakage Current From an Inverter-Driven Motor, *IEEE Transactions on Power Electronics*, Vol. 21, No. 5, September 2006, pp. 1459–1469.

(Albrecht, 1986) Albrecht P. F., Appiarius J. C., McCoy R. M., and Owen E. L., Assessment of the reliability of motors in utility applications, *IEEE Transactions on energy conversion*, Vol. EC-1, No. 1, March 1986, pp. 39–46.

(Alger, 1924) Alger P. and Samson H., Shaft Currents in Electric Machines, *A.I.R.E. Conference*, Philadelphia, February 1924, pp. 235–245.

(Ammann, 1988) Ammann C., Reichert K., Joho R., and Posedel Z., Shaft voltages in generators with static excitation systems – problems and solution, *IEEE Transactions on Energy Conversion*, Vol. 3, No. 2, June 1988, pp. 409–419.

(Baiju, 2004) Baiju M. R., Mohapatra K. K., Kanchan R. S., and Gopakumar K., A Dual Two-Level Inverter Scheme With Common Mode Voltage Elimination for an Induction Motor Drive, *IEEE Transactions on Power Electronics*, Vol. 19, No. 3, May 2004, pp. 794–805.

(Bell, 2001) Bell S. et al., Experience with variable-frequency drives and motor bearing reliability, *IEEE Transactions on industry applications*, Vol. 37, No. 5, Sep./Oct. 2001, pp. 1438–1446.

(Bentley, 1997) Bentley J. M. and Link P. J., Evaluation of motor power cables for PWM ac drives, *IEEE Transactions on Industry Applications*, Vol. 33, No. 2, March/April 1997, pp. 342–358.

(Binder, 2008) Binder A. and Muetze A., Scaling Effects of Inverter-Induced Bearing Currents in AC Machines, *IEEE Transactions on Industry Applications*, Vol. 44, No. 3, May/June 2008, pp. 769–776.

(Boggs, 1982) Boggs S. A. and Stone G. C., Fundamental Limitations in the Measurement of Corona and Partial Discharge, *IEEE Transactions on Electrical Insulation*, Vol. 17, No. 2, 1982, pp.143–150.

(Boyanton, 2002) Boyanton H. E. and Hodges G., Bearing fluting, *IEEE Industry Applications Magazine*, Vol. 8, No. 5, Sept./Oct. 2002, pp. 53–57.

(Busse, 1997) Busse D., Erdman J., Kerkman R., Schlegel D., and Skibinski G. An evaluation of the electrostatic shielded induction motor: a solution for rotor shaft voltage buildup and bearing current, *IEEE Transactions on Industry Applications*, Vol. 33, No. 6, Nov. /Dec. 1997, pp. 1563–1570.

(Busse, 1997B) Busse D., Erdman J., Kerkman R., Schlegel D., and Skibinski G.,System Electrical Parameters and Their Effects on Bearing Currents, *IEEE Transactions on Industry Applications*, Vol. 33, No. 2, March/April 1997, pp. 577–584.

(Busse, 1997C) Busse D., Erdman J., Kerkman R., Schlegel D., and Skibinski G., Bearing Currents and Their Relationship to PWM Drives, *IEEE Transactions on Power Electronics*, Vol. 12, No. 2, March 1997, pp. 243–252.

(Busse, 1997D) Busse D., Erdman J., Kerkman R., Schlegel D., and Skibinski G., Characteristics of Shaft Voltage and Bearing Currents, *IEEE Industry Applications Magazine*, Vol. 3, No. 6, Nov./Dec. 1997, pp. 21–31.

(Busse, 1997E) Busse D., Erdman J., Kerkman R., Schlegel D., and Skibinski G., The Effects of PWM Voltage Source Inverters on the Mechanical Performance of Rolling Bearings, *IEEE Transactions on Industry Applications*, Vol. 33, No. 2, March/April 1997, pp. 567–576.

(Cech, 2007) Cech V. and Foldyna J., Diagnostics of Electrical Damage Cause of Induction Motors' Bearings, in *Proceedings of COMADEM*, Harrogate, United Kingdom, 11–14 June 2007, pp. 283–286.

(Chen, 1996) Chen S. and Lipo T. A., Source of induction motor bearing currents caused by PWM inverters, *IEEE Transactions on Energy Conversion*, Vol. 11, No. 1, March 1996, pp. 25–32.

(Chen, 1996B) Chen S. and Lipo T. A., Circulating Type Motor Bearing Current in Inverter Drives, in *Conference Record of the 31st IEEE-IAS Annual Meeting, IAS'96*, San Diego, CA, pp. 162–167.

(Chen, 1996C) Chen S., Lipo T. A., and Fitzgerald D., Modeling of Motor Bearing Currents in PWM Inverter Drives, *IEEE Transactions on Industry Applications*, Vol. 32, No. 6, Nov./Dec. 1996, pp. 1365–1370.

(Chen, 1998) Chen S. and Lipo T. A., Circulating Type Motor Bearing Current in Inverter Drives, *IEEE Industry Applications Magazine*, Jan./Feb. 1998, pp. 32–38.

(Chmelik, 2007) Chmelik K., Cech V., and Foldyna J., Devices for Prevention of Bearings Devaluation by Electric Current, *IEEE International Symposium on Diagnostics for Electric Machines, Power Electronics and Drives, SDEMPED*, Cracow, Poland, 6–8 September 2007, pp. 316–319.

(Dahl, 2008) Dahl D., Sosnowski D., Schlegel D., Kerkman R. J., and Pennings M., Gear up your bearings, *IEEE Industry Applications Magazine*, Vol. 14, No. 4 July/Aug. 2008, pp. 45–53.

(Delli Colli, 2005) Delli Colli V., Cancelliere, Marignetti F., and Di Stefano R., Influence of voltage and current source inverters on low-power induction motors, *IEEE Proceedings of Electrical Power Applications*, Vol. 152, No. 5, September 2005, pp. 1311–1320.

(Erdman, 1996) Erdman J., Kerkman R., Schlegel D., and Skibinski G., Effect of PWM Inverters on AC Motor Bearing Currents and Shaft Voltages, *IEEE Transactions on Industry Applications*, Vol. 32., No. 2., March/April 1996, pp. 250–259.

(Guttowski, 2006) Guttowski S., Weber S., Schinkel M., John W., and Reichl H., Troubleshooting and fixing of inverter driven induction motor bearing currents in existing plants of large size - an evaluation of possible mitigation techniques in practical applications, in *Proceedings of Twenty-First Annual IEEE Applied Power Electronics Conference and Exposition, APEC*, Dallas, TX, USA, 19– 23 March 2006, pp. 225–230.

(Hayt, 1989) Hayt W. H., *Engineering Electromagnetics*, 5th edition, New York, McGraw-Hill, 1989.

(Hoppler, 2007) Hoppler R. and Errath R.A., Motor Bearings, not just a piece of metal, *IEEE-IAS/PCA Cement Industry Conference*, Charleston, SC, USA, 29 April–3 May, 2007, pp. 214–233.

(Hyypio, 2005) Hyypio D., Mitigation of Bearing Electro-Erosion of Inverter-Fed Motors Through Passive Common-Mode Voltage Suppression, *IEEE Transactions of Industry Applications*, Vol. 41, No. 2, March/April 2005. pp. 576–583.

(IEEE, 2008) IEEE (Institute of Electrical and Electronics Engineers) Virtual Museum, http://www.ieee-virtual-museum.org/, Accessed in November, 2008.

(Jagenbrein, 2005) Jagenbrein A., Buschbeck F., Gröschl M., and Preisinger G., Investigation of the physical mechanisms in rolling bearings during the passage of electric current, *Tribotest journal*, Vol. 11, No. 4, June 2005, pp. 295–306.

(Jouanne, 1998) Jouanne A., Zhang H., and Wallace A. K., An Evaluation of Mitigation Techniques for Bearing Currents, EMI and Overvoltages in ASD Applications, *IEEE Transactions on Industry Applications*, Vol. 34, No. 5, Sept./Oct 1998, pp. 1113–1122.

(Jouanne, 2002) Jouanne A., Dai S., and Zhang H., A Multilevel Inverter Approach Providing DC-Link Balancing, Ride-Through Enhancement, and Common-Mode Voltage Elimination, *IEEE Transactions on Industrial Electronics*, Vol. 49, No. 4, August 2002, pp. 739–745.

(Judd, 2005) Judd M. D., Li Yang, and Hunter I. B. B., Partial Discharge Monitoring of Power Transformers Using UHF Sensors. Part 1: Sensors and Signal Interpretation, *IEEE Electrical Insulation Magazine*, Vol. 21, No. 2, March/April 2005, pp. 5–14.

(Judd, 2005B) Judd M. D., Li Yang, and Hunter I. B. B., Partial Discharge Monitoring of Power Transformers Using UHF Sensors. Part 2: Field Experience, *IEEE Electrical Insulation Magazine*, Vol. 21, No. 3, May/June 2005, pp. 5–13.

(Kempski, 2001) Kempski A., Capacitively coupled discharging currents in bearings of induction motor fed from PWM (pulsewidth modulation) inverters, *Journal of Electrostatics*, No. 51–52, May 2001, pp. 416–423.

(Lindh, 2003) Lindh T., *On the Condition Monitoring of Induction Machines*, Doctoral dissertation, Lappeenranta University of Technology, Lappeenranta, Finland, 2003.

(Link, 1999) Link P.J., Minimizing electric bearing currents in ASD systems, *IEEE Industry Application Magazine*, Vol. 5, No. 4, July/August. 1999, pp. 55–66.

(Macdonald, 1999) Macdonald D. and Gray W., PWM drive related bearing failures, *IEEE Industry Applications Magazine*, Vol. 5, No. 4, July/August. 1999, pp. 41–47.

(Moore, 2005) Moore P. J., Portuques I. E., Glover I. A., Radiometric Location of Partial Discharge Sources on Energized High Voltage Plant, *IEEE Transactions on Power Delivery*, Vol. 20, No. 3, July 2005, pp. 2264–2272.

(Moore, 2006) Moore P. J., Portuques I. E., Glover I. A., Partial Discharge Investigation of a Power Transformer Using Wireless Wideband Radio-Frequency Measurements, *IEEE Transactions on Power Delivery*, Vol. 21, No. 1, January 2006, pp. 528–530.

(Muetze, 2003) Muetze A. and Binder A., Experimental evaluation of mitigation techniques for bearing currents in inverter-supplied drive-systems - Investigations on induction motors up to 500 kW, *Conference Record of the IEEE International Electric Machines and Drives Conference*, 2003, Vol. 3, Madison WI, USA, 1–4 June 2003, pp. 1859–1865.

(Muetze, 2004) Muetze A. and Binder A., Calculation of Circulating Bearing Currents in Machines of Inverter-Based Drive Systems, *IEEE Transactions on Industrial Electronics*, Vol. 54, No. 2, April 2007, pp. 932–938.

(Muetze, 2006) Muetze A. and Binder A., Vogel H., Hering J., What can bearings bear?, *IEEE Industry Applications Magazine*, Vol. 12, No. 6, Nov./Dec. 2006, pp. 57–64.

(Muetze, 2006B) Muetze A. and Binder A., Don't lose your bearings - Mitigation techniques for bearing currents in inverter-supplied drive systems, *IEEE Magazine on Industry Applications*, Vol. 12, No. 4, July/Aug. 2006, pp. 22–31.

(Muetze, 2006C) Muetze A. and Binder A., Calculation of Influence of Insulated Bearings and Insulated Inner Bearing Seats on Circulating Bearing Currents in Machines of Inverter-Based Drive Systems, *IEEE Transactions on Industry Applications*, Vol. 42, No. 4, July/August 2006, pp. 965–972.

(Muetze, 2007) Muetze A. and Binder A., Techniques for measurement of parameters related to inverter-induced bearing currents, *IEEE Transactions on Industry Applications*, Vol. 43, No. 5, Sep./Oct. 2007, pp. 1274–1283.

(Muetze, 2007B) Muetze A. and Binder A., Calculation of Motor Capacitances for Prediction of the Voltage Across the Bearings in Machines of Inverter-Based Drive Systems, *IEEE Transactions on Industry Applications*, Vol. 43, No. 3, May/June 2007, pp. 665–672.

(Muetze, 2008) Muetze A. and, Oh H. W., Design Aspects of Conductive Microfiber Rings for Shaft Grounding Purposes, *IEEE Transactions on Industry Applications*, Vol. 44, No. 6, Nov./Dec. 2008, pp. 1749–1757.

(Mäki-Ontto, 2003) Mäki-Ontto P. and Luomi J., Bearing current prevention of converter-fed AC machines with a conductive shielding in stator slots, in *Conference Record of the IEEE International Electric Machines and Drives Conference, IEMDC 2003*, Vol. 1, Madison WI, USA, 1–4 June 2003, pp. 274–278.

(Mäki-Ontto, 2005) Mäki-Ontto P. and Luomi J., Induction Motor Model for the Analysis of Capacitive and Induced Shaft Voltages, in *Proceedings of IEEE International Conference on Electric Machines and Drives*, San Antonio, TX, USA, 15–18 May 2005, pp. 1653–1660.

(Mäki-Ontto, 2006) Mäki-Ontto P., *Modeling and Reduction of Shaft Voltages in AC Motors Fed by Frequency Converters*, Doctoral dissertation, Helsinki University of Technology, Espoo, Finland, 2006.

(Naumanen, 2008) Naumanen V., Luukko J., Itkonen T., Pyrhönen O., and Pyrhönen J., Modulation Technique for Series-Connected H-Bridge Multilevel Converters with Equal Load Sharing, approved to be published in *IET Electric Power Applications.*

(O'Donnell, 1985) O'Donnell P., IEEE reliability working group, report of large motor reliability survey of industrial and commercial installations. Part I, II and III, *IEEE Transactions on Industry Applications*, 1985, pp. 853–872.

(Ogasawara, 1997) Ogasawara S., Ayano H., Akagi H., Measurement and Reduction of EMI Radiated by a PWM Inverter-Fed AC Motor Drive System, *IEEE Transactions on Industry Applications*, Vol. 33, No. 4, July/Aug. 1997, pp. 1019–1026.

(Oh, 2007) Oh W., Preventing VFD/AC Drive Induced Electrical Damage to AC Motor Bearings, *AEGIS application note*, October 5, 2007.

(Ollila, 1997) Ollila J., Hammar T., Iisakkala J., and Tuusa H., On the bearing currents in medium power variable speed AC drives, in *Proceedings of the International Electric Machines and Drives Conference*, IEMDC'97, Milwaukee, WI, USA, 18– 21 May 1997, pp. MD1-1.1–1.3.

(Ost, 2005) Ost W., and De Baets P., Failure analysis of the deep groove ball bearings of an electric motor, *Engineering Failure Analysis*, Vol. 12, No. 5 October 2005, pp. 772–783.

(Pahlavan, 2002) Pahlavan K., Xinrong L., and Mäkelä J. P, Indoor geolocation science and technology, *IEEE Communication Magazine*, Vol. 40, No. 2, February 2002, pp. 112–118.

(Prashad, 1999) Prashad H., Determination of magnetic flux density on the surfaces of rolling element bearings as an indication of the current that has passed through them - an investigation, *Tribology International*, Vol. 32, No. 8, August 1999, pp. 455–467.

(Prashad, 2001) Prashad H., Appearance of craters on track surface of rolling element bearings by spark erosion, *Tribology International*, Vol. 34, No. 1, January 2001, pp. 39–47.

(Preisinger, 2001) Preisinger G., Gröschl M., and Köttritsch H., Prevention of electric erosion in bearings, *SKF's magazine Evolution*, No. 2, June 2001, pp. 21–25.

(Rappaport, 2002) Rappaport T. S., *Wireless Communications Principles and Practice*, second edition, Prentice-Hall, Inc, Upper Saddle River, New Jersey, USA, 2002.

(Rechberger, 2006) Rechberger T. and Ingruber R., Influence of Different Types of Supply Cables on Shaft Currents in VSI-fed Induction Motors, in *Proceedings* of *International Symposium on Power Electronics, Electrical Drives, Automation and Motion* (SPEEDAM), Taormina, Italy, 23–26 May 2006, pp. 1372–1376

(Revol, 2004) Revol B., Roudet J., Schanen J. L., Loizelet P., EMI study of a three phase inverter-fed motor drives, in *Proceedings of the 2004 IEEE Industry Applications Conference*, Seattle, WA, USA, 3–7 October 2004, pp. 2657–2664.

(Schiferl, 2004) Schiferl R. F. and Melfi M. J., Bearing Current Remediation Options, *IEEE Industry Applications Magazine*, July/Aug. 2004, pp. 40–50.

(Sellars, 1995) Sellars A. G., et al., Calibrating the UHF Technique of Partial Discharge Detection using a PD simulator, *IEEE Transactions on Dielectrics and Electrical Insulation*, Vol. 2, No. 1, Feb. 1995, pp. 46–53.

(Seybold, 2005) Seybold J. S., *Introduction to RF Propagation*, John Wiley & Sons, Inc., Hoboken, New Jersey, 2005.

(Silventoinen, 2001) Silventoinen P., *Electromagnetic compatibility and EMC-measurements in DC-voltage link converters*, Doctoral dissertation, Lappeenranta University of Technology, Lappeenranta, Finland, 2001.

(Singh, 2002) Singh G.K., Sa'ad Ahmed Saleh Al Kazzaz, Induction machine drive condition monitoring and diagnostic research – a survey, *Electric Power Systems Research*, Vol. 64, No. 2, February 2002, pp. 145–158.

(SKF, 2007) SKF AB, Marinov P., Method and device for indicating an electric discharge inside a bearing of an electric drive system, international patent, Patent No. WO2007106015, 2007.

(SKF, 2008) Humbert S., Detection of electrical discharges in bearings, SKF White Paper, November 2008.

(Skibinski, 1999) Skibinski G. L., Kerkman R. J., and Schlegel D., EMI Emissions of Modern PWM ac Drives, *IEEE Industry Applications Magazine*, Nov./Dec. 1999.

(Stack, 2005) Stack J. R., Habetler T. G., and Harley R. G., Experimentally Generating Faults in Rolling Element Bearings Via Shaft Current, *IEEE Transactions on Industry Applications*, Vol. 41, No. 1, Jan./Feb. 2005.

(Stone, 1995) Stone Greg C. and Sedding H. G., In-Service Evaluation of Motor and Generator Stator Windings Using Partial Discharge Tests, *IEEE Transactions on Industry Applications*, Vol. 31, No. 2, March/April 1995.

(Särkimäki, 2008) Särkimäki V., Ahola J., Lindh T., and Tiainen R., Radio Frequency Measurements of Bearing Currents in an Induction Motor, in *Proceedings of the Fifth International Conference on Condition Monitoring and Machinery Failure Prevention Technologies* (CM2008 / MFPT2008), Edinburgh, United Kingdom, 15–18 July 2008.

(Tandon, 1999) Tandon N. and Choudhury A., A review of vibration and acoustic measurement methods for the detection of defects in rolling element bearings, *Tribology International*, Vol 32, No. 8, August 1999. pp. 469–480.

(Tavner, 1999) Tavner P. J. and Hasson J. P., Predicting the design life of high integrity rotating electrical machines, in *Proceedings of the 9th IEEE International conference on electrical machines and drives* (EMD), Canterbury, United Kingdom, 1–3 September 1999, pp. 286–290.

(Tavner, 2008) Tavner P.J., Review of condition monitoring of rotating electrical machines, *IET Electric Power Applications*, Vol. 2, No. 4, July 2008. pp. 215–247.

(Thorsen, 1995) Thorsen O. V. and Dalva M., A survey of faults on induction motors in offshore oil industry, petrochemical industry, gas terminals and oil refineries, *IEEE Transactions on Industry Applications*, Vol. 31, No 5, Sep./Oct. 1995, pp. 1186–1196.

(Thorsen, 1999) Thorsen O. V. and Dalva M., Failure Identification and Analysis for High-Voltage Induction Motors in the Petrochemical Industry, *IEEE Transactions on Industry Applications*, Vol. 35, No. 4, July/Aug. 1999, pp. 810–818.

(Vossiek, 2003) Vossiek M., Wiebking L., Gulden P., Wieghardt J., Hoffmann C., and Heide P., Wireless Local Positioning, *IEEE Microwave magazine*, Vol. 4, No. 4, December 2003, pp. 77–86.

(Wang, 2000) Wang F., Motor Shaft Voltages and Bearing Currents and Their Reduction in Multilevel Medium-Voltage PWM Voltage-Source-Inverter Drive Applications, *IEEE Transactions on Industry Applications*, Vol. 36, No. 5, Sept./Oct. 2000, pp. 1336–1341.

(Zhang, 2000) Zhang H., von Jouanne A., Dai S., Wallace A., and Wang F., Multilevel inverter modulation schemes to eliminate common-mode voltages, *IEEE Transactions on Industry Applications*, Vol. 36, No. 6, Nov./Dec. 2000, pp. 1645–1653.

(Zhou, 2007) Zhou W., Habetler T. G., and Harley R. G., Bearing Condition Monitoring Methods for Electric Machines: A General Review, in *Proceedings of IEEE International Symposium on Diagnostics for Electric Machines, Power Electronics and Drives, 2007* (SDEMPED), Cracow, Poland, 6–8 September 2007, pp. 3–6.

APPENDIX I

The test equipment used in the tests consists of:

- Two identical Invensys T-01F160L4/01 three-phase induction motors
  - 15 kW 4-pole LV and delta-connected
  - V_N = 400 V and I_N = 28.5 A
  - The primary test motor has insulated bearings and the insulation can be shorted with a jumper.
  - The primary test motor has a brush connection for shaft voltage injection and measurement.
  - The drive motor is unmodified.
- Frequency converter ABB ACS 400 series
  - Switching frequency 4 or 8 kHz
  - A shielded and symmetric power cable with a length of 4 meters is used to connect the motor and the frequency converter.
- High-speed oscilloscope Tektronix TDS7104
  - Bandwidth up to 1 GHz
  - 2.5 GS/s real-time sample rate for each of the four channels
  - Maximum record length with one channel is 400000 points and with two channels 200000 points per channel.
- Network analyzer Agilent 4395A with Agilent 87511A s-parameter test set
  - Bandwidth up to 500 MHz
- Current probe Tektronix TCP202 AC/DC
  - Bandwidth DC–50 MHz
- Wide-bandwidth antenna EMCO 93148
  - Bandwidth 200–2000 MHz
  - Average gain of 5 dB over whole bandwidth
- Two monopole whip antennas from RF Solutions
  - Tuned to 433 MHz
- Three passive high-pass filters from Mini-Circuits
  - Filter types are BHP-50+, BHP-100+ and BHP-150+.
  - Passbands of these filters are 41–800 MHz, 90–400 MHz, and 133–1000 MHz, respectively.
  - For the BHP-100+ attenuation in the passband is <1 dB, in the stopband between 40–55 MHz >20 dB, and between DC-40 MHz >40 dB
- Adjustable DC power source with a voltage range of 0–24V

The test setup and the position of the equipment are illustrated below:

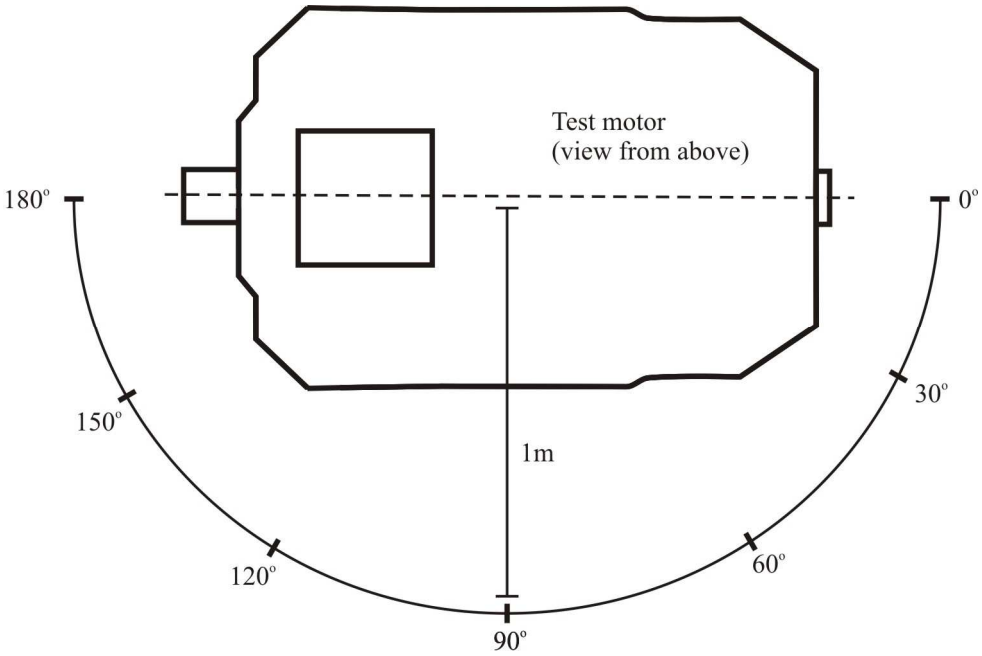

Fig. I. illustrates the position of the receiving antenna with respect to the test motor. If not otherwise mentioned, the measurements are done with the antenna located at the angle of 90^{o}. The distance to the motor centre is one meter in every measurement, measured from the antenna tip. The height of the antenna was kept constant at one meter measured from the ground.

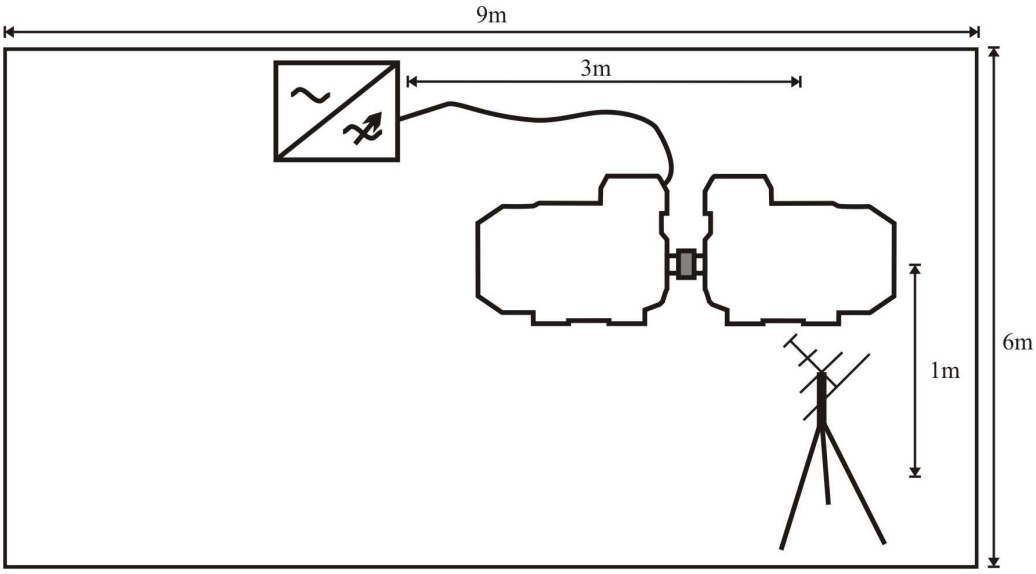

Fig. II illustrates the overall position of the equipment. The dimensions of the laboratory are 9m x 6m x 6m (length x width x height)).

APPENDIX II

Filter coefficients:

Section #1

Numerator:
1
-2
1
Denominator:
1
-1.7009643319435259
0.78849973981529797
Gain:
0.060808892573133759

Section #2

Numerator:
0.99999999999999989
-1.9999999999999998
0.99999999999999989
Denominator:
1
-1.4796742169311936
0.55582154328248901
Gain:
1

Output Gain:
10.88682607410459

ACTA UNIVERSITATIS LAPPEENRANTAENSIS

299. OIKARINEN, TUIJA. Organisatorinen oppiminen – tapaustutkimus oppimisprosessien jännitteistä teollisuusyrityksessä. 2008. Diss.

300. KARHULA, JUKKA. Cardan gear mechanism versus slider-crank mechanism in pumps and engines. 2008. Diss.

301. RAJAMÄKI, PEKKA. Fusion weld metal solidification: Continuum from weld interface to centerline. 2008. Diss.

302. KACHINA, ANNA. Gas-phase photocatalytic oxidation of volatile organic compounds. 2008. Diss.

303. VIRTANEN, PERTTU. Evolution, practice and theory of European database IP law. 2008.

304. TANNINEN, KATI. Diffusion of administrative innovation: TQM implementation and effectiveness in a global organization. 2008. Diss.

305. PUISTO, ANTTI. The initial oxidation of transition metal surfaces. 2008. Diss.

306. FELLMAN, ANNA. The effects of some variables on CO_2 laser-MAG hybrid welding. 2008. Diss.

307. KALLIOINEN, MARI. Regenerated cellulose ultrafiltration membranes in the treatment of pulp and paper mill process waters. 2008. Diss.

308. PELTOLA, SATU. Capability matrix – identifying and evaluating the key capabilities of purchasing and supply management. 2008. Diss.

309. HONKAPURO, SAMULI. Performance benchmarking and incentive regulation – considerations of directing signals for electricity distribution companies. 2008. Diss.

310. KORHONEN, KIRSI. Facilitating coordination improvement efforts in cross-functional process development programs. 2008. Diss.

311. RITVANEN, VIRPI. Purchasing and supply management capabilities in Finnish medium-sized enterprises. 2008. Diss.

312. PYNNÖNEN, MIKKO. Customer driven business model – connecting customer value to firm resources in ICT value networks. 2008. Diss.

313. AL NAZER, RAMI. Flexible multibody simulation approach in the dynamic analysis of bone strains during physical activity. 2008. Diss.

314. The Proceedings of the 7th MiNEMA Workshop. Middleware for Network Eccentric and Mobile Applications. Ed. by Pekka Jäppinen, Jouni Ikonen and Jari Porras. 2008.

315. VÄÄTÄNEN, JUHA. Russian enterprise restructuring – the effect of privatisation and market liberalisation on the performance of large enterprises. 2008. Diss.

316. DABAGHMESHIN, MAHSA. Modeling the transport phenomena within the arterial wall: porous media approach . 2008. Diss.

317. HAIMALA, JUHA. Supplier´s position in project marketing networks. 2008. Diss.

318. UOTILA, TUOMO. The use of future-oriented knowledge in regional innovation processes: research on knowledge generation, transfer and conversion. 2008. Diss.

319. LAPPALAINEN, TOMMI. Validation of plant dynamic model by online and laboratory measurements – a tool to predict online COD loads out of production of mechanical printing papers. 2008. Diss.

320. KOSONEN, ANTTI. Power line communication in motor cables of variable-speed electric drives – analysis and implementation. 2008. Diss.

321. HANNUKAINEN, PETRI. Non-linear journal bearing model for analysis of superharmonic vibrations of rotor systems. 2008. Diss.

322. SAASTAMOINEN, KALLE. Many valued algebraic structures as measures of comparison. 2008. Diss.

323. PEUHU, LEENA. Liiketoimintastrategisten vaatimusten syntyminen ja niiden toteutumisen arviointi keskisuurten yritysten toiminnanohjausjärjestelmähankkeissa: Tapaustutkimus kolmesta teollisuusyrityksestä ja aineistolähtöinen teoria. 2008. Diss.

324. BANZUZI, KUKKA. Trigger and data link system for CMS resistive plate chambers at the LHC accelerator. 2008. Diss.

325. HIETANEN, HERKKO. The pursuit of efficient copyright licensing – How some rights reserved attempts to solve the problems of all rights reserved. 2008. Diss.

326. SINTONEN, SANNA. Older consumers adopting information and communication technology: Evaluating opportunities for health care applications. 2008. Diss.

327. KUPARINEN, TONI. Reconstruction and analysis of surface variation using photometric stereo. 2008. Diss.

328. SEPPÄNEN, RISTO. Trust in inter-organizational relationships. 2008. Diss.

329. VISKARI, KIRSI. Drivers and barriers of collaboration in the value chain of paperboard-packed consumer goods. 2008. Diss.

330. KOLEHMAINEN, EERO. Process intensification: From optimised flow patterns to microprocess technology. 2008. Diss.

331. KUOSA, MARKKU. Modeling reaction kinetics and mass transfer in ozonation in water solutions. 2008. Diss.

332. KYRKI, ANNA. Offshore sourcing in software development: Case studies of Finnish-Russian cooperation. 2008. Diss.

333. JAFARI, AREZOU. CFD simulation of complex phenomena containing suspensions and flow through porous media. 2008. Diss.

334. KOIVUNIEMI, JOUNI. Managing the front end of innovation in a networked company environment – Combining strategy, processes and systems of innovation. 2008. Diss.

335. KOSONEN, MIIA. Knowledge sharing in virtual communities. 2008. Diss.

336. NIEMI, PETRI. Improving the effectiveness of supply chain development work – an expert role perspective. 2008. Diss.

337. LEPISTÖ-JOHANSSON, PIIA. Making sense of women managers´ identities through the constructions of managerial career and gender. 2009. Diss.

338. HYRKÄS, ELINA. Osaamisen johtaminen Suomen kunnissa. 2009. Diss.

339. LAIHANEN, ANNA-LEENA. Ajopuusta asiantuntijaksi – luottamushenkilöarvioinnin merkitys kunnan johtamisessa ja päätöksenteossa. 2009. Diss.

340. KUKKURAINEN, PAAVO. Fuzzy subgroups, algebraic and topological points of view and complex analysis. 2009. Diss.